CONSTITUTIVE PARAMETERS AND THEIR RELATIONSHIP FOR MAGNETOTELLURIC APPLICATION

A Thesis Submitted
in Partial Fulfilment of the Requirements
for the Degree of
DOCTOR OF PHILOSOPHY

by

YASH KANT

to the

DEPARTMENT OF CIVIL ENGINEERING
INDIAN INSTITUTE OF TECHNOLOGY, KANPUR

JULY, 1993

DEDICATED

TO

MY PARENTS

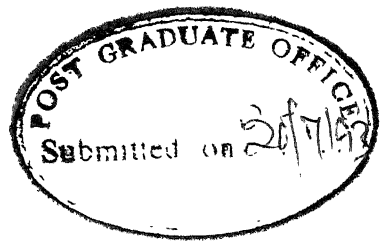

CERTIFICATE

It is certified that the work contained in the thesis entitled "CONSTITUTIVE PARAMETERS AND THEIR RELATIONSHIP FOR MAGNETOTELLURIC APPLICATION" by YASH KANT, has been carried out under my supervision and that this work has not been submitted elsewhere for a degree.

Ramesh P. Singh

Associate professor
Department of Civil Engineering
Indian Institute of Technology
Kanpur - 208 016, INDIA

JULY, 1993

ACKNOWLEDGEMENTS

The author is deeply indebted, first and foremost, to the thesis supervisor Dr. Ramesh P. Singh for providing his research laboratory facilities, valuable guidance, stimulus and constructive criticism during all stages of the thesis. It is his wholehearted support, co-operation and meticulous scientific attitude which inspired and enabled the author in accomplishing this undertaking.

I owe many thanks to Dr. Sri Niwas and Dr. P.S. Moharir who introduced me to the world of electromagnetics. Sincere thanks are also due to Dr. T.M. Rasmussen and Dr. L.L. Vanyan for introducing me to the acquisition and processing of magnetotelluric data and interpretive schemes during their visits on the campus. I also appreciate the timely help, discussion and kindness extended by Dr. S.S. Raghuwanshi during his visit on the campus.

I am thankful to all my teachers at Post-graduation level; especially to Drs. P.S. Moharir, Sri Niwas, P.K. Gupta, R. Chander, H. Sinhval, V.N. Singh, R.G.S. Sastri, B.B.S. Singhal, D.C. Srivastava, A.K. Sen, K.V.G.K. Gokhale, B.C. Raymahasay and Madam (Dr.) I. Sarkar who put efforts and spent their valuable time in understand the subjects inside the class room and outside as well. The help, advice and support at times given to the author is equally important during the stay on the campus. I acknowledge the share of their affection and generosity and would like to render thanks particularly to Mr. N.K. Goel, Mr. E.C. Shekhar, Ms. A. Rastogi, Mr. U.K. Singh, Mr. A.K. Keshari, Mr. A.K. Tiwari, Mr. A.D. Shukla, Mr. A. Sirohi, Dr. B.K. Panigrahi and Dr. N. Patel.

I wish to express my sincere thanks to my parents for their moral support, continuous encouragement, inspiration and affection. My pre-University teacher Mr. B.D. Sharma is also fully acknowledged who has always been with me as a source of inspiration and strength. Financial support during critical stages extended by my younger brothers Mr. Tej Veer Singh and Mr. Yash Veer Singh is equally appreciated and acknowledged. I have no words to express my gratitude to my wife Sunita who has shown a great degree of patience and tolerance throughout my companionship with her. Many many thanks to my lovely kid Nirjhar whose naughtiness and agility have always been pleasing.

I am also thankful to the Ministry of Human Resources and Development, Government of India; and Council of Scientific and Industrial Research, New Delhi for providing me financial support. Part of the work in this thesis is also supported through research projects sponsored by the Department of Science and Technology, New Delhi under the "Himalayan Seismicity" and "Deep Continental" study programs. I am also thankful to the Indian Institute of Technology, Kanpur for providing me financial support and necessary facilities.

Finally, but by no means the least, I would like to thank Mr. Bhatia and Mr. Harish for neat and clean typing of the thesis.

I.I.T., Kanpur (India)

(YASH KANT)

July, 1993

SYNOPSIS

Yash Kant
Department of Civil Engineering
Indian Institute of Technology, Kanpur
India

CONSTITUTIVE PARAMETERS AND THEIR RELATIONSHIP FOR MAGNETOTELLURIC APPLICATION

Magnetotelluric method is one of the geoelectrical methods which imparts information about the electrical resistivity of the Earth's crust and upper mantle. Electrical and electromagnetic methods do not conform well with the response of lumped circuit elements such as resistance, inductance and capacitance. Inhomogeneities and stratification in the subsurface have been found to give unexpected response to incident electromagnetic waves. The overall response of the subsurface to magnetotelluric signals encompasses relatively much larger depths and is found to change significantly. The term 'apparent resistivity' is generally used in electrical and electromagnetic methods, particularly in resistivity and magnetotelluric methods to deduce the subsurface resistivity structure. The characteristic behaviour of apparent resistivity arises primarily from the layered subsurface parameters, and at times is associated with characteristic oscillations and undulations.

Magnetotelluric response in both frequency and time domains are used to express the observable data as apparent resistivity. The apparent resistivity basically is a weighted spatial average of nearby resistivity distribution. To deduce useful information about the geological structure, efforts have been made to explore few possible ways of presenting the Earth's responses. The real, imaginary and

absolute values of the surface impedance have recently been used to define apparent resistivity. These definitions provide additional information and characteristic features of the subsurface, which is otherwise not possible using classical definition alone. Similarly in time domain, the step and impulse responses of the Earth to magnetotelluric signals have been used in arriving at different apparent resistivity definitions. These definitions merely channel different ways of assigning different set of weights to the subsurface resistivity distribution. The apparent resistivity defined in different ways are found to provide subsurface resistivity distribution.

The apparent resistivity over various three layered Earth models (H, K, Q and A type) shows characteristic features of the layered parameters for different definitions of apparent resistivity. The distinctive behaviour of apparent resistivity curves in the broad band periods and delay times can be used as an appropriate definition for a particular H, K, Q and A type Earth models. The special features of apparent resistivity curves obtained using various definitions can be used as rules of thumb in the qualitative interpretation of magnetotelluric data in frequency and time domains.

For the prediction of subsurface resistivity distribution with the help of suitable and adequate mathematical function, it is essential to have the knowledge of functional characteristic over various layered models. Such functions are the characteristic of the changes in behaviour of apparent resistivity in frequency and time domains which are associated with changes in resistivity distribution of the layered Earth. This characterizes the ability of explaining the related phenomena that takes place at depths. The understanding of the changes in a model and corresponding changes in predictable data is important in

developing a mathematical link. The Frechet derivative serves the connecting link for such changes and has been derived for various one-dimensional Earth models. Frechet derivatives provide immediate information about the geophysical environment of the subsurface which is useful in itself or in a second stage of inversion wherein an acceptable resistivity model is deduced. In fact, resistivity often changes by many orders of magnitude, therefore, model perturbation and corresponding data perturbation are best represented on logarithmic scale. Frechet derivatives defined in this manner are known as 'sensitivity functions'. Sensitivity functions have been studied in detail for various multi-layered and continuous Earth models with varying conductivity in both frequency and time domains. The sensitivity variations with depth show contribution of the resistivity structure at depths to the apparent resistivity at a particular period. It also gives the direct estimation of the depth of investigations at a particular period. Moreover, the zones of localized maximum sensitivity in either domain are emphasized with ease. Such zones are found on or near the Earth surface in frequency domain and at depths below the Earth surface in case of time domain. The maximum sensitivity observed on or near the Earth surface can be attributed to the observed static shift in some of the regions. The behaviour of sensitivity functions shows that the static shift problem may not be present in time domain magnetotelluric measurement. The sensitivity functions using analytical expression are found to illustrate the problem of equivalence in magnetotelluric method.

The magnetotelluric data at various locations in the Indo-Gangetic basin have been recorded. Various magnetotelluric parameters at each location have been studied to deduce the resistivity structure of the Indo-Gangetic basin. It has been found that the high conducting top

layer distorts the magnetotelluric data at longer periods. The influence of the high conducting sediments have been studied as a sensitivity on the Earth surface in the period range 1-4000 seconds. The conductance of this conductive sedimentary layer has been removed to avoid the screening effect to extract maximum information about the electrical resistivity of the deeper structure. The lower crustal conductivity zone is also found to be present in the Indo-Gangetic basin. The magnetotelluric data show the subsurface extension of the peninsular shield beneath the Indo-Gangetic basin.

CONTENTS

LIST OF FIGURES

LIST OF SYMBOLS

E_x Horizontal component of electric field along x-axis

E_y Horizontal component of electric field along y-axis E Horizontal component of electric field for one dimensional Earth models or column matrix of of horizontal electric field components

H Horizontal component of magnetic field for one dimensional Earth models or column matrix of horizontal magnetic field components

H_x Horizontal component of magnetic field along x-axis

H_y Horizontal component of magnetic field along y-axis

Z_{xy} Surface impedance for E-ploarization

Z_{yx} Surface impedance for H-polarization

Z Surface impedance for one dimensional Earth models or 2 X 2 impedance tensor

Z_{am} Arithmatic mean of the off-diagonal elements of tensor impedance

Z_{Det} Square root of the determinant of tensor impedance

Z_{gm} Geometric mean of the off-diagonal elements of tensor impedance

$\underline{Z}$ $Z/i\omega$

ρ_{axy} Apparent resistivity for E-ploarization

ρ_{ayx} Apparent resistivity for H-ploarization

ρ_a Apparent resistivity for one dimensional Earth models

ρ_{aDet} Apparent resistivity for Z_{Det}

ϕ_{xy} Phase of Z_{xy}

ϕ_{yx} Phase of Z_{yx}

ϕ Phase of surface impedance (Z) for one-dimensional Earth models

ϕ_{Det} Phase of Z_{Det}

γ Wave number

ω Angular frequency of the signal

f Frequency of the signal

T Period of the signal

μ Magnetic pemeability of free space

E' Rotated electric field components (x or y) or their column matrix

H' Rotated magnetic field components (x or y) or their column matrix

Z' Rotated components (diagonal or off diagonal) of surface imedance or their 2 X 2 tensor impedance

α Angle of rotation

A Tranformation matrix

t Delay time of the signal

E(t) Inverse Fourier Transform of E(w)

H(t) Inverse Fourier Transform of H(w)

$R_s(t)$ Step response of the Earth

$R_i(t)$ Impulse response of the Earth

ρ_n Resistivity of nth layer

σ_n Conductivity of nth layer

d_n Thickness of nth layer

γ_n Propagation constant in nth layer

$K_{n(n-1)}$ Reflection coefficient for interface between nth and (n-1)th layer

$\sigma(z)$ One-dimensional vertical conductivity profile, z is depth

ρ_o Resistivity of surface layer for exponentially varying conductive models with depth

σ_o Conductivityof surface layer for exponentiallyvarying conductive models with depth

δ_{sd} Skin depth either in first layer or surface layer

δ_{dd} Defused depth either in first layer or surface layer

ϑ_1 $\left[2/\pi\right]^{1/2} / (\delta_{dd}\, \sigma_1)$

ξ_1 The ratio of first layer thickness to diffused depth

I_n, K_n The nth order modified Bessel functions of first and second kind

ber_n, bei_n Thomson (Kelvin) function of nth order corresponding to I_n

Ker_n, Kei_n Thomson (Kelvin) function of nth order corresponding to K_n

CHAPTER I

INTRODUCTION

1.1 General

Geophysics is the study of the surface features and the interior of the Earth by systematic measurements of various physical phenomena, associated with their correlative physical property, with appropriate instruments on or above the surface. The physical state of the Earth's concealed regions is characterized by the physical property, deduced from the measurements using interpretive schemes. The inferred physical property is transformed into geologically meaningful section of the subsurface formations. The main geophysical methods used to study the interior of the Earth are seismic, gravity, magnetic, and electrical methods. Each of the methods uses measurements of different physical phenomenon, anticipated to exist among rocks and rock types comprising the concealed regions. The usefulness and suitability of a geophysical method depend upon the optimality of objectives, geological environment of the region to be surveyed, potentiality of the method, rapid coverage, and exploration cost involved. Nevertheless, one 'best' geophysical method simply does not exist for all applications. In practice different combinations of exploration techniques are used for deriving complete information of the region under study. The magnetotelluric method is one of the most potential techniques which is capable of providing deeper information for the region under study.

1.2 The Magnetotelluric Method and its Need in India

Magnetotelluric method is one of the electrical methods, which makes use of naturally occurring electromagnetic phenomenon to elicit information about the spatial distribution of electrical resistivity inside the Earth. The efficacy of magnetotelluric method lies in the systematic application of electromagnetic wave theory to evaluate the response of the solid Earth with a view to elucidate the electrical state, behaviours, composition, thermal regimes and geologic structures of the Earth's surface and interior. The evolution of magnetotelluric method as an exploration tool dates back to at least 1950, when the concept of using natural electromagnetic energy to determine the electrical characteristics of the crust was proposed by Tikhonov (1950). However, the first detailed independent western reference was published by Cagniard (1953). This classical approach uses the frequency-based representation of transfer function as the starting point of magnetotelluric interpretive schemes. A different approach was suggested by Kunetz (1972), which uses the time-based representation of transfer function as the starting point of magnetotelluric interpretive schemes.

The basis of magnetotelluric method is very simple. The electromagnetic fields are induced inside the Earth, by the variations in magnetic field of electromagnetic waves that are attenuated exponentially with depth as these penetrate into the subsurface. In frequency-domain the depth of penetration in a homogeneous medium at which the amplitude of electromagnetic wave is attenuated by a factor of e^{-1} is called skin depth δ_{sd}, and in MKS units is written as (eg. Spies, 1989)

$$\delta_{sd} = \sqrt{\frac{2}{\omega \sigma \mu_o}} \qquad \ldots(1.1)$$

where ω (= $2\pi f$), μ_o and σ are the angular frequency of the electromagnetic wave, magnetic permeability of the free space, and conductivity of the medium, respectively.

In time-domain, the depth of penetration in a homogeneous medium at which the maximum transient electric field is found to be located is called diffusion depth δ_{dd}, and in MKS units is written as (eg. Spies, 1989).

$$\delta_{dd} = \sqrt{\frac{2t}{\sigma \mu_o}} \qquad \ldots(1.2)$$

where, t is delay-time.

The similarity between expressions for skin depth (equation 1.1) and diffusion depth (equation 1.2) is remarkable; the depths are proportional to $1/\sqrt{\omega}$ in the frequency-domain, and $\sqrt{t}$ in time-domain. There is one to one correspondence between period (reciprocal of frequency) and delay-time. For example, at shorter periods shallow information of the subsurface structure are obtained, while at longer periods the deeper information of the subsurface structure are obtained. Similar is the case for early delay-time and late delay-time. Here the adjective 'delay' means how much the signal is delayed in reaching the earth surface after interacting with the subsurface structure. Thus, it is clear from the equation 1.1 and 1.2 that the depth of penetration highly depends upon the resistivity of the medium and the frequency/delay-time of the wave. In a highly conducting region, at high frequencies/early delay-times the waves are confined to shallow regions due to smaller skin/diffused depth and vice-versa. In real Earth situation the greater depths of penetration are achieved at low frequencies/higher delay-times. It follows from the Ampere's law that

the fluctuating amplitudes of the magnetic field on the surface of the Earth determines the total current flowing in the subsurface. Once the current is known, the magnitude of the electric field can be used to determine the Earth's electrical resistivity. This determination takes into account the vertical spread of the current due to the attenuation effect. Different frequencies/delay-times have different depths of penetration, which allow to study the variations of resistivity as a function of depth. By making measurements on the surface of the Earth, at sites along the profile, information about the horizontal variations of resistivity are obtained, and thus an approximate two-dimensional picture of the Earth's resistivity is developed. The data are usually presented in terms of the apparent resistivity (both in frequency and time-domains) and E/H phase (in frequency-domain only) as a function of frequency/delay-time. The apparent resistivity, a parameter which is commonly used in all electrical soundings, is simply the resistivity of an equivalent homogeneous Earth that would give the same magnitude of the observed response (surface impedance in frequency-domain; step and impulse responses in time-domain) of the Earth. In an inhomogeneous Earth, the apparent resistivity varies with frequency/delay-time as well as with position.

The time-domain approach suggested by Kunetz (1972), uses the frequency-domain system (natural source or controlled source) as the traditional magnetotelluric method uses. The difference lies in the response function. The frequency-domain approach uses the surface impedance as the response function, whereas, time-domain uses the step and impulse functions as the response functions. The step and impulse response functions corresponding to step and impulse variations in primary magnetic field exhibit all the properties and contain signature

of Earth's subsurface. However, the approach of Kunetz discussed above has similarity with transient electromagnetic methods, still it constitute a part of interpretation of magnetotelluric data owing to the derivation of step and impulse response functions directly from the surface impedance. Although, frequency-domain and time-domain approaches may be applied to successive phases of the processing and/or interpretation of magnetotelluric measurements, yet both the approaches are independent of each other. However, for the application of aforementioned time-domain approach, a good knowledge of the amplitude and phase responses of the frequency-domain is necessary.

1.2.1 Magnetotelluric Method- A Potential Tool

The application of any geophysical method depends upon its inherent characteristic of target resolution, precision of instrument, detailed method of data acquisition and quality of data, interpretive techniques and the perception of the method that a working group selects and finally adopts. The merits and demerits are better judged by the ratio of success to failure on commercial basis, both in absolute sense and when compared with other methods. Careful study of the geology of the region to be surveyed, well defined objectives, comparative knowledge of successes and failures of various methods under the same geologic environment and of course the experienced group of practitioners inevitably arrive at the most feasible decision to initiate with the proposed method. To begin with magnetotelluric method, therefore, is to begin with an understanding of the signal features and its interaction with the target resulting into various responses and its merits and demerits as compared to other compatible methods. As an exploration tool seismic method has dominated all the other geophysical methods,

therefore, the comparison of magnetotelluric method is always been made with seismic method.

1.2.2 Details of Magnetotelluric Method

In general, volcanic and geologically complex areas are difficult to explore using seismic method. Such areas are generally probed using magnetotelluric method. These areas belong to the following four broad types of regions: First - the basalt layers near or on the surface of the Earth which cause very strong reflections and greatly hinder the imaging of layers beneath them, Second - the areas where tectonic events have disrupted the sedimentary layer geometries and greatly complicated the seismic signature, making the seismic interpretation very difficult, Third - in densely populated areas where strong explosives cannot be used as a source of energy for seismic measurements and finally the Fourth and the last includes areas with rugged topography where layout of seismic measurement unit is not possible. Under such conditions the magnetotelluric method has demonstrated proven potentiality and ability to obtain qualitative and quantitative subsurface information.

Magnetotelluric method measures a different set of physical property, and thus, compliments the data obtained by other geophysical methods such as gravity, magnetic, and seismic. Magnetotelluric data have been particularly helpful in resolving ambiguities and clearing conflicts arising from seismic and gravity/magnetic interpretations. Magnetotelluric logistics are relatively simple as compared to seismic in areas of difficult topography. The effects of electromagnetic field due to induction in subsurface structure can be observed on the surface of the Earth, some distance away from the structure. This enhances the ability of magnetotelluric method to interpret the structure with an

economically wide spaced measurement sites along the profile. For information on deeper parts (eg. lower crust and upper mantle) magnetotelluric method has proven to be a potential method. Deeper information are obtained due to greater depth of penetrations into subsurface at low frequency signal associated with broad-band frequency spectrum of natural source.

1.2.3 Demerits of Magnetotelluric Method

In general, the natural sources of magnetotelluric signals are not discrete and controllable and therefore, are associated with unavoidable noise and dispersion which tends to limit its probing potentiality. The diffuse nature of electromagnetic waves in a conducting medium results as the information content of the medium being smoothly spread out over a wide range of frequencies. This spread of signature for any underlying structure over a wide range of frequencies reduces the vertical resolution of magnetotelluric method. Thus, magnetotelluric method is a low resolution technique as compared to reflection seismic method.

Information contents from the magnetotelluric measurements is possible only if a resistivity contrast between neighbouring geologic formations exists. In environments where similar electrical properties for two geologically different neighbouring formations do exist, the interpretation of magnetotelluric measurements are not usually amenable to the discrimination of the formations.

Often, magnetotelluric inverse solution is non-unique and ambiguous. The degree of ambiguity and non-uniqueness is reduced on supporting the magnetotelluric data from other methods such as gravity, magnetic, and seismic data. However, this demerit is not only associated with magnetotelluric method but also it is shared to some extent by most

of the geophysical methods.

The lateral variations of resistivity in the vicinity of a measuring site have an effect on magnetotelluric data. Such variations might be represented in nature by alluvial-filled depressions, stream beds, narrow valleys bounded by rock outcrops, etc. These effects are termed as static effects and may be manifested by a parallel or near parallel separation of the two apparent resistivity curves for E- and H-polarizations. The effects of near surface inhomogeneities are superimposed upon the effects of deeper structures which cause the so called and aforementioned static shift. The analysis of such data at time, misleads the interpretation. However, there are techniques to correct the magnetotelluric data for static effects which lessen its severity. Current channeling is another problem which affects the magnetotelluric data acquisition and there interpretation.

In India seismic method has widely been used for exploration of hydrocarbon resources. However, the applicability of seismic method has not subtly been appraised to delineate the complete structure due to various reasons and certain local constraints. There are areas in India with volcanic and crystalline rocks on or near the surface of the Earth, (eg. Deccan trap part of Madhya pradesh, Maharastra and Gujarat states) where seismic method reveals no information about the underlying formations. However, under such surface conditions, the hydrocarbon-bearing source and reservoir rocks are known or suspected in the subsurface, beneath the volcanic or crystalline formations. Gangetic-plain is another region where seismic method failed miserably to impart any diagnostic information. This region is densely populated and inhibits the seismic survey. The magnetotelluric method is capable of overcoming some of the limitations and has proven to be an excellent

tool for identifying or confirming the presence of the deep seated rocks that possibly may be the potential hydrocarbon source and reservoirs, and for providing an estimate of the thickness of the surface formations and thickness and gross structural configuration of the sediments (Orange, 1988). Although, the magnetotelluric method has been proved to be the only potential tool under these conditions, yet it has not been used so far in these regions for delineating the structural details. The low cost and fast coverage of magnetotelluric method are its assets for its extended use in geophysical exploration in the Developing Countries like India. The magnetotelluric method undoubtedly may prove to be an excellent exploration technique in India, not only as a regional reconnaissance tool to access the seismic method in unexplored areas but also as singular viable tool in areas of rugged topography, complex geologic conditions and in densely populated regions.

1.3 Magnetotelluric Study in India: A Review

1.3.1 Theoretical Work

Theoretical study of magnetotellurics means analytic conceptualization of physical reality, processes, interpretive schemes and their resolution, and appraisal of models used. In magnetotellurics, one usually analyses various Earth processes both qualitatively and quantitatively, and attempts to find the smallest number of independent ordering principles and/or elementary processes. Each step of theoretical study stated above invariably supports ultimately, directly or indirectly, and progressively in improving models under study to match the reality as far as possible.

The most dominant and productive work in India is being done at National Institute of Geophysical Research, Hyderabad in the field of

magnetotellurics with emphasis on its applications on current distribution in covered conductors, effects of perturbation of the shape on the electromagnetic response of these bodies, influence of inhomogeneity and magnetic permeability of conductors on electromagnetic responses and effect of anisotropy. A list of problems analysed at NGRI during 1961-1973 is given in a unpublished report by Negi (1974). The significant research in theoretical electromagnetics done by Negi and Saraf in the last two decades is covered in their book published recently (1989).

Srivastava (1963) applied the magnetotelluric method to anisotropic and inhomogeneous bodies. Srivastava (1965) given the method of interpretation of magnetotelluric data when source field is considered. Naidu (1965) computed the telluric profiles over an inclined fault. Srivastava (1966) given the theory of magnetotelluric method for a spherical conductor. Mallick (1970) studied the magnetotelluric sounding for layered Earth with transitional boundary. Roy and Naidu (1970) computed the telluric field and apparent resistivity over an anticlinal structure. Mallick (1971) discussed about the detection of transitional electrical properties of the Earth. Mallick (1972) studied the response of conducting sphere in electromagnetic input field. Mallick (1973) studied the response of infinite horizontal cylinder in electromagnetic input field. Roy (1973) carried out the theoretical analysis of telluric field over a faulted basement. Kumar (1979) studied the theoretical magnetotelluric response over two-dimensional dyke. Kumar et al. (1981) studied the detectability of an intermediate layer for magnetotelluric sounding. Roy et al. (1982) studied the telluric fields and their gradients over a step fault at right angles to the strike of the fault planes. They obtained a closed form solution of the boundary problem in

terms of elliptic integrals of the first and third kind by applying the Schwarz-Christoffel method of conformal transformation. Roy and Ghose (1985) interpreted the crust-mantle heterogeneities on the basis of published results of magnetotelluric (and seismic also) for the profile which extends from the Scandinavian Shield to Mariana Islands, and passes through the parts of Europe, Atlantic Ocean, Canada, U.S.A., Pacific Ocean and Hawaiian Islands. Inverted magnetotelluric (and seismic) data were plotted by them against depth on a regional scale to obtain geoelectric and seismic sections and attempted to correlate the electrical conductivities and seismic velocities. A tentative temperature section is then constructed based on the electrical conductivities of the geoelectric section. Sarma et al. (1991) examined the non-uniformity in the magnetotelluric signal in the equatorial region of India. They pointed out the possibility that southern peninsular India could be considered as one of the possible features responsible for non-uniformity in the magnetotelluric source field. Their results indicate that the source field effects may have to be taken into consideration when magnetotelluric surveys for periods greater than 100 sec. are carried out in the day time in this region, particularly in the high resistive shield areas.

1.3.2 Field Work

The first magnetotelluric study using the data from the permanent geoelectric observatory at Choutupal near Hyderabad, established by National Geophysical Research Institute, Hyderabad, was carried out by Sarma et al., (1970). They had analysed the data using the method of Niblett and Sayn-Wittgenstien and concluded a three-layer structure with first and second layer thicknesses as 42 and 24 Km, respectively. The

conductive estimates of the three regions were proposed to be 11 - 12 X 10^{-14}, 6.5 - 9.5 X 10^{-15} and 9 - 12 X 10^{-14} emu, respectively. Sarma et al. (1983) analysed the telluric data near the northern parts of Konkan geothermal province. They concluded depending upon their analysis that i) a distinct well defined telluric anomaly exist in the region, and ii) the anomaly reflects positively the presence of a conducting zone(s) at fairly deeper levels which appears to have a close bearing on the geothermal setting of this region.

In December, 1987, Indian Institute of Technology, Kharagpur carried out the acquisition of magnetotelluric data in Singhbhum region. The results have been discussed in a recent publication (Roy et al., 1989). However, on the Singhbhum batholith the sediment conductance is only a few Siemens, but the level of the apparent resistivity curves are high due to static shift which has not been accounted for.

The Indian Institute of Geomagnetism, Bombay is also associated with the magnetotelluric data acquisition in the western part of Deccan traps. Their analysis of magnetotelluric data were recently presented in a workshop held at Indian Institute of Technology, Kharagpur (Gokaran et al. 1992).

With the collaboration of Uppsala University, Sweden, The Indian Institute of Technology, Kanpur have carried out the magnetotelluric measurements at about 80 various locations covering parts of Indo-Gangetic basin, Indian Peninsular region and Cambay basin during March-May 1989. The processing of data is under way. Some of the results are given in this thesis.

1.4 Scope of the Thesis and its Organization

The present work is undertaken with a view to improve non-intricately an intuition about the electrical state of the material beneath the surface of the Earth, through comparative study of different definitions of apparent resistivity and sensitivity analysis of various one-dimensional vertically inhomogeneous Earth models.

The aim of magnetotellurics does not end up with the solution of inverse problem which reproduces observations only within some specified error limit but extends to the appraisal of the models (solution). The sensitivity analysis accounts for it.

The Indo-Gangetic plain is taken as the area of study. The application of magnetotelluric to this area is not only interesting due to a high probability of occurrence of potential petroleum resources, where seismic methods have failed, but in addition it also gives results which may prove to be important for understanding the tectonic activity.

Besides this introductory Chapter, the thesis contains five more Chapters.

Chapter II, is intended to provide theoretical background and with this aim it reviews the theory of magnetotelluric method. Various interpretive response parameters to magnetotelluric data have been explained. The transfer functions between electric and magnetic (or its time derivative, particularly in time-domain) fields, both in frequency and time-domains are derived analytically or numerically for various vertically inhomogeneous one-dimensional Earth models.

Chapter III, is intended to provide background for interpretation of experimental results through theoretical study of various apparent resistivity definitions which have been given by using real, imaginary and amplitudes of surface impedance/square of the surface impedance (in

frequency-domain); and by using the step and impulse response functions (in time-domain). Comparative study of these theoretical apparent resistivities have been carried out for three-layer Earth models in both frequency and time-domains.

In Chapter IV, analytical and numerical solutions of sensitivity functions for various one-dimensional vertical inhomogeneous Earth models have been discussed. The sensitivity analysis for various Earth models have been carried out. The graphical illustrations of the behaviour of sensitivity functions are included in this Chapter.

In Chapter V, an attempt has been made to interpret the magnetotelluric data recorded in Indo-Gangetic basin. Various magnetotelluric parameters have been used as interpretive tools on several stages of interpretation.

In Chapter VI, summarized conclusions relevant to specific problems studied and scope for future studies have been discussed.

CHAPTER II

MAGNETOTELLURIC THEORY AND INTERPRETIVE PARAMETERS

2.1 General

The magnetotelluric method uses naturally occurring electromagnetic fields, to measure the magnetotelluric response of the Earth's surface and interior at the first stage which enables the determination of the subsurface electrical resistivity as the incident wave penetrates and reflects back. This method utilizes the electrical resistivity of the subsurface which vary from one location to another due to which the magnetotelluric response also changes from one location to another. The measurements of magnetotelluric fields yield subsurface electrical resistivity information due to changes in rock properties, that are used to map the subsurface structure and to estimate and evaluate its physical properties. The estimation of electrical resistivity distribution of the subsurface essentially requires either, the use of forward or inverse method. The forward method involves the known geoelectric model parameters to compute the theoretical magnetotelluric response using predefined model function. From the catalogue of theoretical magnetotelluric responses, a response is chosen which almost is in full agreement with the field observation. The subsurface model, corresponding to this response is the desired solution. The inverse method involves first, the parameterization of the Earth into a number of subsurface layers of constant resistivity (one-dimensional inversion) and then attempts to address the existence, uniqueness, construction, stability and appraisal of the solution (model). The inverse method is

most feasible and is usually preferred. It addresses many questions which are accomplished only by using the deduced parameters of the model to compute the forward functions.

The traditional application of magnetotelluric method involves the estimation of surface impedance at a site, through the measurements of horizontal orthogonal components of electric and magnetic fields in the broad-band frequency range. The broad-band frequency spectrum for the surface impedance contains the signature of the subsurface, is a frequency-based representation of the Earth system transfer function which transfers the magnetic field to the corresponding electric field. The conventional and current usage involves the theoretical expression of transfer function (surface impedance) to define the apparent resistivity using the Cagniard (1953) formula. The unconventional usage, includes determination of theoretical expressions of transfer functions, especially in time-domain, leading from the magnetic field or its time derivative to the corresponding electric field (Kunetz, 1972; Wieladek and Ernst, 1977; McMechan and Barrodale, 1985; Gomez-Trevino, 1987b; and Yee et al. 1988). At this point a series expansion of the frequency-domain transfer function ($Z(\omega)/i\omega$ or $Z(\omega)$) which leads to an expression well adapted to a transposition into the time-domain, giving transfer function, step response ($R_s(t)$) or impulse response ($R_i(t)$). The step and impulse response functions are time-based representation of the transfer characteristics of the Earth, which are used to define the corresponding apparent resistivities. In principle, all these apparent resistivities, which are related to different transfer functions, should give rise to similar visualization and quantification of subsurface resistivity distribution since they sample the same underground structure. This ideal requirement is seldom met in practice due to the

loss of information on the part of corresponding transfer functions during theoretical formulation of forward problem and because of different averaging processes which are involved in evaluating corresponding transfer functions. The characteristics of these transfer functions are only realized after detailed comparative study of apparent resistivity defined through them.

2.2 Sources of Natural Electromagnetic Variations

The magnetotelluric measurements over the depths of interest including regions between crust and upper mantle requires naturally occurring source signals ranging approximately from 0.0005 - 500 Hz. In the present study signals ranging approximately from 0.0003 - 10.0 Hz have been used. There are two primary sources, responsible for variations in the electromagnetic fields which provide this bandwidth over more than five decades. One of the sources of incident energy at the Earth's surface which causes variations in the electromagnetic field at low frequency below roughly 1.0 Hz is the upper ionosphere and magnetosphere. These variations include magnetic storms, substorms and micropulsations are the consequences of the interaction of Earth magnetic field with the solar wind which consists of the stream of charged particles emanating from the Sun, and the plasma layers in the magnetosphere and upper ionosphere. The second source of energy, at high frequencies above roughly 1.0 Hz, is the world-wide cloud-to-cloud and cloud-to-ground lightning activities (i.e. spherics), propagating in and exciting the Earth's ionosphere cavity. The first resonance of this cavity occurs at roughly 8.0 Hz and the signals are attenuated rapidly below this frequency. These energy bands do not quite overlap, and there is an energy 'hole' or minimum in the frequency range of roughly 0.1 -

2.0 Hz. In this band, it is difficult to obtain high-quality magnetotelluric data. In addition to covering a broad frequency range, the magnetotelluric energy also encompasses an extremely broad dynamic range for both electric and magnetic power spectra. The dynamic ranges for electric and magnetic field densities cover a range of approximately seven and nine decades, respectively (Orange, 1989).

For magnetotelluric signal range, especially at low frequencies, the wavelengths of the incident electromagnetic waves are much larger than the inductive scales of the Earth's structure under investigation. Therefore, electromagnetic waves for magnetotelluric case are sufficiently planar, and thus, the wave number γ can be assigned zero value to electromagnetic field components. Moreover, the primary source is farther from the Earth's surface which provides nearly normal incidence of the primary energy on the Earth surface. Thus, the planar and primary electromagnetic field is assumed to be propagating nearly vertically downward to the surface of the Earth, which induces electric and magnetic fields that are linearly related to the primary sources of excitation. Figure 2.1 describes schematically the interaction of the source magnetic induction field with the geoelectrical medium.

2.3 Theory of Magnetotelluric Method

The magnetotelluric theory for one-dimensional stratified Earth in which resistivity varies as a function of depth only, was first formulated by Cagniard in 1953. This requires only one set of horizontal electric and perpendicular magnetic field components to describe the Earth structure. Cantwell (1960) generalized the theory for real Earth, replacing the over simplified theory for one-dimensional stratified structure which is hardly realized in real situations. Cantwell defined

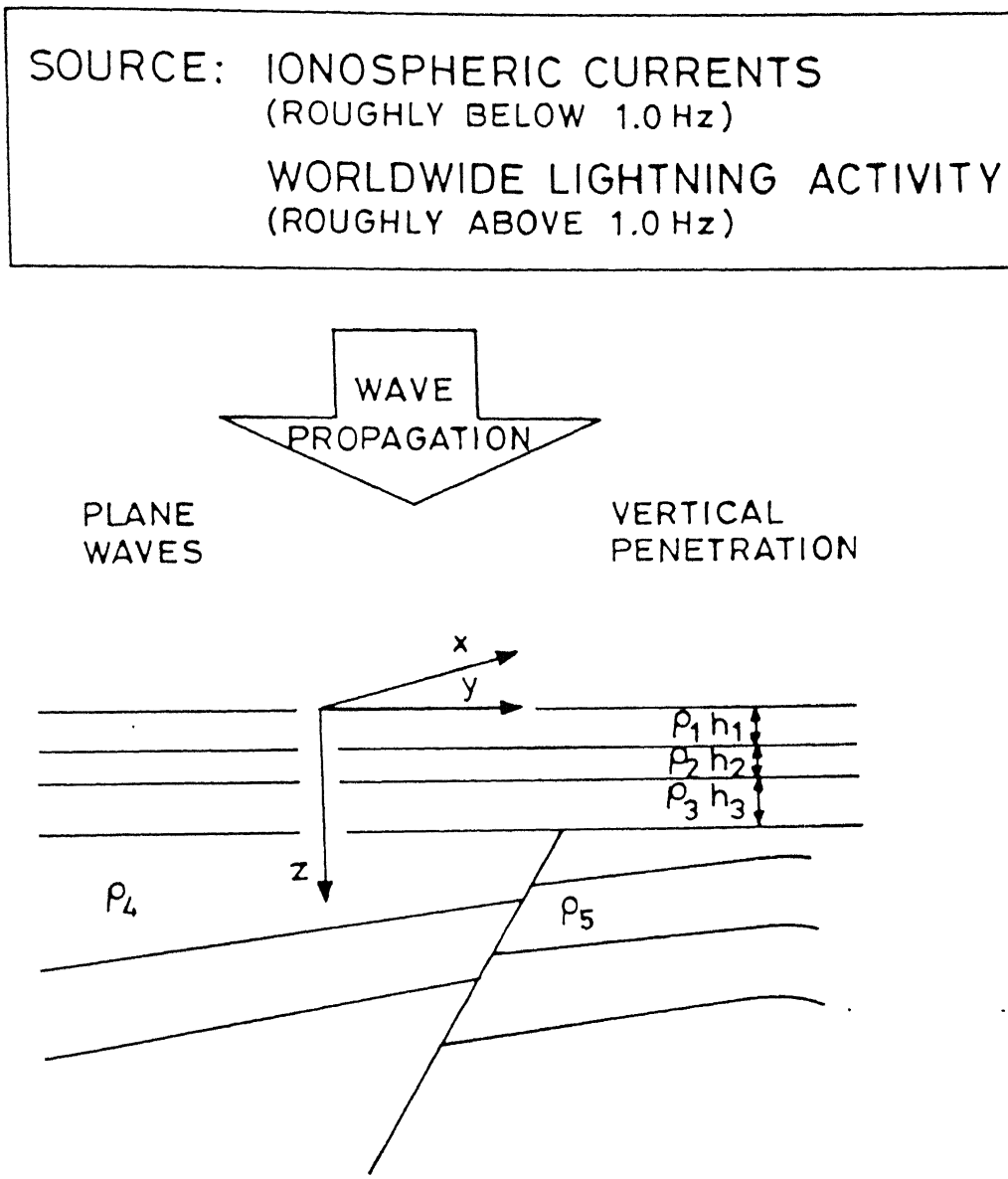

Figure 2.1 The interaction of the natural electromagnetic source with conductive geoelectric model (redrawn from Dobrin and Savit, 1988).

the signature of a particular measurement site through impedance tensor, which relates horizontal magnetic components to the horizontal electric components at a particular frequency and wave number of the source field. The wave number γ is ignored due to planar assumption for the source field.

The four horizontal orthogonal components - E_x, E_y, H_x and H_y and one vertical magnetic field component H_z of time varying total electromagnetic field of the Earth are measured at a physical site on the Earth surface. The measuring directions, the x-axis and y-axis are taken North-South and East-West, respectively. The z-axis points vertically downward. The electric field sensors (grounded electrodes) and the magnetometers are typically deployed along with recording unit as shown in Figure 2.2. The linearity of Maxwell's equations ensure that for any plane and normally incident electromagnetic wave at angular frequency ω, the following relations hold between the horizontal

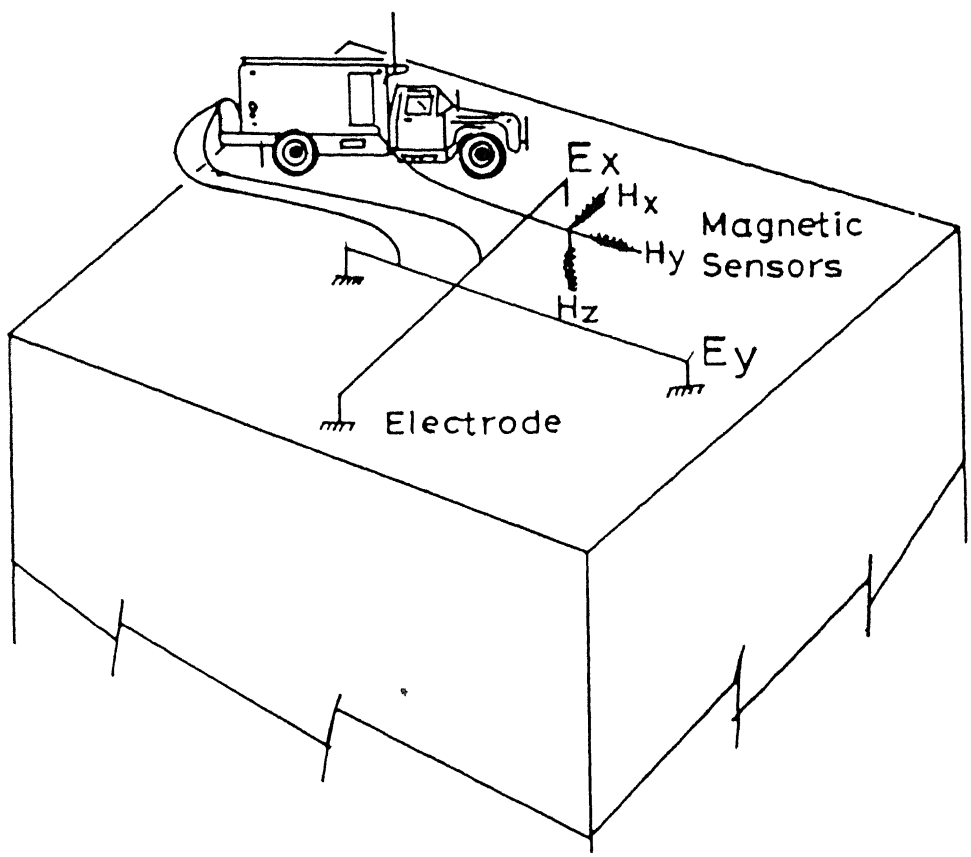

Figure 2.2 The layout of the magnetotelluric field sensors and recording unit.

orthogonal components of electric and magnetic fields (Cantwell, 1960).

$$\begin{bmatrix} E_x(\omega, \gamma) \\ E_y(\omega, \gamma) \end{bmatrix} = \begin{bmatrix} Z_{xx}(\omega, \gamma) & Z_{xy}(\omega, \gamma) \\ Z_{yx}(\omega, \gamma) & Z_{yy}(\omega, \gamma) \end{bmatrix} \begin{bmatrix} H_x(\omega, \gamma) \\ H_y(\omega, \gamma) \end{bmatrix} \quad \ldots(2.1)$$

or in compact notation

$$E(\omega, \gamma) = Z(\omega, \gamma)\, H(\omega, \gamma) \quad \ldots(2.2)$$

where, $\omega = 2\pi f$ is the angular frequency, and f is the frequency of the signal. $E(\omega, \gamma) = [E_x(\omega, \gamma) \quad E_y(\omega, \gamma)]^T$, and $H(\omega, \gamma) = [H_x(\omega, \gamma) \quad H_y(\omega, \gamma)]^T$ represent the respective electric and the magnetic fields on the Earth surface; superscript T represents the transposition of the row matrices of electric and magnetic field components; and γ is wave number which is assumed to be zero due to planar assumption of the source field and can be dropped. The 2 X 2 impedance tensor is thus written as

$$Z(\omega) = \begin{bmatrix} Z_{xx}(\omega) & Z_{xy}(\omega) \\ Z_{yx}(\omega) & Z_{yy}(\omega) \end{bmatrix} \quad \ldots(2.3)$$

From the view point of linear system theory, a set of tensor components $Z_{xx}(\omega)$ and $Z_{xy}(\omega)$ or $Z_{yx}(\omega)$ and $Z_{yy}(\omega)$ are transfer functions of a dual input, single output linear system through which the horizontal magnetic field components H_x and H_y (input) are related deterministically to the horizontal electric field components E_x or E_y (output). The schematic diagram for Earth transfer linear system is shown in Figure 2.3. The electric field $E(\omega)$, magnetic field $H(\omega)$ and impedance tensor $Z(\omega)$ are

not only the function of angular frequency ω, but also vary with

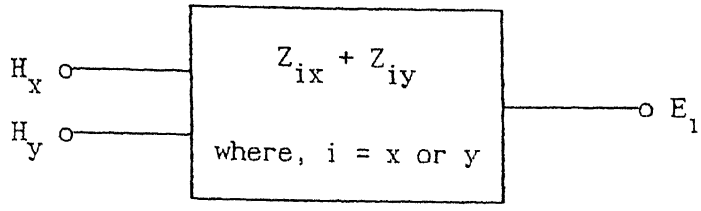

Figure 2.3 The schematic diagram of the transmission of single output (one electric field component) by the dual input (both magnetic field components) Earth transfer linear system.

with position on the surface of the Earth. The apparent resistivity ρ_{al} and the phase ϕ_l (l = xy or yx) of the impedance are defined for two measuring directions, respectively as

$$\rho_{axy} = \frac{|Z_{xy}(\omega)^2|}{\omega \mu_o} \quad \text{and} \quad \rho_{ayx} = \frac{|Z_{yx}(\omega)^2|}{\omega \mu_o} \qquad \ldots(2.4)$$

$$\phi_{xy} = \arg (Z_{xy}) \quad \text{and} \quad \phi_{yx} = \arg (-Z_{yx}) \qquad \ldots(2.5)$$

Thus in one-dimensional environment, the apparent resistivity in two directions is

$$\rho_{axy} = \rho_{ayx} = \rho_a \qquad \ldots(2.6)$$

2.3.1 Rotation of Impedance Tensor

The rotation of impedance tensor $Z(\omega)$ and its elements $Z_{ix}(\omega)$ and $Z_{iy}(\omega)$ (i = x or y), given in equation 2.3, is carried out by rotating the co-ordinate axes. The set of rotated co-ordinate axes (x', y') may be obtained after clockwise rotation through an angle 'α' degree with respect to the set of measuring axes (x, y). The relationship of horizontal orthogonal electric and magnetic field components between

measuring axes (x, y) and rotated axes (x′, y′) is shown in Figure 2.4 by vector diagram. The rotation is performed to understand and deduce the azimuthal and some other important characteristics of the impedance tensor elements such as the assignment of principal directions, the visualization of the current density of the surveyed region, and the dimensionality of the subsurface. The relationship shown by vector diagram in Figure 2.4, can be written mathematically as (denoted by primes)

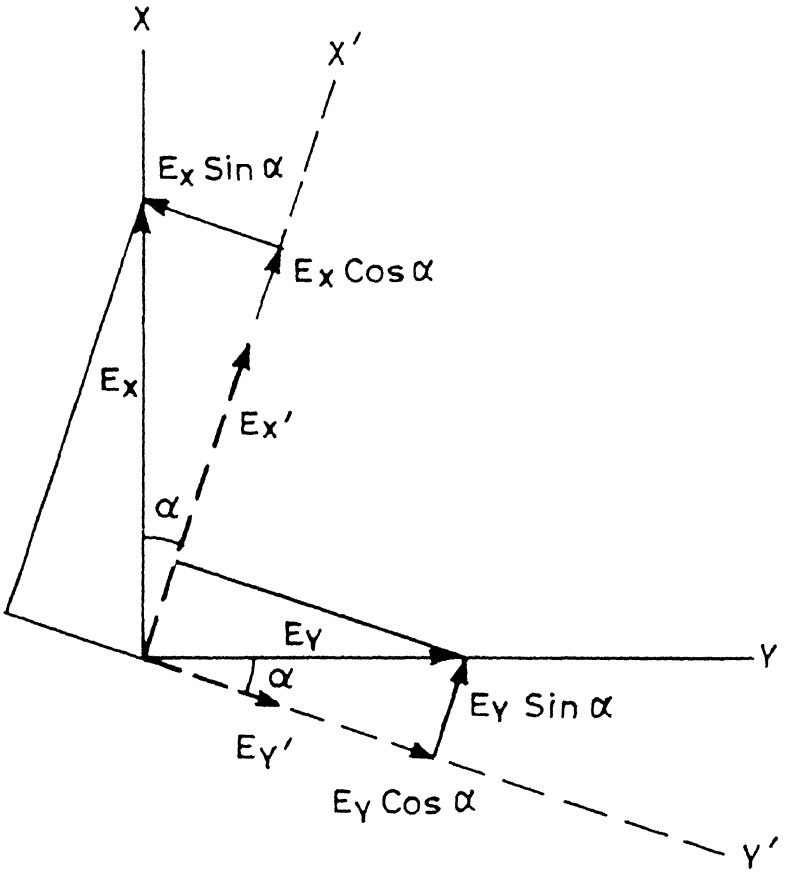

Figure 2.4 The relationship of horizontal orthogonal electric and magnetic field components between measuring axes (x, y) and rotated axes (x′, y′).

$$E' = A\,E \quad \text{and} \quad H' = A\,H, \quad \text{where } A = \begin{bmatrix} \cos\alpha & \sin\alpha \\ -\sin\alpha & \cos\alpha \end{bmatrix} \qquad \ldots(2.7)$$

For a transformation such that $E' = Z'\,H'$, the transformed

impedance tensor is written as

$$Z' = A\ Z\ A^{-1} = A\ Z\ A^{T} \qquad \ldots(2.8)$$

In expanded form, the general expressions for rotated impedance elements are

$$\left.\begin{aligned} Z_{x'x'} &= Z_{xx}\cos^2\alpha + (Z_{xy} + Z_{yx})\sin\alpha\cos\alpha + Z_{yy}\sin^2\alpha \\ Z_{x'y'} &= Z_{xy}\cos^2\alpha + (Z_{yy} - Z_{xx})\sin\alpha\cos\alpha - Z_{yx}\sin^2\alpha \\ Z_{y'x'} &= Z_{yx}\cos^2\alpha + (Z_{yy} - Z_{xx})\sin\alpha\cos\alpha - Z_{xy}\sin^2\alpha \\ Z_{y'y'} &= Z_{yy}\cos^2\alpha - (Z_{xy} + Z_{yx})\sin\alpha\cos\alpha + Z_{xx}\sin^2\alpha \end{aligned}\right] \qquad \ldots(2.9)$$

2.3.2 Properties of Impedance Iensor Elements

For one-dimensional Earth structure,

$$Z_{xx} = Z_{yy} = 0, \quad \text{and} \quad Z_{xy} + Z_{yx} = 0 \qquad \ldots(2.10)$$

For two-dimensional Earth structure,

$$Z_{xx} + Z_{yy} = 0, \quad \text{and} \quad Z_{xy} + Z_{yx} \neq 0 \qquad \ldots(2.11)$$

After rotation of the coordinate system to the strike of the structure

$$Z_{x'x'} = Z_{y'y'} = 0, \quad \text{and} \quad Z_{x'y'} + Z_{y'x'} \neq 0 \qquad \ldots(2.12)$$

For three-dimensional structure there are no such constraints. These properties are necessary but not sufficient. For example, three-dimensional structure exist even when $Z_{xx} = Z_{yy} = 0$ for all frequencies, but there are exceptions and from a practical point of view

the above criteria are also sufficient.

If an impedance tensor is measured over a two-dimensional resistivity Earth structure such that one of the measuring axes (x-axis) is parallel and another axis (y-axis) is perpendicular to the strike of the structure as shown in Figure 2.5, then rotated tensor elements away from its principal axes are determined by substituting $Z_{xx} = Z_{yy} = 0$ in equation 2.9, giving

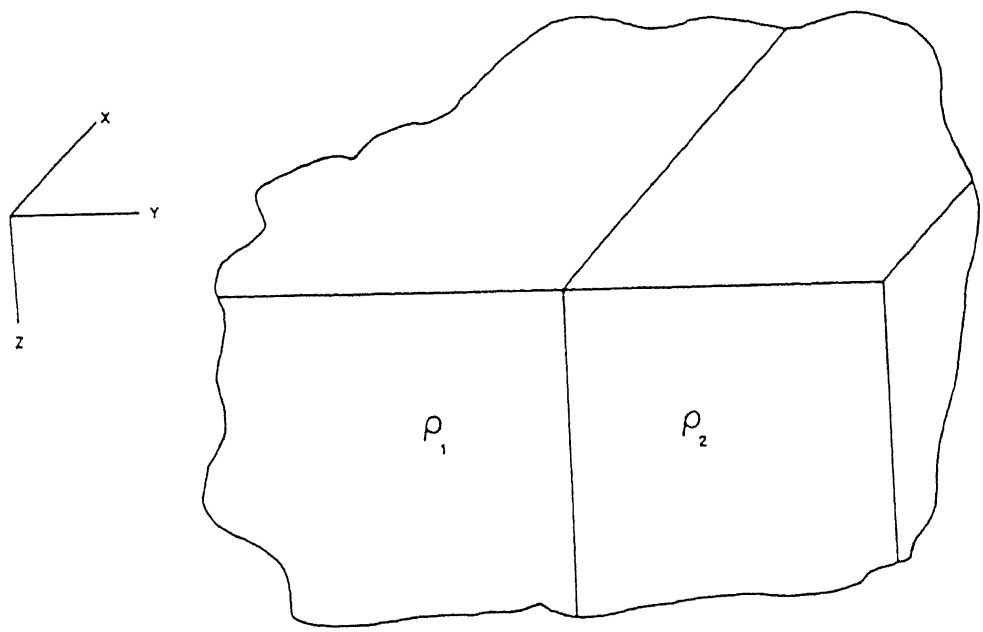

Figure 2.5 Cross-section of simple two-dimensional structure case. ρ_1 and ρ_2 extend to infinity to the left and right, respectively.

$$\left.\begin{aligned} Z_{x'x'} &= \frac{1}{2}(Z_{xy} + Z_{yx}) \sin 2\alpha \\ Z_{x'y'} &= Z_{xy} \cos^2\alpha - Z_{yx} \sin^2\alpha \\ Z_{y'x'} &= Z_{yx} \cos^2\alpha - Z_{xy} \sin^2\alpha \\ Z_{y'y'} &= -\frac{1}{2}(Z_{xy} + Z_{yx}) \sin 2\alpha \end{aligned}\right] \quad \ldots(2.13)$$

2.3.3 Polar Diagrams

A convenient way of representing the impedance tensor elements over two or three-dimensional Earth structure is by polar diagrams where the normalized absolute value and rotation angle 'α' are represented by the radial distance and azimuth, respectively. The normalization factor is $(\omega\ \mu_o)^{1/2}$. In the case of rotated $Z_{x'x'}$ and $Z_{y'y'}$, the absolute values are controlled by the function 'sin 2α', 'α' being the rotation angle which varies from 0 to 2π and the polar diagram shows four distinct lobes as shown by third row in Figure 2.6. The distinct four lobes have clover leaf-like symmetric shape at sites where two-dimensional effects are dominating. At sites where three-dimensional effects are severe, the symmetric four lobed figure degrades into a strongly asymmetric figure (Hermance, 1982) as shown by fourth row in Figure 2.6. The rotated

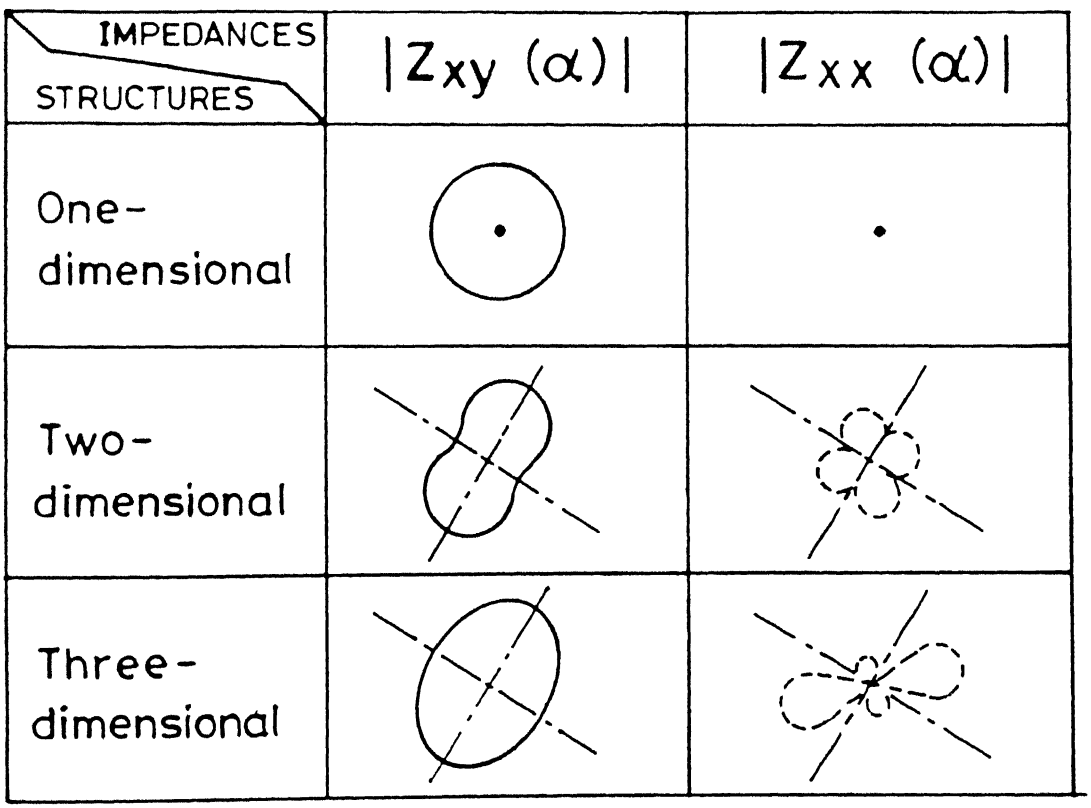

Figure 2.6 The polar diagrams for impedance tensor elements over one-, two- and three-dimensional Earth structure.

off-diagonal tensor elements $Z_{x'y'}$ and $Z_{y'x'}$ are controlled by a combination of '$\sin^2 2\alpha$' and '$\cos^2 2\alpha$' and produce a two-lobed polar diagram. In general, the polar diagrams are patterns with four asymmetric leaves, each of which repeats itself through an angle π. As follows from the equation 2.13, the polar diagrams for $Z_{y'x'}$ and $Z_{y'y'}$ are turned with respect to the polar diagrams for $Z_{x'y'}$ and $Z_{x'x'}$ by $\pi/2$.

The polar diagrams calculated from measured impedance tensor elements have been used by various workers as a criterion for two-dimensional resistivity structure (Berdichevsky et al., 1970). Swift (1967) has shown that the direction in which the diagonal elements are minimized, is either parallel or perpendicular to structural strike in a two-dimensional environment. Thus, a standard method of analysis is to rotate the tensor until the off-diagonal elements are maximized. The impedance tensor for this rotation, in the absence of noise, simplifies to impedance tensor containing only off-diagonal elements which are (i) equal in amplitude and opposite in sign over one-dimensional structure (ii) not equal over two-dimensional structure. However, impedance tensors over three-dimensional structure can still have four non-zero elements after rotation (Park, 1985). The apparent resistivities along the directions where off-diagonal elements are maximum and minimum at each frequency are called maximum and minimum apparent resistivities respectively.

2.3.4 Rotationally Invariant Impedances

The interpretation of magnetotelluric data in complex geologic environment, where field behaviour is complicated and one-dimensionality is not even partially met, is misleading. Wright (1970) and Reddy and Rankin (1972) suggested that one-dimensional use of E-polarization mode in a two-dimensional environment may give an accurate estimate of the structure, whereas, H-polarization mode can not be used owing to less sensitive to deeper structure. Park et al. (1983) and Wannamaker et al. (1984) showed that the E-polarization mode is also distorted in three-dimensional environment and that one-dimensional interpretation of either mode leads to severe errors. However, two-dimensional interpretation of H-polarization mode along the profiles far from the ends of three-dimensional bodies yield accurate structure (Wannamaker et al. 1984). The most difficult problem with three-dimensional environment is the identification of E- and H-polarization modes, which are coupled together. However, in two-dimensional environment both the modes are found decoupled (Swift, 1967). Park et al. (1983) and Wannamaker et al. (1984) showed that maximum and minimum apparent resistivities contain the effects of both E- and H-polarization modes and the separation of the modes is not possible. These results show that one-dimensional modelling is the most widely available interpretive tool, which is always erroneous. The two-dimensional modelling is useful only under certain circumstances and three-dimensional modelling is rare, expensive, slow, and the density of the measurements sites is normally too sparse to warrant a detailed three-dimensional modelling exercise.

Nevertheless, the interpretation and inversion of magnetotelluric data have almost always been done with one-dimensional or at the most with two-dimensional models. The efforts have been made to approximate the three-dimensional Earth by one-dimensional models for which there are well developed inversion schemes (Jupp and Vozoff, 1975; Parker, 1980; Fischer et al., 1981). Different forms of impedance tensors are used to carry out one-dimensional interpretation. The first method finds the rotation angle 'α' which maximizes the off-diagonal elements in some least square sense. This is done for all frequencies. The rotation angle 'α' is found to vary for different frequencies. It is often assumed that these directions (in terms of angle α's) define the E-polarization with an ambiguity of 90° and thus, for low frequencies the above procedure should lead to maximum or minimum apparent resistivity and corresponding phase that are relatively less distorted by near surface inhomogeneities and represent the one-dimensional Earth. The geology of the area provides an additional tool to separate E- and H-polarizations and hence the ambiguity of 90°. The results are correct if the defined rotations, at which off-diagonal elements are maximized, coincide with the strike of the overburden. However, unless the regional structure can be well approximated by a one-dimensional structure, there is no guarantee of such coincidence. The second method uses the rotations defined above as a function of frequencies to estimate an average strike, which is then kept constant for all frequencies to define the maximum or minimum apparent resistivity and corresponding phase used for formal one-dimensional interpretation or two-dimensional modelling (Zhang et al., 1987)

The third method was introduced by Berdichevsky and Dmitriev (1976a). They have proposed two rotationally invariant elements of the

impedance tensor using arithmetic mean of the off-diagonal elements and the square root of the determinant of 2 X 2 impedance tensor matrix (given by matrix equation 2.3). The arithmetic mean Z_{am} is

$$Z_{am} = 0.5\ (Z_{xy} - Z_{yx}) \qquad \ldots(2.14)$$

and the square root of the determinant Z_{Det} is

$$Z_{Det} = (Z_{xx}\ Z_{yy} - Z_{xy}\ Z_{yx})^{1/2} \qquad \ldots(2.15)$$

The geometric mean Z_{gm}, which has also been proposed (Kaufman and Keller, 1981)

$$Z_{gm} = (-Z_{xy}\ Z_{yx})^{1/2} \qquad \ldots(2.16)$$

The three invariant impedances given by equations 2.14 - 2.16 reduce to the same scalar impedance for one-dimensional structure. The invariant impedances given by equations 2.15 and 2.16 reduce to the same value when the structure is two-dimensional, but the arithmetic mean is still different. All three impedances are different if the structure is three-dimensional.

Ingham (1988) analyzed the utility of the arithmetic mean for interpreting the subsurface structure and hypothesized that the determinant form might be better because it accounts for all impedance tensor elements. Among others who have used the arithmetic mean are Ingham and Hutton (1982), Jones and Garland (1986), Green et al. (1987), and Park and Livelybrooks (1989). The determinant form of impedance (equation 2.15) have been used by Berdichevsky et al. (1980), Hutton et

al. (1987), Zhang et al. (1987, 1988) and Ranganayaki (1984). Ranganayaki using the determinant form of impedance showed a good internal consistency in the interpretation of large number of data sets from a sedimentary area. It was also shown that the phase of the determinant is not severely affected by near surface lateral inhomogeneities whereas, arithmetic mean form is affected. According to Berdichevsky and Dmitriev (1976a) the interpretation of magnetotelluric data based on determinant form generally give better results than interpretation based arithmetic mean form. The apparent resistivity and phase using determinant form are given as

$$\rho_{aDet} = \frac{|Z_{Det}(\omega)|^2}{\omega \mu_o} \qquad (2.17)$$

$$\phi_{Det} = \arg (Z_{Det}) - \Pi/2 \qquad (2.18)$$

2.4 Theoretical Transfer Functions for One-dimensional Earth

In frequency-domain, the electric and magnetic fields on the the surface of the Earth are derived from the governing Maxwell's equations in a source free medium, with appropriate boundary conditions. For one-dimensional Earth, there are only an x-component of electric field and a y-component of magnetic field, therefore fields can be denoted by $E(z, \omega)$ and $H(z, \omega)$, respectively, where z is depth axis pointing downward, with the origin located on the surface of the Earth. The transfer function (surface impedance) is obtained by taking ratio of electric to magnetic fields, for $z = 0$. Equation 2.2 describes this relationship, where $E(\omega)$ and $H(\omega)$ are the electric and magnetic fields on the Earth surface for one-dimensional Earth.

It is possible to derive theoretical expressions of the time-based

representation of transfer functions by using frequency-based transfer function (equation 2.2). The latter function is the one usually derived by solving the Maxwell's equations, as described above, and experimentally estimated from the measurements of electric and magnetic fields on the surface of the Earth at sites. The former are the response functions in time-domain and are characterized by step $R_s(t)$ and impulse $R_i(t)$ response functions, respectively. The step response function represents the response of the Earth to a step variation in magnetic field and the impulse response function represents the corresponding impulse response of the Earth and can be viewed as the time derivative of step response function. In order to find the theoretical expressions for time-based representation of transfer functions, the frequency-based transfer function given by equation 2.2 can be written as (Kunetz, 1972; Wieladek and Ernst, 1977; McMechan and Barrodale, 1985; Gomez-Trevino, 1987b; Yee et al. 1988)

$$E(\omega) = \underline{Z}(\omega)\ i\omega H(\omega) \qquad \ldots(2.19)$$

and

$$E(\omega) = Z(\omega)\ H(\omega) \qquad \ldots(2.20)$$

where $\underline{Z}(\omega) = Z(\omega)/i\omega$. The Inverse Fourier Transform of equations 2.19 and 2.20 leads to the following two convolutions (denoted by *)

$$E(t) = R_s(t) * \frac{dH(t)}{dt} \qquad \ldots(2.21)$$

and

$$E(t) = R_i(t) * H(t) \qquad \ldots(2.22)$$

where

$$R_s(t) = \frac{1}{2\pi} \int_0^{\infty} \underline{Z}(\omega)\ e^{i\omega t}\ d\omega \qquad \ldots(2.23)$$

and

$$R_i(t) = \frac{1}{2\pi} \int_0^{\infty} Z(\omega)\, e^{i\omega t}\, d\omega \qquad \ldots(2.24)$$

Equations 2.23 and 2.24 give the theoretical expressions for step and impulse response functions, respectively. Both the equations require series expansions of frequency-based transfer function $\underline{Z}(\omega)$ (in equation 2.23) and $Z(\omega)$ (in equation 2.24) for well adapted transformation into time-domain. In case, if Inverse Fourier Transform of these series expansion is not derivable, the time-based transfer functions are obtained numerically. For numerical solution, the $\underline{Z}(\omega)$ and $Z(\omega)$ are discretized and sampled at uniform interval Δ (using the sampling theorem) to give the discretized sampled vector sequences $\{\underline{Z}(m)\}$ and $\{Z(m)\}$ for $m = 0, 1, 2, 3, \ldots$. These discretized frequency-based functions are related to time-based step and impulse response sequences of matrices $\{R_s(n)\}$ and $\{R_i(n)\}$, respectively, by means of Discrete Fourier Transforms as following

$$R_s(n) = \frac{1}{2\pi} \sum_{m=0}^{\infty} \underline{Z}(m)\, e^{imn\Delta}; \quad n = 0, 1, 2, 3, \qquad \ldots(2.25)$$

$$R_i(n) = \frac{1}{2\pi} \sum_{m=0}^{\infty} Z(m)\, e^{imn\Delta}; \quad n = 0, 1, 2, 3, \qquad \ldots(2.26)$$

The number of terms appearing in summation, given in equations 2.25 and 2.26 are kept finite and are truncated after the first N terms. The value of N is a trade off between two conflicting requirements, namely; it should be sufficiently large to achieve a good approximation to $\underline{Z}(\omega)$ and $Z(\omega)$ and at the same instant it should be sufficiently small to meet the restrictions of a finite discretized sampled vector sequences $\{\underline{Z}(m)\}$ and $\{Z(m)\}$ consistent with computational practicality.

2.4.1 Two-layer Earth Model

Two-layer Earth model (shown in Figure 2.7) is characterized by resistivities ρ_1 and ρ_2 (or the conductivities σ_1 and σ_2) of first and second layers and thickness d_1 of first layer. Two-layer case is a particular case of multi-layer Earth model. The surface impedance as a recurrence relation for multi-layer Earth model is widely available in magnetotelluric related literature. The surface impedance recurrence relation for multi-layer Earth model

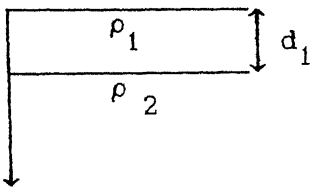

Figure 2.7 Sketch of a one-dimensional, two-layer Earth model.

and herein follows from Porstendorfer (1975) and Kaufman and Keller (1981).

i) Frequency-domain

For two-layer Earth model, the surface impedance $Z(\omega)$ is written as (Porstendorfer, 1975; Kaufman and Keller, 1981)

$$Z(\omega) = \frac{\gamma_1}{\sigma_1} \frac{1 + K_{12} \exp(-2\, d_1 \gamma_1)}{1 - K_{12} \exp(-2\, d_1 \gamma_1)} \qquad \ldots(2.27)$$

where $\gamma_1 = \left[i\omega\mu_o\sigma_1 \right]^{1/2}$ is the propagation constant in first layer. $K_{12} = (\sqrt{\sigma}_1 - \sqrt{\sigma}_2)/(\sqrt{\sigma}_1 + \sqrt{\sigma}_2)$ is the reflection coefficient at the interface between first layer and second layer.

ii) Time-domain

The theoretical expressions for step and impulse response functions for two-layer model follow from the Inverse Fourier Transform of series expansions of $\underline{Z}(\omega)$ $(=Z(\omega)/i\omega)$ and $Z(\omega)$, respectively. The series expansions of $\underline{Z}(\omega)$ and $Z(\omega)$ for two-layer case are written as

$$\underline{Z}(\omega) = \frac{\mu_o}{\gamma_1}\left[1 + 2\sum_{n=1}^{\infty} K_{12}^n \exp(-n\ 2d_1\gamma_1)\right] \qquad ...(2.28)$$

and

$$Z(\omega) = \frac{\gamma_1}{\sigma_1}\left[1 + 2\sum_{n=1}^{\infty} K_{12}^n \exp(-n\ 2d_1\gamma_1)\right] \qquad ...(2.29)$$

The step and impulse response functions obtained using Inverse Fourier Transform of series expansions $\underline{Z}(\omega)$ and $Z(\omega)$, given by equation 2.28 and 2.29, respectively, are written as (Gomez-Trevino 1987b; Kunetz 1972)

$$R_s(t) = \vartheta_1\left[1 + 2\sum_{n=1}^{\infty} K_{12}^n \exp(-2n^2\ \zeta_1^2)\right] \qquad ...(2.30)$$

and

$$R_i(t) = \frac{-\vartheta_1}{2t}\left[1 + 2\sum_{n=1}^{\infty} K_{12}^n\ (1-4n^2\ \zeta_1^2)\ \exp(-2n^2\ \zeta_1^2)\right] \qquad ...(2.31)$$

where $\vartheta_1 = \left[\frac{2}{\pi}\right]^{1/2} \frac{1}{\delta_{dd}\ \sigma_1}$, $\delta_{dd} = (2t/\mu_o\sigma_1)^{1/2}$ is the diffused depth in first layer at delay-time t, and $\zeta = d_1/\delta_{dd}$ is the ratio of first layer thickness to diffused depth.

2.4.2 Three-layer Earth Model

Three-layer Earth model (shown in Figure 2.8) is characterized by resistivities ρ_1, ρ_2, and ρ_3 (or the conductivities σ_1, σ_2 and σ_3) of first, second and third layers and thickness d_1 and d_2 of first and second layers. Three-layer case is also a particular case of multi-layer Earth model.

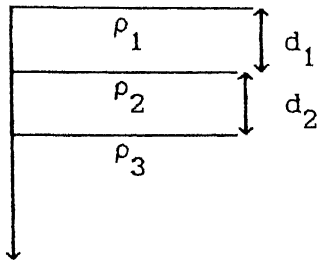

Figure 2.8 Sketch of a one-dimensional, three-layer Earth. model.

i) Frequency-domain

The surface impedance on the Earth surface for three-layer in frequency-domain is written as (Porstendorfer, 1975; Kaufman and Keller, 1981)

$$Z(\omega) = \frac{\gamma_1}{\sigma_1} \frac{1 + R_1 \exp(-2 d_1 \gamma_1)}{1 - R_1 \exp(-2 d_1 \gamma_1)} \qquad \ldots(2.32)$$

where $R_1 = [K_{12} + K_{23} \exp(-2\gamma_2 d_2)] / [1 + K_{12}K_{23} \exp(-2\gamma_2 d_2)]$, $\gamma_j = [i\omega\mu_o\sigma_j]^{1/2}$; $j = 1, 2$ is the propagation constant in jth layer, and $K_{j(j+1)} = [\sqrt{\sigma_j} - \sqrt{\sigma_{j+1}}] / [\sqrt{\sigma_j} + \sqrt{\sigma_{j+1}}]$ is the reflection coefficient between jth and (j+1)th layer.

ii) Time-domain

The series expansions of $\underline{Z}(\omega)$ ($=Z(\omega)/i\omega$) and $Z(\omega)$ are written as

$$\underline{Z}(\omega) = \frac{\mu_o}{\gamma_1}\left[1 + 2\sum_{n=1}^{\infty} K_{12}^n X_1^n \sum_{r=o}^{n} C_1(n,r)\, X_2^r \sum_{s=o}^{\infty} C_2(-n,s)\, X_3^s\right] \qquad ...(2.33)$$

and

$$Z(\omega) = \frac{\gamma_1}{\sigma_1}\left[1 + 2\sum_{n=1}^{\infty} K_{12}^n X_1^n \sum_{r=o}^{n} C_1(n,r)\, X_2^r \sum_{s=o}^{\infty} C_2(-n,s)\, X_2^s\right] \qquad ...(2.34)$$

where $C_1(n,r) = {}^nC_r \left[\frac{K_{23}}{K_{12}}\right]^r$; $C_2(-n,s) = {}^{-n}C_s \left[K_{12}K_{23}\right]^s$;

$X_1 = \exp(-2\gamma_1 d_1)$ and $X_2 = \exp(-2\gamma_2 d_2)$.

The theoretical expressions for step and impulse response functions for three-layer model are obtained by taking the Inverse Fourier Transform of series expansions of $\underline{Z}(\omega)$ and $Z(\omega)$, and are given as (only final forms are given)

$$R_s(t) = \vartheta_1\left[1 + 2\sum_{n=1}^{\infty} K_{12}^n \sum_{r=o}^{n} \sum_{s=o}^{\infty} C_1(n,r)\, C_2(-n,s)\, e^{-\beta/4t}\right] \qquad ...(2.35)$$

and

$$R_i(t) = \frac{-\vartheta_1}{2t}\left[1 + 2\sum_{n=1}^{\infty} K_{12}^n \sum_{r=o}^{\infty} \sum_{s=o}^{\infty} C_1(n,r)\, C_2(-n,s)\left(1-\frac{\beta}{4t}\right) e^{-\beta/4t}\right] \qquad ...(2.36)$$

where $C_1(n,r) = {}^nC_r \left[\frac{K_{23}}{K_{12}}\right]^r$; $C_2(-n,s) = {}^{-n}C_s \left[K_{12}K_{23}\right]^s$;

$\beta^{1/2} = 2\left[nd_1\sqrt{\mu_o\sigma_1} + (r+s)\, d_2\sqrt{\mu_o\sigma_2}\right]$ and $\vartheta_1 = \left[\frac{2}{\pi}\right]^{1/2} \frac{1}{\delta_{dd}\,\sigma_1}$

2.4.3 Exponentially Varying Vertical Conductivity Profiles

The variation of electrical resistivity for one-dimensional vertically inhomogeneous Earth where conductivity changes continuously with depth has been studied by many workers. Mallick and Roy (1968), Patella (1977), Koefoed (1979), Mallick and Jain (1979) and Banerjee et al. (1980) studied electrical resistivity sounding using Earth models with a transition layer. For magnetotelluric sounding, Mallick (1970), Abramovici (1974), Kao and Rankin (1980), and Kao (1981) studied Earth models of conductivity varying linearly with depth. Kao (1982) studied Earth models of conductivity varying exponentially within a transition layer.

2.4.3.1 Exponentially Increasing Vertical Conductivity Profile

i) Frequency-domain

The electromagnetic wave equation for one-dimensional vertical conductivity profile is written as

$$\frac{d^2E(z,\omega)}{dz^2} - i\omega\mu_o\sigma(z)\,E(z,\omega) = 0 \qquad \ldots(2.37)$$

and

$$H(z,\omega) = -\frac{1}{i\omega\mu_o}\frac{dE(z,\omega)}{dz} \qquad \ldots(2.38)$$

The exponentially increasing conductivity Earth model is defined as

$$\sigma(z) = \sigma_o\, e^{pz} \qquad \ldots(2.39)$$

where σ_o is the conductivity on the Earth's surface ($z = 0$), p is real positive number and is responsible for slow or fast increases

conductivity inside the Earth. On introducing the variable y such that

$$y^2 = \frac{4}{p^2}\omega\mu_o\sigma_o e^{pz} \qquad \ldots(2.40)$$

and differentiating the resulting equation with respect to z, one obtains

$$2y\frac{dy}{dz} = \frac{4}{p^2}\omega\mu_o\sigma_o . pe^{pz} = py^2$$

which further reduces to

$$\frac{dy}{dz} = \frac{p}{2}y \qquad \ldots(2.41)$$

The first and second derivative of electric field with respect to depth can be written as

$$\frac{dE}{dz} = \frac{dE}{dy}\frac{dy}{dz} = \frac{p}{2}y\frac{dE}{dy} \qquad \ldots(2.42)$$

and

$$\frac{d^2E}{dz^2} = \frac{p}{2}\left[y\frac{d^2E}{dy^2}\frac{dy}{dz} + \frac{dy}{dz}\frac{dE}{dy}\right]$$

$$= \left(\frac{p}{2}\right)^2 y\left[y\frac{d^2E}{dy^2} + \frac{dE}{dy}\right] \qquad \ldots(2.43)$$

From equations 2.37 and 2.38, the governing differential electromagnetic wave is written as

$$\frac{d^2E(z,\omega)}{dy^2} + \frac{1}{y}\frac{dE(z,\omega)}{dy} - iE(z,\omega) = 0 \qquad \ldots(2.44)$$

The solution of the above modified Bessel's equation of zero order is given by (Abramowitz and Stegun, 1964).

$$E(z,\omega) = A\, I_o(y\sqrt{i}) + B\, K_o(y\sqrt{i}) \qquad \ldots(2.45)$$

where I_o and K_o are zeroth order modified Bessel functions of first and second kind, respectively. As a valid assumption, the electric field E must not increase indefinitely as depth z increases. Therefore, solution $I_o(y\sqrt{i})$ is no longer valid deep inside the Earth (As $z \longrightarrow \infty$, so the $y \longrightarrow \infty$ which implies $I_o(y\sqrt{i}) \longrightarrow \infty$). Under this condition

$$E(z,\omega) = B\, K_o(y\sqrt{i}) \qquad \ldots(2.46)$$

The magnetic field is linked with electric field through equation 2.38 which can be written as

$$H(z,\omega) = \frac{-B}{i\omega\mu_o}\frac{\partial\{K_o(y\sqrt{i})\}}{\partial z}$$

$$= \frac{-B}{i\omega\mu_o}\,\frac{\partial\{K_o(y\sqrt{i})\}}{\partial(y\sqrt{i})}\,\frac{\partial(y\sqrt{i})}{\partial z}$$

$$= \frac{-B}{i\omega\mu_o}\left\{-K_1(y\sqrt{i})\right\}\left\{\sqrt{i\omega\,\mu_o\sigma_o}\,e^{pz}\right\}$$

$$= \frac{-B}{i\omega\mu_o}K_1(y\sqrt{i})\,\gamma_o\,e^{pz/2}$$

and finally is written as

$$H(z,\omega) = \frac{B\gamma_o e^{pz/2}}{i\omega\mu_o}\,K_1(y\sqrt{i}) \qquad \ldots(2.47)$$

where $\gamma_o = (i\omega\,\mu_o\sigma_o)^{1/2}$ is propagation constant on the Earth surface (z = 0) and K_1 is first order modified Bessel function of second kird. From equation 2.45 and 2.46, it is easy to write the impedance on the surface

of the Earth (surface impedance) as

$$Z(\omega) = \frac{E(\omega)}{H(\omega)} = \left. \frac{K_o(y\sqrt{i})}{\gamma_o e^{pz/2} \frac{K_1(y\sqrt{i})}{i\omega\mu_o}} \right|_{z = 0}$$

or

$$Z(\omega) = \frac{i\omega\mu_o}{\gamma_o} \frac{K_o(x\sqrt{i})}{K_1(x\sqrt{i})} \qquad \ldots(2.48)$$

where $x = \frac{2}{p} (\omega \mu_o \sigma_o)^{1/2}$. The modified Bessel functions K_o and K_1 are not as easy to compute as are the Thomson (Kelvin) functions. Therefore, representation of surface impedance in terms of Thomson functions is computationally easy and efficient. The following relationship holds between modified Bessel functions and Thomson functions (Abramowitz and Stegun, 1964).

$$e^{-n\pi i/2} K_n(x\sqrt{i}) = Ker_n(x) + i\, Kei_n(x) \qquad \ldots(2.49)$$

where n is the order of the respective function. $Ker_n(x)$ and $Kei_n(x)$ are called as nth order Thomson functions corresponding to nth order modified Bessel function of the second kind. Using equations 2.48 and 2.49, the surface impedance can be written as

$$Z(\omega) = \frac{i\omega\mu_o}{\gamma_o} \frac{(Ker_o(x) + i\, Kei_o(x)}{(Kei_1(x) - i\, Ker_1(x)} \qquad \ldots(2.50)$$

ii) Time-domain

The series expansions of $\underline{Z}(\omega)$ and $Z(\omega)$ is not easily derivable in the present case. The numerical solution for step and response functions is carried out using equations 2.25 and 2.26, respectively.

2.4.3.2 Exponentially Decreasing Vertical Conductivity Profile

i) Frequency-domain

The model for exponentially decreasing conductivity profile is described as

$$\sigma(z) = \sigma_o e^{-pz} \qquad \ldots(2.51)$$

The introduction of variable $y^2 = \frac{4}{p^2} \omega\mu_o\sigma_o e^{-pz}$, transforms the governing differential electromagnetic wave equations, given by 2.37 and 2.38, into a form known as modified Bessel's equation of zero order.

$$\frac{dy}{dz} = -\frac{p}{2} y \qquad \ldots(2.52)$$

$$\frac{dE}{dz} = -\frac{p}{2} y \frac{dE}{dy} \qquad \ldots(2.53)$$

and

$$\frac{d^2E}{dz^2} = -(\frac{p}{2})^2 y \left[y \frac{d^2E}{dy^2} + \frac{dE}{dy} \right] \qquad \ldots(2.54)$$

From equation 2.37 and 2.54, the following zeroth order modified Bessel's equation is obtained

$$\frac{d^2E}{dz^2} + \frac{1}{y} \frac{dE}{dy} - iE = 0 \qquad \ldots(2.55)$$

which renders the solution of the form

$$E(z,\omega) = AI_o(y\sqrt{i}) + B K_o(y\sqrt{i}) \qquad \ldots(2.56)$$

The second term $K_o(y\sqrt{i})$ is no longer valid deep inside the Earth as $z \longrightarrow \infty$, $y \longrightarrow 0$ and hence $K_o(y\sqrt{i}) \longrightarrow \infty$. Thus,

$$E(z,\omega) = AI_o\,(y\sqrt{i}) \qquad \ldots(2.57)$$

The corresponding horizontal magnetic field component perpendicular to horizontal electric field component is obtained by differentiating the later with respect to depth 'z' and substituting it into equation 2.38. Therefore,

$$H(z,\omega) = \frac{-A}{i\omega\mu_o}\frac{\partial}{\partial z}\{\, I_o(y\sqrt{i})\}$$

$$= -\frac{A}{i\omega\mu_o}\left[\frac{\partial\{I_o(y\sqrt{i})\}}{\partial(y\sqrt{i})}\;\frac{\partial(y\sqrt{i})}{\partial z}\right]$$

$$= -\frac{A}{i\omega\mu_o}\left\{\, I_1(y\sqrt{i})\right\}\left\{-\sqrt{i}\,\frac{p}{2}\,y\right\}$$

$$= -\frac{A}{i\omega\mu_o}\left\{\, I_1(y\sqrt{i})\right\}\left\{-\sqrt{i\omega\,\mu_o\sigma_o e^{-pz}}\right\}$$

$$= -\frac{A}{i\omega\mu_o}\; I_1(y\sqrt{i})\;\gamma_o\; e^{-pz/2}$$

Finally,

$$H(z,\omega) = \frac{A\,\gamma_o\; e^{-pz/2}}{i\omega\;\mu_o}\; I_1(y\sqrt{i}) \qquad \ldots(2.58)$$

where $I_1(y\sqrt{i})$ is the first order modified Bessel function of first kind. From equation 2.56 and 2.57, the surface impedance is written as

$$Z(\omega) = \left.\frac{I_1(y\sqrt{i})}{\dfrac{\gamma_o\; e^{-pz/2}}{i\omega\;\mu_o}\; I_1(y\sqrt{i})}\right|_{z\,=\,0}$$

or

$$Z(\omega) = \frac{i\omega \mu_o}{\gamma_o} \frac{I_o(x\sqrt{i})}{I_1(x\sqrt{i})} \qquad \ldots(2.59)$$

where $x = \frac{2}{p}\sqrt{\omega \mu_o \sigma_o}$. The Bessel functions in the form of Thomson's functions lead the computation more efficiently than the present form. The following relationship relates the modified Bessel function of first kind to Thomson functions (Abramowitz and Stegun, 1964).

$$e^{n\pi i/2} I_n(x\sqrt{i}) = ber_n(x) + ibei_n(x) \qquad \ldots(2.60)$$

where n is the order of the respective functions. $Ber_n(x)$ and $Bei_n(x)$ are known as nth order Thomson functions corresponding to nth order modified Bessel functions of Ist kind. From equation 2.59 and 2.60, one may write

$$Z(\omega) = \frac{i\omega \mu_o}{\gamma_o} \left[\frac{ber_o(x) + i\, bei_o(x)}{bei_1(x) - i\, ber_1(x)} \right] \qquad \ldots(2.61)$$

ii) Time-domain

The series expansion of $\underline{Z}(\omega)$ and $Z(\omega)$ is not easily derivable in present case. The numerical solution for step and response functions, following the approach mentioned through the equations 2.25 and 2.26 is carried out.

2.5 Conclusions

The derivation of analytical expressions for step and impulse response functions in time-domain, following the Inverse Fourier Transform of the series expansions of $\underline{Z}(\omega)$ and $Z(\omega)$, especially for three-layer model is significant and is extremely useful in the analysis

and interpretation of magnetotelluric data in time domain. The importance of transfer functions (step and impulse) lies in the basic nature of their capability in producing forward functional response for any three-layer Earth models. The form of expression for step response function, which was derived by Kunetz (1972) by using methods of images, has an constraint according to which the product of layer conductivity with the square of the layer thickness should be constant in each layer. Though this condition has always been satisfied by subdividing the layers into elementary layers (integers only), but there have been some models for which integer subdivision is not possible and thus, one can not compute the forward model function. The form of expression derived in this Chapter has no such constraint for three-layer Earth models. However, the computation of the summation of series takes significant computational time but still it is quite accurate.

The main interpretive parameters for the magnetotelluric method are transfer functions i.e. surface impedance in frequency-domain, step and impulse response functions in time-domain. From these, many other directly measurable parameters can be extracted to facilitate interpretation and provide clear insight into the subsurface. The most common parameters are apparent resistivity or conductivity, depth of investigation (both in frequency and time-domains); rotation of impedance tensor to estimate regional principal directions and dimensionality check of the subsurface through polar diagrams, rotationally invariant impedance (in frequency-domain only). The development of this Chapter is an adequate foundation for further developments and applications in the subsequent Chapters of this thesis.

CHAPTER III

VARIOUS DEFINITIONS OF MAGNETOTELLURIC APPARENT RESISTIVITY

3.1 General

The panorama of application of magnetotelluric method in exploration geophysics started in Russia by Tikhonov (1950) and in France by Cagniard (1953). As mentioned in Chapter II, the source of energy is the naturally occurring electromagnetic plane waves, incident normal to the Earth's surface. The pair of horizontal orthogonal components of the electric and magnetic fields are measured at a chosen sequence of points on the Earth surface. The surface impedance is the response of the Earth to continuously and harmonically varying magnetic field derived from a plane electromagnetic wave propagating vertically into the Earth and is estimated for broad-band frequency spectrum at each site as the ratio of electric to magnetic field components. The magnetotelluric problem lies in estimation of surface impedance $Z(\omega)$ and to decipher the spatial variations of subsurface resistivity using parametric dependence of the $Z(\omega)$ values upon the frequency used.

The magnetotelluric method is an extension of the geoelectrical methods which information about the frequency dependent complex electrical resistivity of the subsurface. It is well known that the electrical and electromagnetic methods do not conform very well with the response of the lumped circuit elements such as resistance, inductance and capacitance. The inhomogeneities and stratification inside the Earth have been found to give varying response for broad-band frequency spectrum and differently polarized incident electromagnetic waves.

Because of the low frequency application of electromagnetic waves, the overall response of the Earth subsurface to magnetotelluric signals encompasses relatively much larger depths and is found to change significantly depending upon the changes in the resistivity of subsurface and the changes in the frequency of the signal used.

3.2 Apparent Resistivity as Viewed and Used

The concept of apparent resistivity follows from the most general and conventional paradigm of electrical geophysical exploration set up by Schlumberger in the years nineteen twenties. Since then it is being used generally in electrical and electromagnetic methods, particularly in resistivity and for deducing different parameters of the stratified Earth. It has made claim to be a paragon for providing complete signature of conducting Earth. The term 'apparent resistivity' is very vital towards proper understanding of the subtle changes in subsurface formations and for carrying out the analysis of experimentally procured data using standard interpretive techniques. The understanding of variations in apparent resistivity with the period accelerates the modus operandi of interpretations into geologically meaningful ones. The characteristic behaviour arises primarily from the layered subsurface parameters, and at times is associated with characteristic oscillations and undulations. This has been discussed as 'paradoxes' (Satpathy, 1974) arising from interference effects (Morrison et al., 1969). The use and misuse of the term apparent resistivity in geophysical exploration have been discussed by Spies and Eggers (1986) and this has been working as an important guideline as well as caution for exploration scientists.

The apparent resistivity is simply the resistivity of a homogeneous Earth that would give the same magnitude for equivalent resistivity of

inhomogeneous Earth. Thus, it characterizes differences in the Earth response caused by departures in the homogeneous half-space from the condition of uniform resistivity. These departures may be caused either by the existence of horizontal stratification or lateral inhomogeneities in the half-space. The apparent resistivity is a formal rather artificial concept and should not be treated as an exact representative of true resistivity of the Earth. This is evident from the fact that the shape of apparent resistivity curve bears little relationship with the subsurface resistivity distribution. For a proper assessment of this quantity, one should always consider the interaction of signal wavelength to inhomogeneous medium of comparable dimensions with which it has been influenced. Incomparable sizes of the inhomogeneities with the signal wavelengths give rise to typical magnitude and shape of apparent resistivity which is very different from the expected values of apparent resistivity.

Berdichevsky and Dmitriev (1976b) have shown that for one-dimensional Earth, the apparent resistivity is a weighted average resistivity of subsurface layers. The weights have been the difference of square of magnetic fields between upper and lower boundaries of the layers normalized by the square of the magnetic field on Earth's surface. Stronger the magnetic field absorption within an inhomogeneity, lower is the weight of the inhomogeneity. Gomez-Trevino (1987a) also have shown that the apparent resistivity is a weighted average of spatial distribution of resistivity of the Earth's subsurface. The weights have been the generalized derivatives of apparent resistivity with respect to spatial distribution of resistivity of the Earth's subsurface.

The practitioners of magnetotelluric method, often, have stressed

more on the quantitative interpretation of apparent resistivity than the qualitative interpretation. However, quantitative subsurface information is intractable without complete knowledge of apparent resistivity and its behaviour under subtle changes in subsurface geology. Thus, its study and behaviour for various Earth models avoids the rigmaroles associated with quantitative interpretation.

3.3 Definitions of Apparent Resistivities

i) Frequency-domain

In magnetotelluric method, the change in behaviour of apparent resistivity with frequency or period gives characteristic features which are used to deduce the physical parameters of the layered Earth's subsurface. Cagniard (1953) first time defined the apparent resistivity in the frequency-domain, as

$$\rho_a = \frac{1}{\omega \mu_0} |Z|^2 \qquad \ldots(3.1)$$

where $\omega = 2\pi f$, f is frequency, $\mu_0 = 4\pi \times 10^{-7}$ Henry m^{-1} for most of geological materials and Z is the surface impedance of the stratified Earth.

In discussing alternatives to the basic definition of the apparent resistivity, Spies and Eggers (1986) pointed out that the apparent resistivity is merely a normalizing procedure with little physical significance. Using the real and imaginary parts of the surface impedance, they further defined independent pairs of apparent resistivities as

$$\rho_a = \frac{2}{\omega \mu_0} [\text{Real } (Z)]^2 \qquad \ldots(3.2)$$

and

$$\rho_a = \frac{2}{\omega \mu_o}[\text{Im } (Z)]^2 \qquad \ldots(3.3)$$

Further definitions are given in terms of real, imaginary and absolute values of the square of the impedance, i.e.

$$\rho_a = \frac{1}{\omega \mu_o}[\text{Im } (Z^2)] \qquad \ldots(3.4)$$

$$\rho_a = \frac{1}{\omega \mu_o} |Z^2| \qquad \ldots(3.5)$$

and

$$\rho_a = \frac{2}{\omega \mu_o} [\text{Real } (Z^2)] \qquad \ldots(3.6)$$

Definitions (3.1) and (3.5) are the same (Spies and Eggers, 1988). Definitions (3.1) - (3.4) are valid only in the sense that they yield the true resistivity in the case of a homogeneous half-space Earth model (Spies and Eggers, 1986). The definition (3.6), which uses the real part of the square of impedance, is not valid in the case of a homogeneous Earth model.

Using the above definitions, Spies and Eggers (1986) have shown the variation of the normalized apparent resistivity with the normalized wave frequency for three-layer models. The apparent resistivity have been computed for different models, and it is found that none of the four valid definitions given above show the characteristic features of a given subsurface contrast over the entire frequency range. Only one or two of the four valid definitions show the significant characteristic features for a given subsurface model. In this frequency range, the responses of all the definitions are better delineated and may be

and

$$\rho_a = \frac{4\pi\, t^3}{\mu_o} R_i^2(t) \qquad \ldots(3.8)$$

where t is the delay-time, $R_s(t)$ and $R_i(t)$ are the step and impulse response functions, respectively. The definitions of apparent resistivities using equations (3.1) - (3.6) and (3.7) - (3.8), respectively, in frequency and time-domains have been termed as D1, D2, D3, D4, D5, D6, D7 and D8, respectively, for convenience of their subsequent use.

3.4 Results and Discussion

The apparent resistivity curves in frequency and time-domains provide useful and equivalent information about the subsurface resistivity distribution. For various reasons, this equivalence is not fully realized. The fundamental difference lies in the use of the transfer function in deriving individual definition of apparent resistivity. The transfer function between continuously and harmonically varying magnetic field and electric field, in frequency-domain, is the surface impedance; the real, imaginary and absolute values of it or of its square have been used to define various definitions. On the other hand, transfer functions between magnetic field varying in steps or impulses (with respect to time) and electric field are step and impulse responses, respectively in time-domain, which have been used to define apparent resistivity, correspondingly.

Each of the apparent resistivity definitions defined in frequency and time-domains behave characteristically. In some aspects, these definitions are similar in behaviour and in some aspects are dissimilar for a given layer parameters. The characteristic behaviour in

frequency-domain is shown by definitions D2 and D3. The apparent resistivities in both the domains differ in the way of their approach to the resistivity of the successive horizons and in the way of their transition which takes place in terms of period/delay-time required to scan the vertical resistivity profile from Earth surface resistivity to the resistivity of deepest horizon.

The salient features of apparent resistivity definitions D1, D2, D3, and D4 in frequency-domain; and D7 and D8 in time-domain for various Earth models have been computed and illustrated graphically. The various Earth models allow the comparison of sounding curves in frequency-domain with those in time-domain. The variations in apparent resistivity using these definitions are shown as a function of varying periods (in frequency-domain) or delay-times (in time-domain) of magnetotelluric signal. In three-layered models, one may encounter with four different types of models depending upon the resistivity contrast of the layers. These models can be represented as K-, H-, Q- and A-type models. The details of apparent resistivity curves using various definitions over these models are discussed in the following sections.

3.4.1 K-type Models ($\rho_1 < \rho_2 > \rho_3$)

i) Frequency-domain

The apparent resistivity given by definitions D1 - D4 is illustrated in Figure 3.1 for K-type models. The behaviour of apparent resistivity curves for D1, D2 and D4 are almost the same; only the curve for D3 shows a minimum in the range of lower periods. The apparent resistivity variations shown using definitions D1 - D4 together show the formation of two loops with a crossover point. The crossover points and the size of the loop vary with the model parameters. The apparent

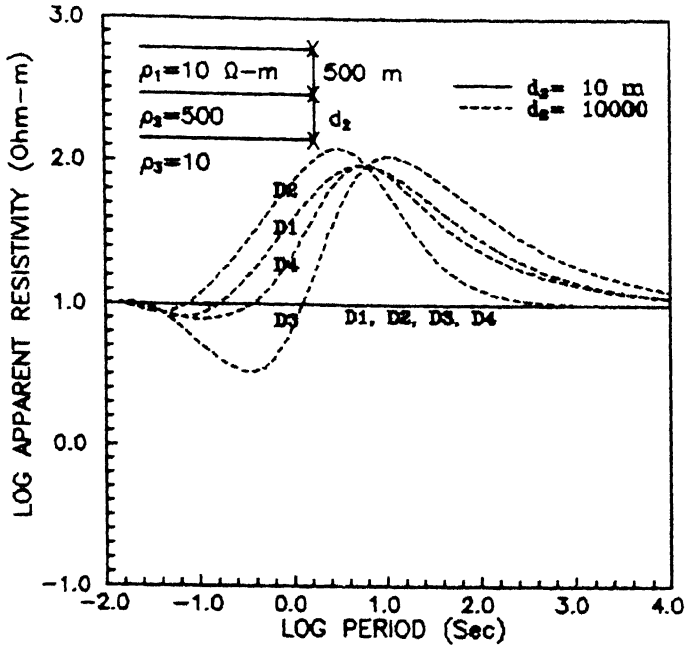

Figure 3.1 Variation of apparent resistivity curves obtained by various definitions with period, for K-type models.

resistivity curves (first loop) show an increase in value with increase in period, whereas the apparent resistivity shown by curves for D1 - D4 (second loop) show a decreasing trend until they attain a constant resistivity value for the bottom layer. The size of the loop depends on the resistivity contrast of the three-layered models. The curves for D1 - D4 show an almost constant value for a very small value of d_2 = 10 m (see Figure 3.1). It is very clear from the illustrations that the analysis of apparent resistivity variations using definitions D1 - D4 together can give qualitative information about the existing subsurface model.

In Figure 3.2, comparison has been made for the apparent resistivity behaviour using definition D3 and the conventional definition D1, for a three-layer K-type Earth model in which the

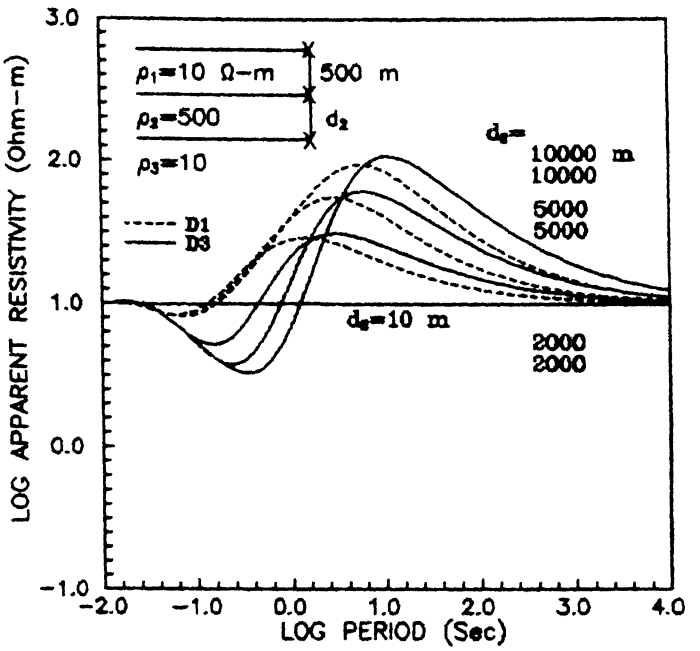

Figure 3.2 Variation of apparent resistivity curves obtained by definitions D1 and D3 for K-type models with period, for various values of d_2.

thickness of the intermediate layer varies. The effect of the change in thickness of the intermediate layer is sharply distinguishable in the lower period on the curves for D3 compared with those obtained using the other definitions, especially the conventional definition D1 (Figure 3.2).

ii) Time-domain

The apparent resistivity curves for definitions D7 and D8 corresponding to step and impulse responses, respectively, are shown in Figure 3.3. The behaviour of apparent resistivity curves, for both D7 D8, is almost same at longer (more than 800 msec) delay-times. The significant difference in their apparent resistivity curves is observed in the delay-time interval 1 - 200 msec. The apparent resistivity shown

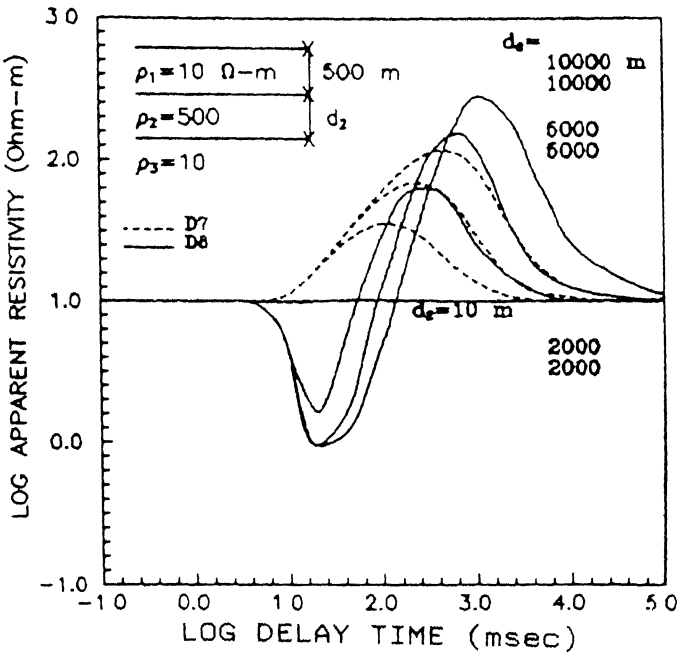

Figure 3.3 Variation of apparent resistivity curves obtained by definitions D7 and D8 for K-type models with delay-time, for various values of d_2.

for definition D8 shows undershoot before transition to second layer whereas D7 shows smooth transition. The apparent resistivity curves using definition D7 and D8 show increase in apparent resistivity corresponding to their middle segments with the increase of thickness of the intermediate layer. The apparent resistivity after attaining maximum value decreases until the value of last layer resistivity is obtained.

The undershoot observed in the apparent resistivity curve (D8) increases with the increase of thickness of intermediate layer. For sufficiently high thickness of intermediate layer 10000 m, the maximum amplitude of apparent resistivity approaches to true resistivity of this layer. The apparent resistivity curves show a constant value for a very small value of d_2 = 10 m for both D7 and D8. It shows that a very

thin resistive layer in the homogeneous half space does not show any subtle effect on apparent resistivity.

3.4.2 H-type Models ($\rho_1 > \rho_2 < \rho_3$)

i) Frequency-domain

The apparent resistivity variation for H-type models are shown in Figures 3.4 - 3.6. The apparent resistivity curves for D1 and D4 show very similar behaviour. The variations in the curves for D2 and D3 differ from those in the curves for D1 and D4. The resistivity and thickness contrast of the models affect the contrast of apparent resistivity curves for D1 - D4. The strong contrast of apparent resistivity corresponds to strong contrast resistivity of models, as shown in Figure 3.4 for resistivity values (ρ_1 = 50, ρ_2 = 2.0, ρ_3 =

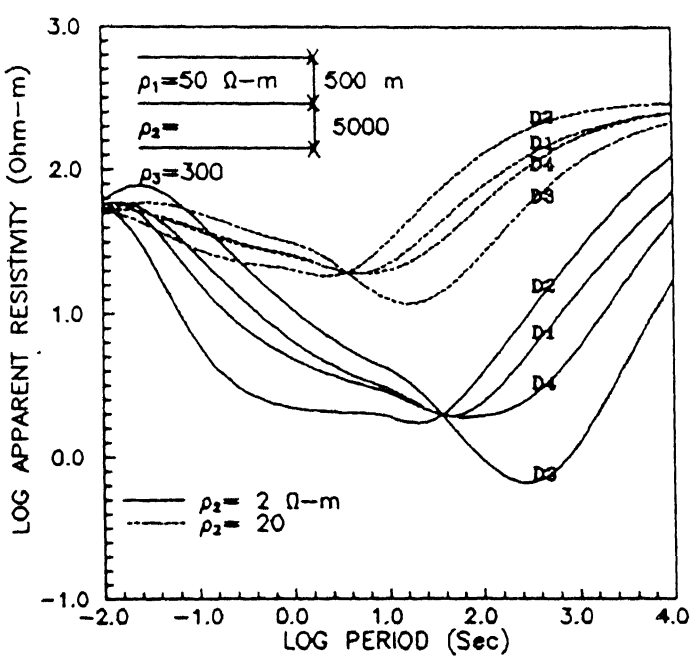

Figure 3.4 Variation of apparent resistivity curves obtained by various definitions for H-type models with period for two values of intermediate layer resistivity (2.0 and 20.0 Ω-m).

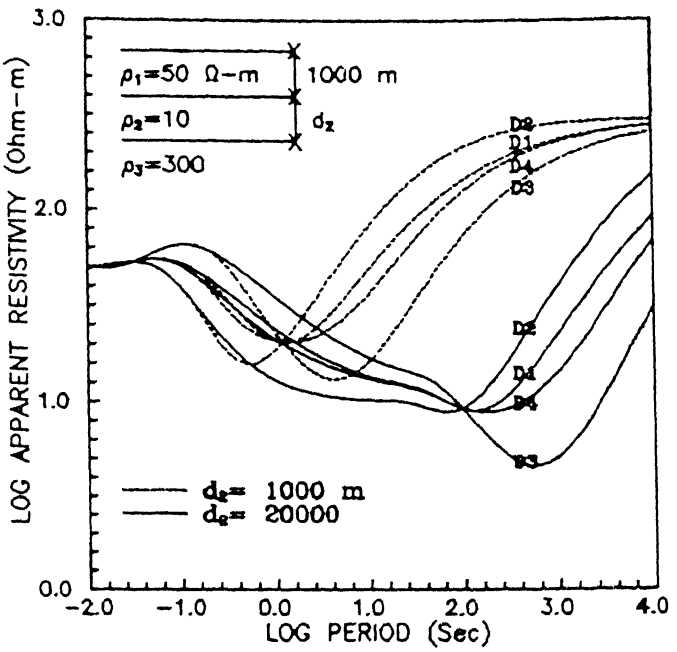

Figure 3.5 Variation of apparent resistivity curves obtained by various definitions for H-type models with period for two values of d_2 (1 and 20 km).

300.0 Ω-m) and(ρ_1 = 50, ρ_2 = 20.0, ρ_3 = 300 Ω-m). The change of layers thickness d_1 and d_2 yields similar apparent resistivity curves except shift of the branch point (Figures 3.4 and 3.5).

As shown in Figure 3.6, in the case of thin intermediate layer, apparent resistivity curves for D3 show a distinct difference from those for D1, D2 and D4 in entire range of periods whereas, in the case of a thick intermediate layer, the curve for D2 shows a distinct difference in the higher period. In the lower periods, the curve for D3 shows distinct differences from the other curves for greater thickness of the intermediate layer.

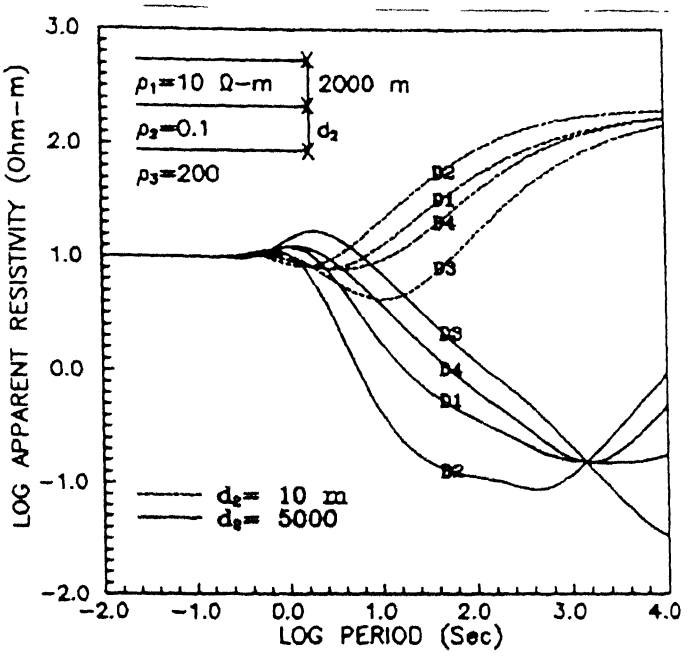

Figure 3.6 Variation of apparent resistivity curves obtained by various definitions for H-type models with period for two values of d_2 (10 and 5000 m).

ii) Time-domain

The apparent resistivity variations for H-type models are shown in Figures 3.7 - 3.9. The apparent resistivity curves for D7 and D8 show peculiar characteristics on various combination of model parameters. Figure 3.7, shows the apparent resistivity curves for definitions D7 and D8 for two values of resistivity of intermediate layer. The decrease in resistivity of intermediate layer from 20 to 2 Ω-m is clearly seen from the apparent resistivity curve. At longer delay-time, the apparent resistivity curve seems to approach the resistivity of the last layer. The apparent resistivity curve defined by D8 shows overshoot at early time, during the transition from first layer to second layer, and undershoot at longer delay-time, during the transition from second layer to third layer. Therefore, undershoot and overshoot are the

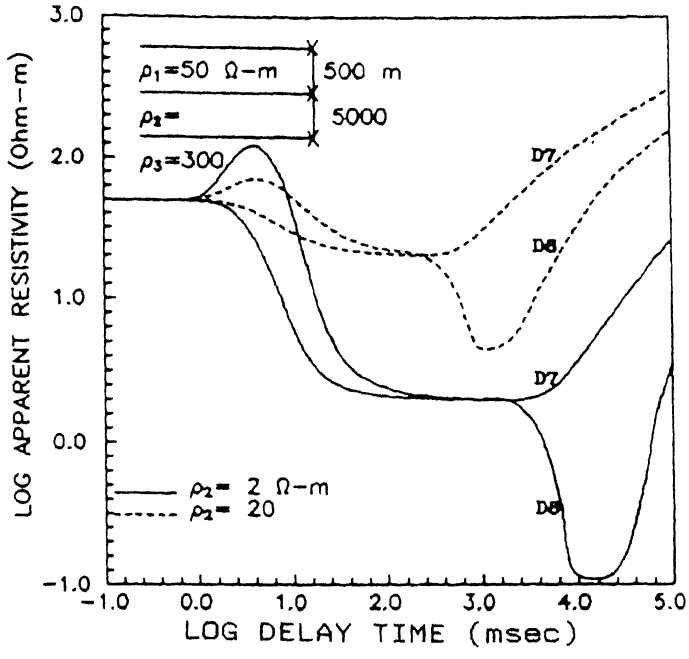

Figure 3.7 Variation of apparent resistivity curves obtained by definitions D7 and D8 for H-type models with delay-time for two values of intermediate layer resistivity (2.0 and 20.0 Ω-m).

characteristics of the boundary of the Earth model.

Figure 3.8 shows variation in apparent resistivity for two values of d_2. The increasing d_2 have an effect of delaying the transition of apparent resistivity from second layer to lower half-space for both D7 and D8. Moreover, the apparent resistivity curve D8 for d_2 = 20000 m does not recover from the undershoot at late delay-time and this is because of higher thickness d_1 causes a shift in curves towards higher time. On comparing with Figure 3.7, it is observed that the nature of shift in apparent resistivity curves is due to increase of thicknesses of both layers(first and second). In Figure 3.8, the complete undershoot is not observed in the delay-time range of the curves, however, the nature is expected at longer delay-time.

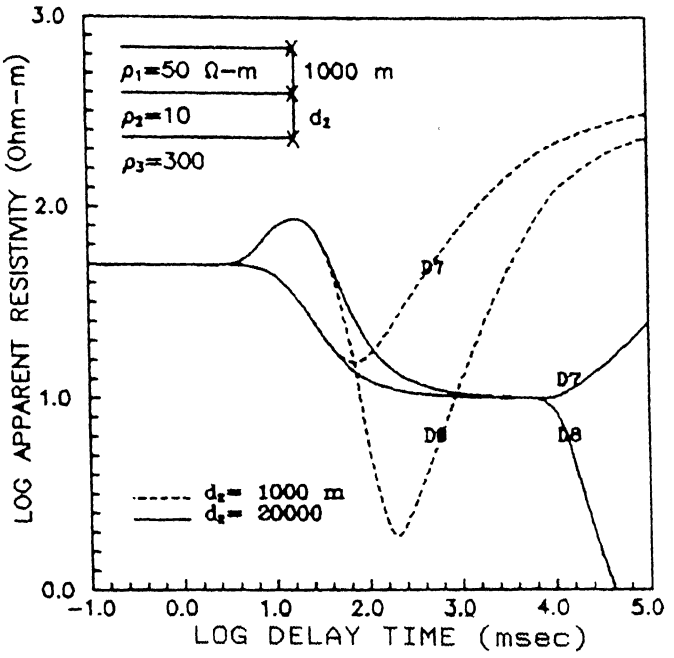

Figure 3.8 Variation of apparent resistivity curves obtained by definitions D7 and D8 for H-type models with delay-time for two values of d_2 (1 and 20 km).

The Figure 3.9 shows the variations in apparent resistivity curves for a model with ρ_1 = 0.1 Ω-m, much smaller than previous two cases, d_1 = 2000 m, even larger than the previous two cases, and d_2 = 10 and 5000 m. The behaviour of the curves for both D7 and D8 are exactly the same as observed in Figure 3.8. The difference lies because of larger thickness of the top layer, due to which the curves are shifted towards higher delay-time. From the Figure 3.9, it is clearly seen that only higher delay-time (>>10^5 msec), more than the present threshold, can show the effect of last layer resistivity on apparent resistivity curves for D8 particularly.

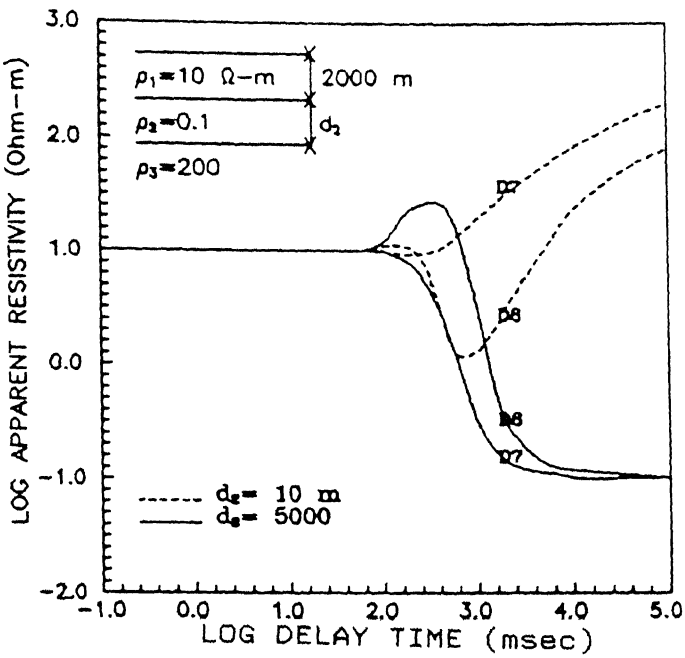

Figure 3.9 Variation of apparent resistivity curves obtained by definitions D7 and D8 for H-type models with delay-time for two values of d_2 (10 and 5000 m).

3.4.3 Q-type Models ($\rho_1 > \rho_2 > \rho_3$)

i) Frequency-domain

The apparent resistivity curves for Q-type models are shown in Figures 3.10 - 3.12. The apparent resistivity curves for D2 show distinct differences from the other curves, in the apparent resistivity contrast for thickness and resistivity of the intermediate layer at lower periods. The large intermediate layer thickness results in a distinct feature in curves for D2 compared with definitions D3 and D4 (Figure 3.10) and with the well-known conventional definition D1 (Figure 3.11) and the other.

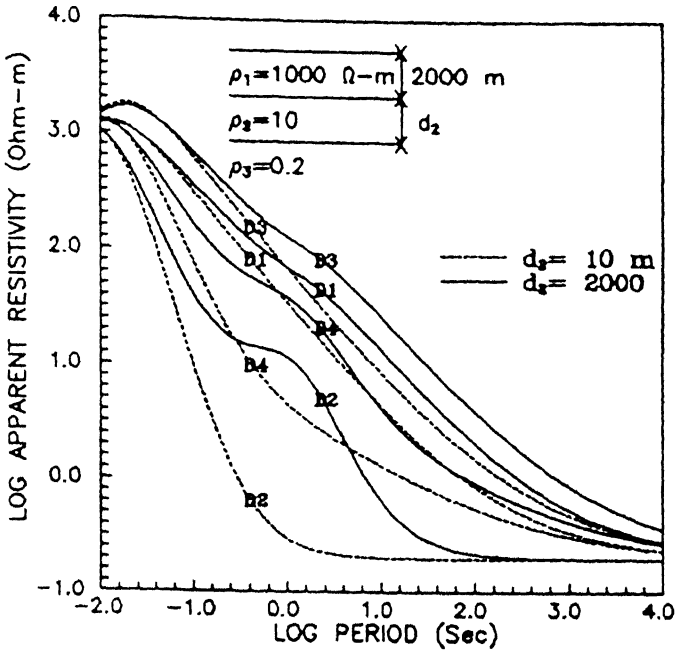

Figure 3.10 Variation of apparent resistivity curves obtained by various definitions for Q-type models with period, for two values of d_2 (10 and 2000 m).

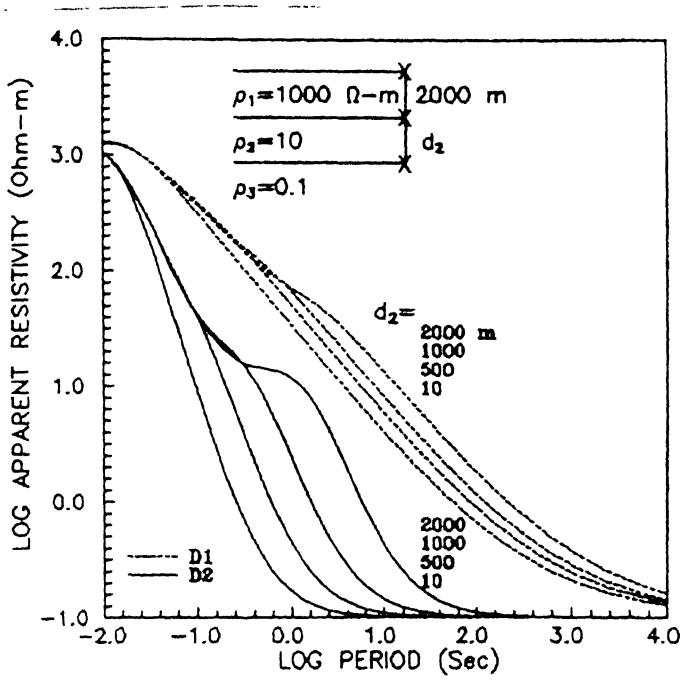

Figure 3.11 Variation of apparent resistivity curves obtained by definitions D1 and D2 for Q-type models with period, for d_2 values of 10, 500, 1000 and 2000 m.

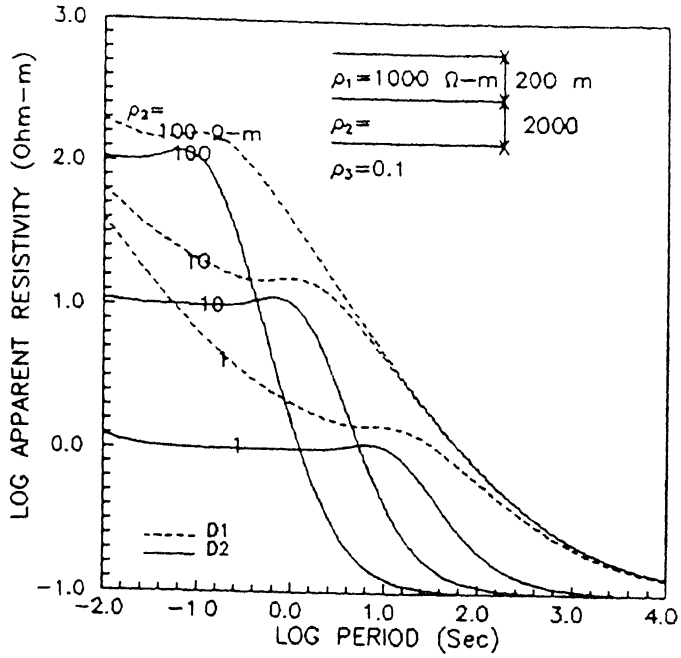

Figure 3.12 Variation of apparent resistivity curves obtained by definitions D1 and D2 for Q-type models with period, for three values of ρ_2 (1, 10 and 100 Ω-m).

Figure 3.12 shows the apparent resistivity variations for definition D1 and D2 for three values of second layer resistivity ρ_3 = 100, 10 and 1 Ω-m. The apparent resistivity curves for definition D2 clearly give the details of the second layer resistivity owing to its characteristic behaviour, whereas, these details are found to intricate to some extent in apparent resistivity curves for definition D1.

ii) Time-domain

The apparent resistivity curves for Q-type models are shown in Figure 3.13 and 3.14. The apparent resistivity curves for both step (D7) and impulse (D8) responses show distinct characteristics for variation in second layer thickness d_2 (Figure 3.13) and resistivity (Figure 3.14). The apparent resistivity curves obtained for definitions D7 show

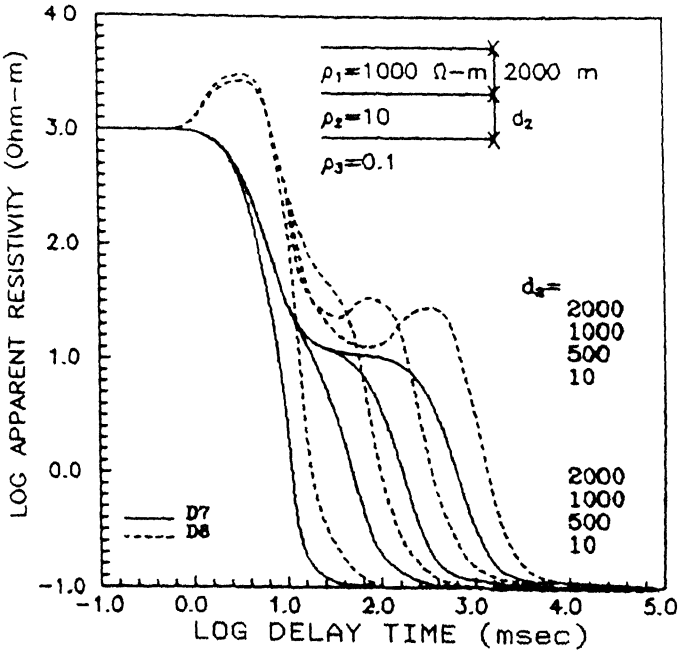

Figure 3.13 Variation of apparent resistivity curves obtained by definitions D7 and D8 for Q-type models with delay-time, for d_2 values of 10, 500, 1000 and 2000 m.

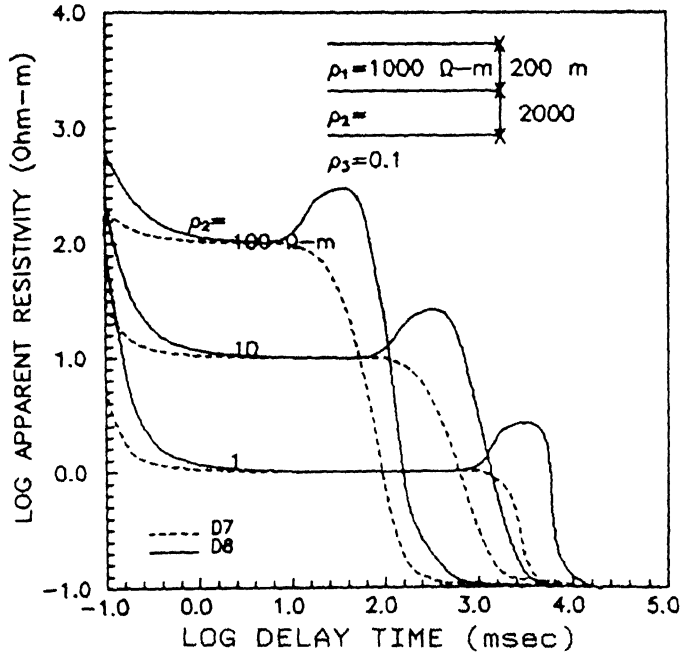

Figure 3.14 Variation of apparent resistivity curves obtained by definitions D1 and D2 for Q-type models with delay-time, for three values of ρ_2 (1, 10 and 100 Ω-m).

the smooth transition from first layer to second layer resistivity ; and from second layer to third layer resistivity, whereas, the smooth transition is obscured by the presence of overshoots at first and second interface in curves for D8. Moreover, the effect of second layer thickness d_2 on apparent resistivity curves for both is visible for values of d_2 greater than 500 m.The fast transition in the apparent resistivity curves for D7 and D8 is seen when the thickness of the intermediate layer is small. The effect of thickness of the intermediate layer is clearly seen in D7 and D8. The transition time either from first layer to second or second layer to lower half-space, is larger in D8 than those in D7.

Figure 3.14 show the effect of second layer resistivity on the apparent resistivity curves for definition D7 and D8. The nature of the curves in Figure 3.14 are similar to the curves in Figure 3.13. However, both the definitions D7 and D8 match perfectly with each other over a sufficient length of delay-time. This length of delay-time increases with the decrease in second layer resistivity.

The apparent resistivity curves in time-domain show up better subtle variations corresponding to changes in model parameter settings of second layer compared to curves those in frequency- domain i.e. the visual discrimination of curves in time-domain has more clarity than those in frequency-domain. The influence of second layer thickness, in frequency-domain, on the apparent resistivity curves for D2 is distinguishable for d_2 values greater than 1000 m whereas in time-domain it is for d_2 values greater than 500 m (in D7) and 10 m (in D8).

3.4.4 A-type Models ($\rho_1 < \rho_2 < \rho_3$)

i) Frequency-domain

Figures 3.15 - 3.19 show the apparent resistivity behaviour for A-type Earth models. This behaviour, using definitions D1 - D4, is found to be almost the same, although the curve for D3 is qualitatively different from the other curves. Therefore, the study of apparent resistivity behaviour using definition D3 and comparison of it with the apparent resistivity behaviour using the conventional definition D1 have been carried out. Figures 3.15 and 3.16, show the apparent resistivity behaviour for a three-layer A-type model with varying top (d_1) and intermediate (d_2) layer thicknesses, respectively. The effect of varying d_1 is clearly seen in the apparent resistivity curves for D1 and D3 (Figure 3.15); however, this effect on varying d_2 is clearly different in the curves for D3 (Figure 3.16).

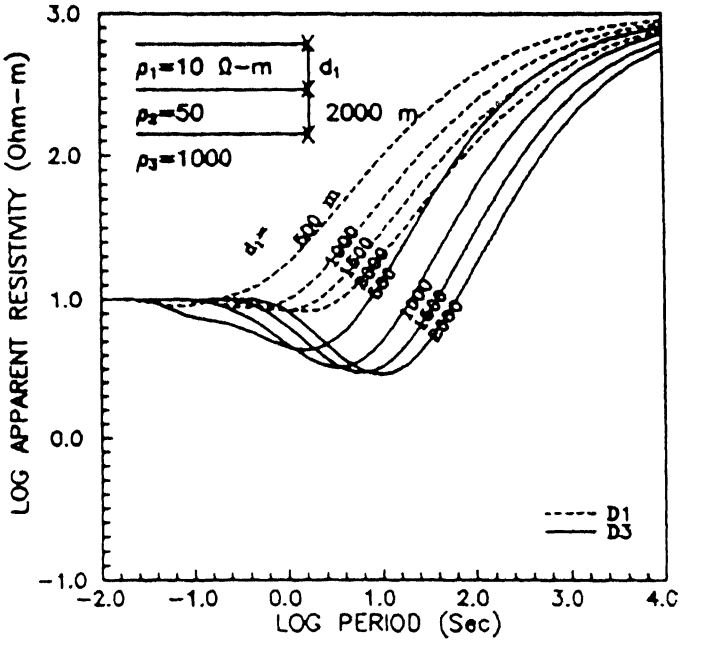

Figure 3.15 Variation of apparent resistivity curves obtained by definitions D1 and D3 for A-type models with period, for various values of first layer thickness (d_1 = 500, 1000, 2000 and 10000 m)

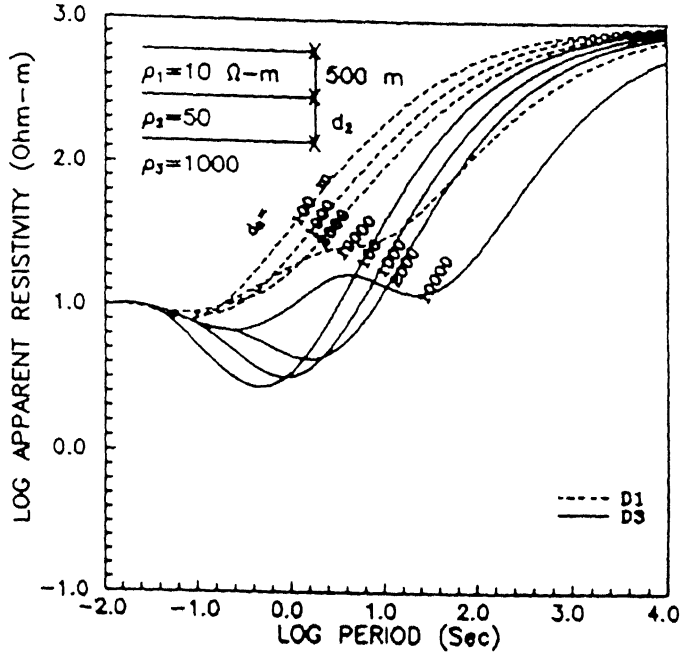

Figure 3.16 Variation of apparent resistivity curves obtained by definitions D1 and D3 for A-type models with period, for various values of intermediate layer thickness (d_2 = 100, 1000, 2000 and 10000 m)

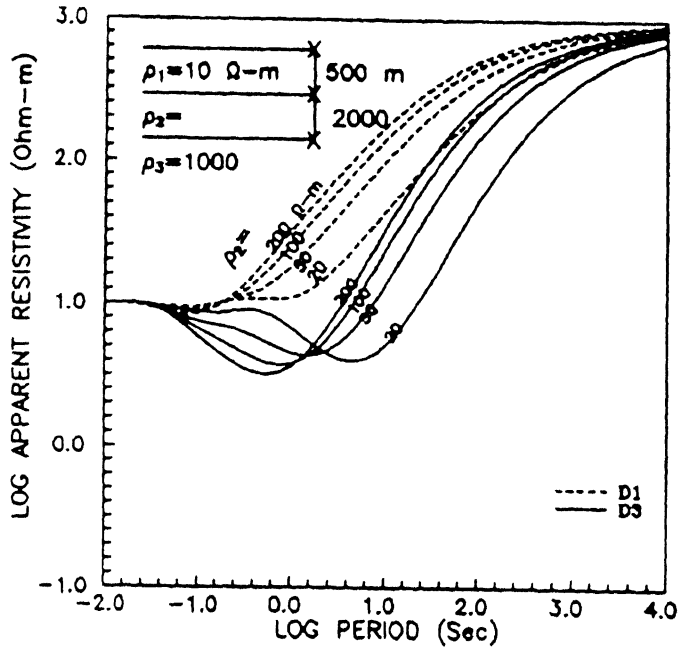

Figure 3.17 Variation of apparent resistivity curves obtained by definitions D1 and D3 for A-type models with period, for various resistivity values of intermediate layer (ρ_2=100, 1000, 2000 and 10000 m)

In Figure 3.17, the change in behaviour of the curves for D1 and D3 with changes in the intermediate layer resistivity have been studied. The resistivity curves for D1 show realistic values of resistivity for the upper layer at lower periods. At higher periods they seem to attain the resistivity value of the bottom layer. The curve for D3 shows similar behaviour to that of the other curves at lower and higher periods. At intermediate periods it show a minima before reaching the resistivity of the bottom layer. The minima depends on the resistivity and thickness contrast of the layers. However, the curves for ρ_2 = 20 Ω-m show both maxima and minima.

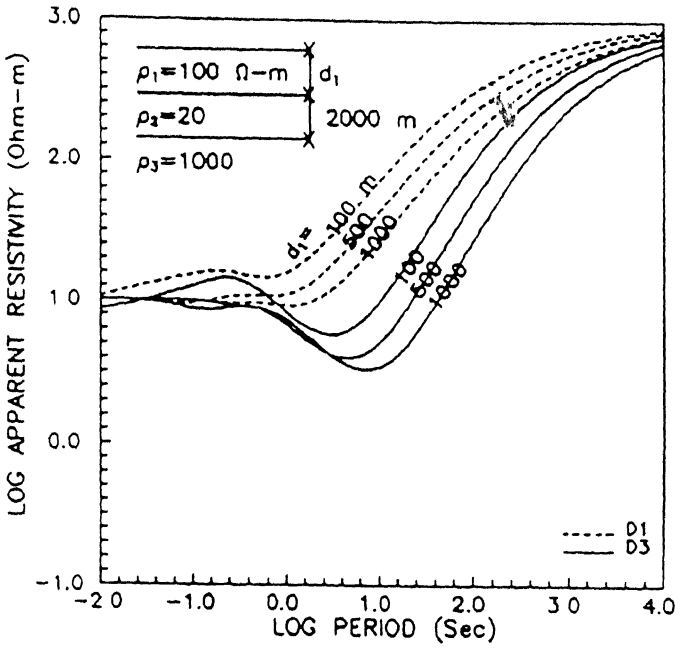

Figure 3.18 Variation of apparent resistivity curves obtained by definitions D1 and D3 for A-type models with period, for the same model as in Figure 3.15 with various thicknesses of top layer (d_2 = 100, 500 and 1000 m) and ρ_2 = 20 Ω-m

The Figures 3.18 and 3.19 show the effect of top layer thickness (d_1) on the apparent resistivity curves for definition D1 and D3 with ρ_2 = 20 and 30 Ω-m, respectively. In both Figures the behaviour of D1 and

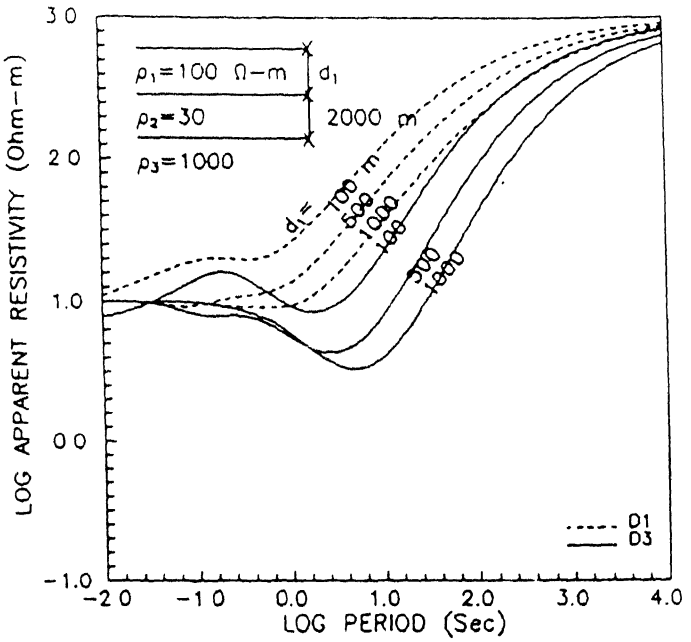

Figure 3.19 Variation of apparent resistivity curves obtained by definitions D1 and D3 for A-type models with period, for the same model as in Figure 3.15 with various thicknesses of top layer (d_2 = 100, 500 and 1000 m) and ρ_2 = 30 Ω-m.

D3 at d_1 = 100 m is clearly different from the curves for top layer thickness (d_1) greater than 100 m. Maxima, the peculiar feature, around 0.2 sec in both D1 and D2 is not seen for top layer thickness (d_1) greater than 100 m.

ii) Time-domain

Figures 3.20 - 3.24 show the apparent resistivity behaviour for A-type Earth models. The behaviour of apparent resistivity using definition D7 is found to be almost the same for various variations in parameters d_1, d_2 and ρ_2 in Figures 3.20 - 3.22, respectively; except for d_2 = 10000 m in Figure 3.21 where the presence of second layer is observed. The behaviour of apparent resistivity using definition D8 is clearly distinct in respective Figures 3.20 - 3.22.

Figure 3.20 shows the effect of top layer thickness (d_1) on apparent resistivity curves for D7 and D8. The apparent resistivity

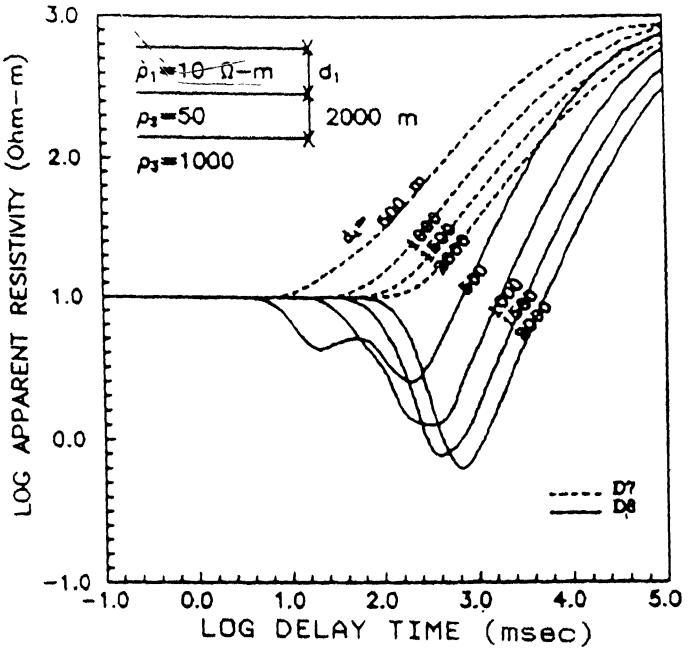

Figure 3.20 Variation of apparent resistivity curves obtained by definitions D7 and D8 for A-type models with delay-time for various values of first layer thickness (d_1 = 500, 1000, 2000 and 10000 m)

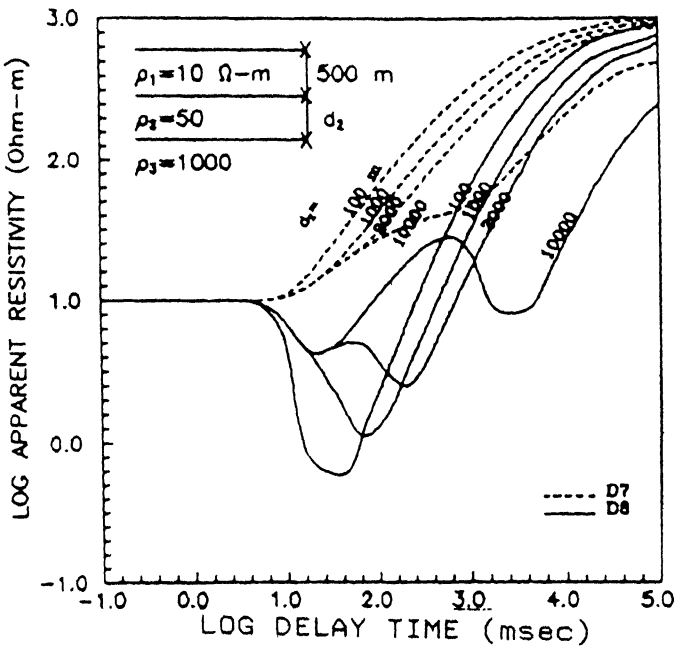

Figure 3.21 Variation of apparent resistivity curves obtained by definitions D7 and D8 for A-type models with delay-time, for various values of intermediate layer thickness (d_2 = 100, 1000, 2000 and 10000 m)

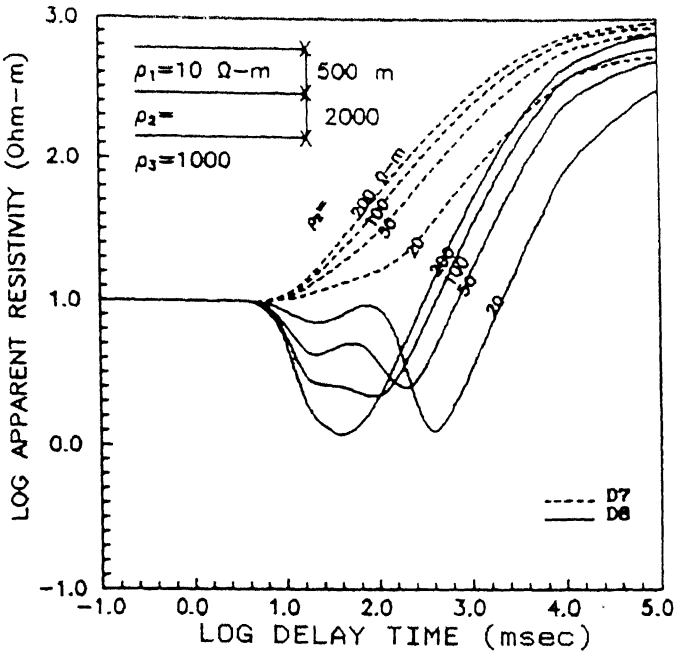

Figure 3.22 Variation of apparent resistivity curves obtained by definitions D7 and D8 for A-type models with delay-time, for various resistivity values of intermediate layer (ρ_2=100, 1000, 2000 and 10000 m).

curves for D7 and D8 shifts towards higher delay-time with the increase of top layer thickness. The behaviour for D8 is distinct in the sense that the size of the undershoot increases on increasing d_1; and for thin intermediate layer (equal and less than 500 m) two undershoots are observed which are indicative of middle layer. This observation of showing two undershoots is further investigated by taking d_1 = 500 m for various values of d_2 in Figure 3.21. The apparent resistivity curves for D7 (in Figure 3.21) show the indication of second layer for d_2 values equal and larger than 10,000 m. Curves for D8 shows the indication of second layer, owing to two undershoots, for d_2 values equal and greater than 2000 m. Further investigation for two undershoots is extended by taking various values of resistivity of second layer with d_1 = 500 m and d_2= 2000 m in Figure 3.22. The apparent resistivity

curves for D7 do not show any indication of second layer. The curves for D8 show two undershoots for ρ_2 values equal and less than 100 Ω-m. The apparent resistivity curves for D2 at ρ_2 = 20 Ω-m is remarkably different from other curves at higher values of ρ_2 than 20 Ω-m.

The Figures 3.23 and 3.24 show the details of peculiarity (seen in Figure 3.22 for definition D8 at ρ_2 = 20 Ω-m) of the apparent resistivity curves for D7 and D8 at ρ_2 = 20 (Figure 3.23) and 30 Ω-m (Figure 3.24) and various values of d_2. The curves in Figure 3.23 are not much different in behaviour from the curves in Figure 3.24, except the curves for D7 and D8 at d_1 = 100 m which are remarkably different from other curves.

From the above illustrations it has been found that the behaviour of apparent resistivity for step response (D7) is very similar to the behaviour of apparent resistivity in frequency-domain shown by

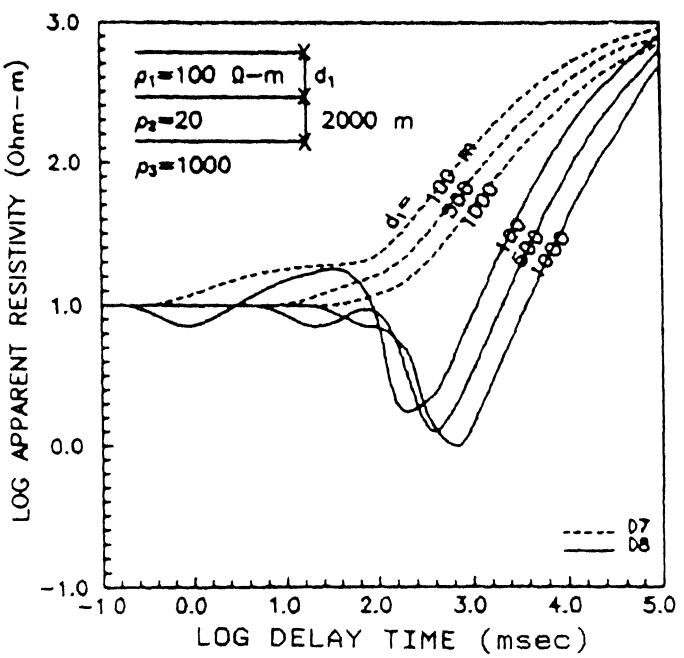

Figure 3.23 Variation of apparent resistivity curves obtained by definitions D1 and D3 for A-type models with delay-time, for the same model as in Figure 3.15 with various thicknesses of top layer (d_2 = 100, 500 and 1000 m) and ρ_2 = 20 Ω-m.

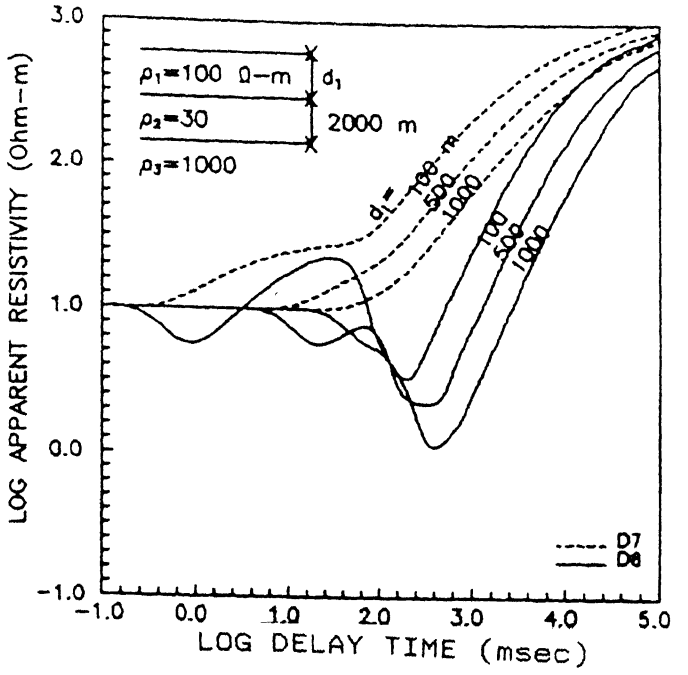

Figure 3.24 Variation of apparent resistivity curves obtained by definitions D7 and D8 for A-type models with delay-time, for the same model as in Figure 3.20 with various thicknesses of top layer (d_2 = 100, 500 and 1000 m) and ρ_2 = 30 Ω-m.

definitions D1, D2 and D4, however, it is more closer to D2. The behaviour of apparent resistivity for impulse response (D8)shows similarity with D3 curves. The apparent resistivity for impulse response is characterized by undershoot and overshoot which are also shown by definition D3 in frequency-domain. However, the undershoot and overshoot characteristics are very pronounced for impulse response. In both frequency and time-domains it has been found that the undershoot and overshoot are the characteristics of the presence of resistive interfaces. The overshoot is attributed to the transition from high resistive to the low resistive substratum, whereas undershoot is attributed to the low resistive to high resistive substratum. It has also been found that if the resistivity contrast is small, oscillation in the undershoot is observed. When the resistivity contrast is higher the apparent resistivity is characterized by sharp undershoot. The

oscillation in the undershoot also increases when the thickness of the layer increases. The undershoot becomes sharp when the thickness is small. On comparing the nature and behaviour of apparent resistivity curves in frequency-domain, it is seen that the definition D1, D2, D4, D7 gives the realistic nature of resistivity variation of the layer, whereas the resistivity curves D3 and D8 do not give the true resistivity of the layered model. However, the definition D3 and D8 shows characteristic features. These characteristic features are attributed to the intermediate layer.

3.5 Conclusions

Detailed numerical results using various definitions of apparent resistivity for different models of Earth's subsurface show similar or distinct behaviours in the broad-band periods or delay-times. In some of the models the set of apparent resistivity curves, or some of the curves defined by various definitions, show characteristic variations in the curves as compared to other definitions for various three-layer models. This distinctive behaviour in the broad-band or shorter/longer periods or delay-times of apparent resistivity curves can be used as an appropriate definition for a particular H-, K-, Q- or A-type three-layered model. The special features of apparent resistivity curves obtained by various definitions as discussed in this Chapter can be used as rules of thumb in the qualitative interpretation of magnetotelluric data in the field. It is concluded that together with the conventional definition of apparent resistivity D1 given by Cagniard (1953) and other definitions D2 - D4 may also be used to extend the interpretation capability of the magnetotelluric method in deducing the resistivity and thickness of subsurface layers. The definitions in frequency and

time-domains provide useful visualization of how individual definitions show the characteristics of subsurface resistivity distribution. Various three-layer Earth models have been considered with simple situations, but to a certain extent this suffices as rule of thumb in the qualitative interpretation of magnetotelluric data in the field. Theoretical apparent resistivity curves obtained for various Earth models based on various definitions in both frequency and time-domains show the characteristic features of transition; in terms of length of period T or delay-time t required to go from one resistivity to the other; and in terms of their early/late succession to second layer resistivity at different values of the period T or delay-time t. The apparent resistivity definition D2 in frequency-domain, seems to have minimum transition time and an early succession. The comparison of frequency-domain with time-domain suggests that definition D7 has the most efficient transition and succession followed by D8, D2, D4 and D3, respectively. This, however, does not prove an advantage over the depth of investigation using time-domain definitions (D7, D8) or D2 in frequency-domain. The main advantage lies in the visualization of detailed response of the Earth's subsurface which the individual definitions provides. Despite all these details, it is obvious that none of the definitions provide a characteristic apparent resistivity variation for all models under consideration.

CHAPTER IV

SENSITIVITY STUDIES OF ELECTROMAGNETIC MEASUREMENTS

4.1 General

The electrical resistivity distribution of the Earth's subsurface, using magnetotelluric method, is deduced from the observed response of the Earth to the incident electromagnetic energy. However, the true resistivity distribution of the Earth's subsurface can not be deciphered completely and directly due to several reasons; one of them being the ever existing fundamental difference between field observations and theoretical measurements (and this provides the basis for inverse theory). In field observations, the real Earth situation is considered whereas, in theoretical measurements mathematical model is considered to represent the real Earth. The pseudo ability of mathematical model to simulate the real Earth, introduces the first source of error. The second source of error is associated with non-linearity of the apparent resistivity which necessarily involves approximations on linearization.

It is highly desirable in solving the non-linear inverse problems to know the quantifiable difference between the data obtained theoretically and from field observations. Moreover, the evaluation of degree of correspondence between theoretically predicted and observed data is needed a priori. This is because a posteriori information on the degree of correspondence between the two data through accumulation of practical knowledge is rather late. The obvious answer to this problem lies in establishing a relationship between changes in a theoretically proposed model and consequent changes in theoretically predicted data.

This results in derivation of Frechet derivative which is also known as weighting function or sensitivity function (Gomez-Trevino, 1987a). Such a relationship serves to modify input model in obtaining an improved model. For simple problems it is possible to describe the Earth by a mathematical function and then derive an analytical expression for Frechet derivative. For complicated problems associated more to realities, it is customary to parameterize the Earth and solve it numerically for parameter sensitivities - partial derivatives of the data with respect to model parameters.

4.2 Sensitivity Functions and Their Roles: A Review

The electromagnetic response over Earth models and the determination of the model parameters from the electromagnetic measurements are associated with forward and inverse modeling, respectively. In mathematical representation, the model space M (the Earth) is considered to be the Hilbert space of functions over a sufficient and suitable interval. The data space D, which represents response of the model, is an N-dimensional euclidean vector space with complex or real elements. Then $F : M \longrightarrow D$ is the mathematical notation of forward mapping which means the mapping F with domain M and range in D i.e. the function F maps model space M into data space D. Mathematically, it is written as

$$d_j = F_j(m); j=1,2,..,N \qquad ...(4.1)$$

where F is linear or non-linear functional. Equation 4.1 states that functional F assigns exactly one element $d \in D$ of its range to each element $m \in M$ in its domain. In simple words, it relates the given model m(z) to the jth component of data d_j. If the problem is linear then

equation 4.1 is written as (Gomez-Trevino, 1987a)

$$d_j = (1-C_j)^{-1} \int_0^{\infty} G(\tau_j, m, z)\, m(z)\, dz \qquad \ldots(4.2)$$

where $j = 1,2,..,N$ are number of observations, τ is period T in frequency-domain and delay-time t in time-domain, $G(\tau_j, m, z)$ is known as Frechet derivative or Kernel of the functional F associated with jth data, and C_j is a dimensionless quantity independent of the vertical co-ordinate z. Explicitly, C_j represents a simple function of logarithmic derivative of d_j with respect to period in frequency-domain or with respect to time in time-domain.

In electromagnetic inverse problems, it is desirable to find a model $\underline{m}(z)$ such that it can reproduce the observed data as

$$d_j^{obs} = F_j(\underline{m}); \quad j = 1,2..,N \qquad \ldots(4.3)$$

where d_j^{obs} is the jth observation.

In linear geophysical problems, numerous schemes are available to solve the set of equations, given by equation 4.3, for $\underline{m}(z)$ using the direct inverse mapping (Parker 1977b, Menke 1984, Oldenburg 1984). In non-linear geophysical problems there are two possible ways of solving the set of equations, given by equation 4.3, for $\underline{m}(z)$. First- use of non-iterative direct inverse mapping eg. Gel'fand-Levitan approach for inverse scattering problems (Weidelt, 1972), which is often unstable in the presence of noisy data. Moreover, no direct inverse mapping is possible in most of the non-linear problems encountered in geophysics. The second method involves the use of iterative schemes with

theoretically predicted model $m_{thp}(z)$ to obtain the predicted data using forward model function (eg. Wu, 1968). A perturbation $\delta m(z)$ is required in each iteration to add in the initially predicted model $m_{thp}(z)$ to improve in such a manner that the observed data are reproduced. Therefore, the solution $\underline{m}(z)$ for non-linear problem to the set of equations in 4.3, is restricted to the 'second' kind of strategy. This is accomplished by expanding the functional F in equation 4.3 around the predicted model $m_{thp}(z)$. For jth observation, Taylor series expansion of the functional F can be written as a right hand side of the following equation

$$d_j^{obs} = F_j(m_{thp}) + F_j^{(1)}(m_{thp})\delta m_j + F_{thp}^{(2)}(m_{thp})(\delta m)^2 + \quad \ldots(4.4)$$

where $j = 1,2..,N$; $\delta m = \underline{m} - m_{thp}$ is the difference between desired and predicted models and $F_j^{(n)}(m_{thp})$ is the nth order Frechet derivative of $F_j(m_{thp})$ (Griffel 1981, Zelder 1985). The first order derivative $F_j^{(1)}(m_{thp})$ is simply referred to as the Frechet derivative.

Let d_j^{thp} be the jth predicted observation. After substituting it for $F_j(m_{thp})$ in equation 4.4, it can be written as

$$d_j^{obs} - d_j^{thp} = F_j^{(1)}(m_{thp})\delta m + R(m_{thp}, \delta m) \quad \ldots(4.5)$$

where $R(m_{thp}, \delta m)$ is remainder term and can be neglected if it is second order in model perturbation i.e. if observations are Frechet differentiable which implies that $R(m_{thp}, \delta m)$ tends to zero faster than δm. Mathematically, it can be written as

$$\lim_{\delta m \to 0} \frac{||R(m_{thp}, \delta m)||}{||\delta m||} = 0$$

It is very important to prove the differentiability of electromagnetic observations because the linearization in equation 4.5 breaks down in lack of differentiability. This has been observed in geophysical non-linear inverse problems. It was Anderssen (1975) who first stated the possibility that Frechet derivative given by Parker (1970) for problem of electrical conductivity in the mantle, might be incorrect since the neglected remainder term may not be of second order in conductivity model perturbation. Woodhouse (1976) shown the first order error terms in Frechet derivatives for seismic normal mode (free oscillations in the Earth) when the model contains discontinuities. This invalidated the derivation of Frechet derivatives by Backus and Gilbert (1967). Moreover, Woodhouse showed that if the discontinuity boundary is moved, a new term of first order in remainder term $R(m_{thp}, \delta m)$ in equation 4.5 appears. Thus, the problem is not Frechet differentiable in usual norm for models with discontinuities. This first order error term and its cause if pertains to the electromagnetic problem might invalidate the work by Parker (1972) in which Frechet derivatives with respect to discontinuous models were used to establish bounds on conductivity. After seeing the seriousness of Frechet differentiability, efforts have been made to establish it for electromagnetic problem in a wide class of conductivity profiles, including the discontinuous ones.

The first attempt was made by Parker (1977a) who established the differentiability of Frechet derivative for one-dimensional electromagnetic induction problem in a general functional space. Parker (1980) has shown that the fundamental space for the inverse problems is larger even than L_1 (the space of integratable functions) in that it should admit delta functions as valid elements. Chave (1984), using the approach of Parker (1977a), established the Frechet differentiability

for low frequency electromagnetic measurements in toroidal and poloidal magnetic modes, where both magnetotelluric and electrical resistivity problems are special cases of poloidal and toroidal modes. The two response functions are shown to be Frechet differentiable in L_2 norm for a general class of conductivity models. The general proof of differentiability in L_1 is also illustrated by Weidelt (1985) in which the Frechet derivative is employed in a variational approach to provide rigorous bounds on the integrated conductivity of the Earth model. MacBain (1986) established that the components of electric fields and the magnetotelluric response function, each has a Frechet derivative with respect to conductivity model when the conductivity functions are twice continuously differentiable in depth. The importance of MacBain's results was reiterated by Parker (1986). Parker suggested that results could have been more important if MacBain might have proved results in a larger space (L_1) of conductivity functions. MacBain (1987) developed a generalized formulations for magnetotelluric problems which remain valid when the conductivity becomes complex to the point that the standard differential equation representation are invalid. MacBain (1987) established the desired general Frechet derivative results in L_1, L_2 and L_1 augmented by the finite delta comb models. The L_1 results have been pursued due to the work of Parker (1980) and Weidelt (1985).

The proofs for Frechet differentiability discussed above are important and entail justification for avoiding the unappealing task of examining the full non-linear problem in present sensitivity studies. Therefore, on neglecting the remainder term, the equation 4.5 can be written as

$$\delta d_j \simeq \int_0^{\infty} G(\tau_j, m_{thp}, z)\, \delta m(z)\, dz; \quad j = 1,2,..,N \qquad ...(4.6)$$

where $\delta d_j = d_j^{obs} - d_j^{thp}$.

From equations 4.2 and 4.6 it is explicit to express that Frechet derivative not only, through a normalization factor, directly relates the data to the model (Gomez-Trevino 1987a), but also relates small changes in data to small changes in the model (Gomez-Trevino 1987b). The equations 4.2 and 4.6 hold for both frequency and time-domains. The equivalent equations in time- domain can be obtained either on replacing period T by delay-time t (Gomez-Trevino 1987a) in equations 4.2 and 4.6, or on Inverse Fourier Transforming (Gomez-Trevino 1987b) the corresponding equations 4.2 and 4.6. Frechet derivatives in time-domain will be real as opposed to being complex in frequency-domain. The Frechet Kernel/derivative $G(\tau_j, m_{thp}, z)$ given by equations 4.2 and 4.6 have an advantage of having both depth (z) and frequency/delay-time dependence. Therefore, it can characterize the importance of deeper parts of conductivity structure through direct visualization of $G(\tau_j, m_{thp}, z)$ along depth and through skin/diffused depth as well.

Efforts have been made to use the equation 4.6 for obtaining solution of the inverse problems. The inverse problems have been solved using Frechet derivative by Weidelt (1972) using a Gel'fand-Levitan technique for the magnetotelluric data; Parker (1972) inverted the grossly inadequate data using Frechet derivatives with discontinuous models; Oldenberg (1978) for electrical resistivity measurements; Oldenberg (1979) for one-dimensional inversion of natural source magnetotelluric observations; Gomez-Triveno (1987a) through non-linear integral equations obtained from the principle of similitude for

electromagnetic problems; Weidelt (1985) used variational approach to provides bounds for the integrated conductivity and Boerner and Holladay (1990) used approximated Frechet derivatives to invert the inductive electromagnetic synthetic data.

Frechet derivatives have been widely used for several non-linear inverse problems. These have been used and represented by resolving Kernels of Backus and Gilbert (1968). Guptasarma (1978) used the Frechet derivatives in the interpretation of electrical resistivity measurements and has shown that the Frechet derivative represents the electric field variations inside the Earth. It has also been shown that the Frechet derivatives diminish at some depth for all types of conductivity distribution. Chave and Cox (1982) described the results in model study of Frechet derivatives for a poloidal magnetic mode of electromagnetic induction. The poloidal magnetic mode is suitable for describing the electromagnetic response for any layered Earth to a purely inductive source. The complimentary nature of electromagnetic induction and electrical resistivity soundings have been illustrated through the sensitivity of surface measurements by Gomez-Trevino and Edwards (1983). Similar applications have been described by Chave (1984) and by Edwards et al. (1984) in relation to electrical soundings on the sea floor. Gomez-Trevino (1987a) has shown that Frechet derivatives of electromagnetic observations play a dual role as sensitivity functions and weighting functions for electrical conductivity despite the non-linear dependence of the model and data. Gomez-Trevino (1987b) has shown the existence of different kinds of sensitivity functions to different types of measurements in both the domains and within the same domain. Pedersen and Rasmussen (1989) used the sensitivity functions for the choice of layer thickness distribution for a model close to a

homogeneous half-space. Spies (1989) presented a number of heuristic depth of investigation rules for inductive electromagnetic sounding methods based on the sensitivity functions to detect an electrical basement. Boerner and West (1989b) presented a simplified analysis of the sensitivity functions for electrical methods for a layered Earth models. In this case electromagnetic fields are factored into geometrical operators and electrical kernels using the approach given in their earlier work (Boerner and West 1989a), and illustrated the spatial variations and frequency dependence of the sensitivity function to buried layers for various electrical prospecting methods. Boerner and West (1989c) have shown that sensitivity function for a model are just an integral over Green's function. However, Frechet differentiability is established and the proof of this is shown to depend on the smoothness of the fields at the boundaries of the perturbed volume. They have given a physical interpretation to Frechet derivative in terms of scattering theory. Sasaki (1989) has carried out study on the sensitivity analysis of magnetotelluric measurements in relation to static effects. The two-dimensional analysis for frequency response reveals that static effect can be explained by high pass filter characteristic for the near surface, while the averaging process at depth is characterized by the low pass filter (Sasaki 1989). Boerner and Holladay (1990) approximated the Frechet derivatives in one-dimensional inductive electromagnetic soundings and have shown that these are not strongly model dependent, even for quite diverse Earth models. They have shown using a scaled version of the Frechet derivative for a uniform half-space to approximate the exact Jacobian in a layered Earth, that the inversion program improves the convergence to an acceptable model. The lack of strong model dependence makes it possible to consider the capabilities

and limitations of electromagnetic "imaging" methods from the prospective of Frechet derivatives. They also have shown that the Frechet derivatives are strongly model dependent for non-inductive sources and therefore, the electromagnetic fields generated by non-inductive sources are less amenable to imaging techniques.

The Frechet derivative $G(\tau_j, m_{thp}, z)$ as given in equation 4.6 establishes the relationship between first order small changes in the model and corresponding changes in the data. When the analytical expression for Frechet derivative is not derivable easily, the linkage between small changes in model and corresponding changes in data can be developed by parameterizing the vertical conductivity profile (the model) into layered models of finite thicknesses and conductivities. For P number of layers there are M parameters which can be represented by m_k; k = 1,2,..,M (first P-1 are thicknesses and rest P are conductivities). For such cases, the equation 4.5 can be written as

$$d_j^{obs} - d_j^{thp} = \sum_{k=1}^{M} \frac{\partial}{\partial m_k}\left[F_j(m_{thp})\right] \delta m_k + R(m_{thp}, \delta m_k) \qquad \ldots(4.7)$$

where j =1,2,..,N are number of observations; $\delta m_k = m_k - m_{thp}$ and $\frac{\partial}{\partial m_k}\left[F_j(m_{thp})\right]$ is the first order sensitivity of $F_j(m_{thp})$ with respect to the kth parameter and $R(m_{thp}, \delta m_k)$ is second order remainder term. If all the observations are taken into account, the equation 4.7 after neglecting the remainder term, can be written in matrix form as

$$\mathbf{D} = \mathbf{J}\,\mathbf{M} \qquad \ldots(4.8)$$

where $\mathbf{D}$ is a column matrix of perturbation in data, $\mathbf{J}$ is N X M Jacobian matrix whose elements $J_{jk} = \frac{\partial}{\partial m_k}\left[F_{jk}(m_{thp})\right]$ are the first order sensitivities and $\mathbf{M}$ is column matrix of perturbation in model

parameters. Practically, the computation of perturbation in parameters, makes use of generalized inverse for J (Jackson, 1972; Wiggins 1972; Jupp and Vozoff 1975 and Menke 1984). Moreover, J has been widely used as the linear inverse 'resolution' matrix (Wiggins 1972; Jupp and Vozoff 1975; Glenn and Ward 1976 and Ward et al. 1976); as in the eigen-parameter decomposition methods (Edwards et al. 1981) and as the variances of model parameters for uncertainty measures (Pedersen and Rasmussen, 1989). In equation 4.8, the first order parameter sensitivities do not have the depth (z) dependence to characterize the explicit importance of deeper parts of conductivity structure.

The major drawback with all of these methods is that they are inherently dependent on the chosen reference model and there is sometimes little indication how one might extend the results to various other Earth models. Moreover, the results represent a posteriori information specific to the real Earth model at the site which may not be useful for suggesting how precautions and improvements (if any) be improvised in subsequent surveys. These difficulties are compounded by the fact that electromagnetic problems are functionally non-linear. The non-linear problems require an investigation of all possible characteristics of Frechet derivatives from simpler to complex models. Several other general and/or specific conclusions concerning electromagnetic methods are only possible after detailed study of the characteristics of Frechet derivatives or their parameter sensitivities.

4.3 Sensitivity Analysis

Lineralized analysis is generally used in solving non-linear inverse problems encountered in electrical and electromagnetic methods. This requires either the use of Frechet derivatives (Oldenberg 1978,

1979; Mcgillivary and Oldenberg, 1990) or partial derivatives to evaluate quantitative change in observed data on a change in model. Therefore, sensitivity functions, which are related with Frechet derivatives or partial derivatives of the data with respect to model parameters, play an important role in both forward as well as in inverse problems through mappings between model space and data space. In order to draw meaningful physical interpretation of the various Earth models, it is essential to parameterize the Earth models and then define sensitivity through Frechet/partial derivatives.

4.3.1 Parameterization of Earth Models

Consider a vertically inhomogeneous model whose conductivity varies as a function of depth is represented by one-dimensional conductivity profile $\sigma(z)$. Depth axis is taken vertically downward with origin on the Earth surface. Let the Earth (H, the Hilbert space) be divided into N number of sub-spaces H_k(k=1, N). Each sub-space H_k may have thicknesses from very small (as of finite delta function) to very large (as of finite homogeneous half-space). The vertical conductivity profile $\sigma(z)$ at any depth z_i can be described as

$$\sigma(z_i) = \sum_{k=1}^{N} \sigma_k \Psi_k \qquad \ldots(4.9)$$

where σ_k is conductivity defined within kth sub-space H_k, and $\{\Psi_k\}$ is a set of basis functions for entire Earth space H. The choice of basis functions determines the type of model to be taken.

i) Layered Earth Models

For layered Earth models, the kth basis function Ψ_k is defined to

$$\delta\sigma_{ar}(\tau_j, \sigma_{thp}) = \int_0^\infty \sigma(z)\, G_r(\tau_j, \sigma_{thp}, z)\, \delta[\ln\{\sigma(z)\}]\, dz \ . \qquad \ldots(4.12)$$

where, $j = 1,2,..,N$; τ is period (T) in frequency-domain and delay-time (t) in time-domain; the subscript 'r' is indicative of the response function used to derive this equation. For response function in frequency-domain (the surface impedance), $r = f$; and for step or impulse response function in time-domain, $r = s$ or i. $\delta\sigma_{ar}$ and G_r are perturbation in apparent conductivity and sensitivity function, respectively, corresponding to response function in either domain.

The sensitivity function for logarithmic changes in the model $\sigma(z)$ is

$$S_r(\tau_j, \sigma_o, z) = \sigma(z)\, G_r(\tau_j, \sigma_{thp}, z) \qquad \ldots(4.13)$$

For a physical interpretation of sensitivity functions, second way is to introduce at depth z_o an additional thin sheet of conductance (integrated conductance) ΔS, such that $\delta\sigma(z) = \Delta S\ \delta(z-z_o)$, and then to calculate the change $\delta\sigma_{ar}(\tau_j)$ in the apparent conductivity. The fractional change in conductivity distribution at depth z_o is related with fractional change in data through the fractional sensitivity function given below.

$$S_r^n(\tau_j, z_o) = \frac{\sigma(z)}{\Delta z}\, G_r(\tau_j, z_o) \qquad \ldots(4.14)$$

The above equation for fractional sensitivity function S_r^n, where super script n denotes the fractional change, is the general expression valid for both frequency and time-domains.

Third way to interpret the variations in sensitivity function is to normalize it with skin depth (in frequency-domain) or diffused depth (in time domain) scaled by $(2\pi)^{-1/2}$ and then to compute it as a function of normalized depth. The expression which relates sensitivity function $G_r(\tau_j, z)$ with the normalized sensitivity function $\varphi_r[\tau_j, \sigma(z)/\sigma_1, \delta_r^{-1}z]$ can be written as

$$G_r(\tau_j, z) = \delta_r^{-1} \varphi_r[\tau_j, \sigma(z)/\sigma_1, \delta_r^{-1}z] \qquad \ldots(4.15)$$

where, δ_r is the factor of normalization which in frequency-domain is the skin depth (δ_{sd}) and in time-domain is the diffused depth (δ_{dd}) scaled by $(2\pi)^{-1/2}$ in the first layer of conductivity σ_1. The function φ_r, with dimensionless arguments, is dimensionless (normalized) sensitivity function in in either domain. Graphical display of normalized sensitivity function φ_r as a function of $\delta_r^{-1}z$ with $\sigma(z)/\sigma_1$ as parameters, gives some useful information on the models under consideration.

The fourth way to interpret the sensitivity of the measurements is to calculate the differential sensitivities by approximating the apparent conductivity using one sided forward or backward finite difference formula. This can be shown by following expression

$$S_r^d(\tau_j, \sigma_o) = \left. \frac{\sigma_{ar}(\tau_j, \sigma_o + \Delta\sigma) - \sigma_{ar}(\tau_j, \sigma_o)}{\Delta\sigma(z)} \right|_{\Delta\sigma(z) \longrightarrow 0}$$

$$= \frac{\partial\sigma_{ar}(\tau_j, \sigma_o)}{\partial\sigma(z)} = G_r^d(\tau_j, \sigma_o) \qquad \ldots(4.16)$$

Similarly parameter differential sensitivity can be defined and computed. This definition suggests that whether one arrive at analytical

expression for Frechet derivative or not, it is always possible to calculate differential sensitivity/Frechet derivative, numerically (also called 'brute force Method') which is of course very inefficient. Nevertheless, this impart fruitful results on conductive structure (Edwards, et al. 1984) Here, the qualifying adjective differential is often omitted in literature and merely implied. This definition is better suited to high sensitive response with respect to model.

4.3.3 Derivation of Sensitivity Functions in Frequency- domain

One-dimensional magnetotelluric data on the Earth surface in frequency-domain is generally characterized by apparent conductivity or resistivity as defined by Cagniard (1953) together with phase. For variations of real, imaginary and amplitude parts of sensitivity functions, based on equations 4.14 and 4.15, it is the complex apparent conductivity which is more suitable form to represent data and is defined as (Gomez-Trevino, 1987b)

$$\sigma_{af}\,(T,\,\sigma) = i\,\frac{2\pi}{T}\,\mu_o Z^{-2}(T) \qquad \ldots(4.17)$$

where $T = f^{-1}$ is the period (sec) reciprocal of frequency f (Hz); μ_o is the magnetic permeability of the free space and Z is the surface impedance for any one-dimensional Earth model. A relationship between perturbation $\delta\sigma(z)$ in model and corresponding perturbation $\delta Z(T)$ in surface impedance has been established for one-dimensional Earth models and is written as (Parker 1977a, Oldenberg 1979)

$$\delta Z(T) = -\int_o^\infty \left[\frac{E(z,T)}{H(0,T)}\right]^2 \delta\sigma(z)dz \qquad \ldots(4.18)$$

The complex apparent conductivity in equation 4.17 allows to

relate perturbation $\delta Z(T)$ in surface impedance to perturbation $\delta\sigma_{af}(T)$ in apparent conductivity through the following relationship

$$\delta\sigma_{af}(T) = -\frac{i4\pi}{T}\,\mu_o Z^{-3}(T)\,\delta Z(T) \qquad \ldots(4.19)$$

After substituting $\delta Z(T)$ from equation 4.18 into equation 4.19, one gets

$$\delta\sigma_{af}(T,\sigma) = \int_o^\infty G_f(T,\sigma,z)\,\delta\sigma(z)\,dz \qquad \ldots(4.20)$$

where

$$G_f(T,\sigma,z) = 2\,\frac{\gamma_1^2}{\sigma_1}\,Z^{-3}(T)\,\left[\frac{E(z,T)}{H(0,T)}\right]^2 \qquad \ldots(4.21)$$

is the general expression for Frechet derivative for any one-dimensional Earth model. The surface impedance Z(T) for multi-layered and exponentially varying conductivity models in frequency-domain have been derived in chapter II. The ratio of electric field in the subsurface to magnetic field on Earth surface [i.e. E(z,T)/H(0,T)] for various one-dimensional Earth models have been derived in following sections.

i) Two-layer Case

For a two-layer Earth model, the electric and magnetic fields for any layer can be derived from their governing differential equations. Therefore, it is possible to express the ratio E(z,T)/H(0,T) in each layer as

$$\frac{E(z,T)}{H(0,T)} = \alpha_2 \begin{cases} e^{-\gamma_1 z}\left[1+K_{12}\,e^{-2\gamma_1(d_1-z_1)}\right]; & 0 \le z \ge d_1 \\ \left[1+K_{12}\right]\,e^{-\gamma_1 d_1-\gamma_2(z-d_1)}; & z \ge d_1 \end{cases} \qquad \ldots(4.22)$$

where, $\alpha_2 = \dfrac{\gamma_1}{\sigma_1\left[1-K_{12}e^{-2d_1\gamma_1}\right]}$; $\gamma_1 = (i\,\omega\,\mu_o\sigma_1)^{1/2}$ is the propagation constant in first layer; σ_1 and d_1 being the conductivity and thickness of the first layer, respectively; $K_{12} = \left[\sqrt{\sigma_1} - \sqrt{\sigma_2}\right] \Big/ \left[\sqrt{\sigma_1} + \sqrt{\sigma_2}\right]$ is the reflection coefficient at the interface between first layer and half-space of conductivity σ_2.

ii) Three-layer Case

For three-layer Earth model, the electric and magnetic fields in any layer can be derived from their governing differential equations. Therefore, it is possible to express the ratio E(z,T)/H(0,T) in each layer as

$$\frac{E(z,T)}{H(0,T)} = \alpha_3 \begin{cases} e^{-\gamma_1 z}\left[1+ e^{-2\gamma_1(d_1-z)}R_1\right]; & 0 \le z \le H_1 \\ \dfrac{\left[1+K_{12}\right] e^{-\left[\gamma_2(z-d_1)+ \gamma_1 d_1\right]} \left[1+K_{23}\, e^{-2\gamma_2(H_2-z)}\right]}{\left[1 + K_{12}\, K_{23}\, e^{-2\gamma_2 d_2}\right]} & ; H_1 \le z \le H_2 \\ \dfrac{\left[1+K_{12}\right]\left[1+K_{23}\right] e^{-\left[\gamma_3(z-H_2)+ \gamma_2 d_2+ \gamma_1 d_1\right]}}{\left[1 + K_{12}\, K_{23}\, e^{-2\gamma_2 d_2}\right]} & ; H_2 \le z \end{cases} \quad \ldots(4.23)$$

where $R_1 = \dfrac{\left[K_{12} + K_{23}\, e^{-2\gamma_2 d_2}\right]}{\left[1 + K_{12}\, K_{23}\, e^{-2\gamma_2 d_2}\right]}$; $\alpha_3 = \dfrac{\gamma_1}{\sigma_1\left[1-R_1\, e^{-2\gamma_1 d_1}\right]}$; σ_1, σ_2, σ_3 are the conductivities of successive layers. The d_1 and d_2, respectively are the first and second layer thicknesses. The H_1 and H_2,

respectively are the depth from Earth surface to first and second interfaces. K_{12} and K_{23}, respectively are the reflection coefficients at the interfaces between first and second layer; and between second layer and half-space.

iii) Exponentially Increasing Vertical Conductivity Profile

For exponentially increasing vertical conductivity profile $\sigma(z)$, the electric and magnetic fields at any depth inside the Earth can be derived from their governing differential equations given in Chapter-II. Therefore, it is possible to express the ratio E(z,T)/H(0,T) in each layer as following

$$\frac{E(z,T)}{H(o,T)} = -\left[\frac{\gamma_o}{\sigma_o}\right] \frac{\left[\overline{Ker}_o(y) + i\, Kei_o(y)\right]}{\left[\overline{Kei}_1(x) - i\, Ker_1(x)\right]} \qquad \ldots(4.24)$$

where, γ_o is propagation constant in surface layer of conductivity σ_o; Ker_n and Kei_n (n = 0,1) are nth order Thomson (or Kelvin) functions corresponding to nth order modified Bessel function of the second kind; $x = \frac{2}{p}\left[\omega\, \mu_o \sigma_o\right]^{1/2}$ and $y = \frac{2}{p}\left[\omega\, \mu_o \sigma_o\, e^{pz}\right]^{1/2}$. In equation 4.21, when values are substituted for surface impedance Z(o,T) (given by equation 2.47 in Chapter II) and for ratio $\frac{E(z,T)}{H(o,T)}$, given by equation 4.24, gives the desired Frechet derivative for exponentially increasing vertical conductivity profile $\sigma(z)$.

iv) Exponentially Decreasing Vertical Conductivity Profile

For exponentially decreasing vertical conductivity profile $\sigma(z)$, the electric and magnetic fields at any depth inside the Earth can be derived from their governing differential equations given in Chapter-II.

Therefore, it is possible to express the ratio E(z,T)/H(0,T) in each layer as following

$$\frac{E(z,T)}{H(o,T)} = -\left[\frac{\gamma_o}{\sigma_o}\right] \frac{\left[ber_o(y) + i\, bei_o(y)\right]}{\left[bei_1(x) - i\, ber_1(x)\right]} \qquad \ldots(4.25)$$

where, γ_o is the propagation constant in surface layer of conductivity σ_o; ber_n and bei_n (n = 0,1) are nth order Thomson (or Kelvin) functions corresponding to nth order modified Bessel function of the first kind; $x = \frac{2}{p}\left[\omega\, \mu_o \sigma_o\right]^{1/2}$ and $y = \frac{2}{p}\left[\omega\, \mu_o \sigma_o\, e^{-pz}\right]^{1/2}$. In equation 4.21, when values are substituted for surface impedance Z(o,T) (given by equation 2.58 in Chapter II) and for ratio $\frac{E(z,T)}{H(o,T)}$, given by equation 4.25, gives the desired Frechet derivative for exponentially decreasing vertical conductivity profile $\sigma(z)$.

4.3.4 Derivation of Sensitivity Functions in Time-domain

The transfer functions in time-domain have been derived theoretically or calculated numerically in Chapter-II, section 2.4 for various Earth models. For variations in time-domain sensitivity functions, based on equations 4.14 and 4.15, and following the analogy with frequency-domain sensitivity functions, the apparent conductivity functions have been used to represent the data. The apparent resistivity for step and impulse response functions are defined in Chapter-III, section 3.3 ii). On rewriting the apparent conductivity for step and impulse response functions as the reciprocal of apparent resistivity, one obtains

$$\sigma_{as}(t,\sigma) = \frac{\mu_o}{\pi t} R_s^{-2}(t) \qquad \ldots(4.26)$$

and

$$\sigma_{a1}(t,\sigma) = \frac{\mu_o}{4\pi t^3} \cdot R_1^{-2}(t) \qquad \ldots(4.27)$$

where, t is delay-time; $R_s(t)$ and $R_i(t)$ are step and impulse response functions for any one-dimensional Earth model.

Equations 4.26 and 4.27 relate small changes in apparent conductivities to small changes in corresponding response functions through the equations

$$\delta\sigma_{as}(t) = \frac{\mu_o}{\pi t} R_s^{-3}(t)\, \delta R_s(t) \qquad \ldots(4.28)$$

and

$$\delta\sigma_{a1}(t) = \frac{\mu_o}{4\pi t^3} R_i^{-3}(t)\, \delta R_i(t) \qquad \ldots(4.29)$$

The small changes in step and impulse response functions are related to small changes in vertical conductivity profile and thus define the Frechet derivatives in time-domain for both step response and impulse response functions, respectively. One point to bear in mind is that each of $\delta R_s(t)$ and $\delta R_i(t)$ will have expression containing integral, the same way as $\delta Z(\omega)$. Only integrand of the expression has to be used according to the definition of sensitivity function. These relationships are either determined theoretically or numerically, following the same approach as has been applied to obtain $R_s(t)$ and $R_i(t)$ in Chapter-II, section 2.4. On substituting, for $R_s(t)$ and $R_i(t)$ (from Chapter-II, section 2.4) and for $\delta R_s(t)$ and $\delta R_i(t)$, which have also been determined theoretically or numerically in following sections for various one-dimensional Earth models, into the equations 4.28 and 4.29, the general expressions for any one-dimensional Earth model is obtained.

i) Two-layer Earth Model

The expressions for step and impulse response functions for two layer model are given (Gomez-Trevino 1987b, Kunetz 1972) in Chapter II, section 2.4.1 ii). The expressions for small perturbation (δR_s and δR_i), in step and impulse response functions, can be derived by the same way as response functions themselves have been. These are given as

$$\delta R_s(t) = -\sqrt{\frac{\pi}{2}}\,\vartheta_1^2 \int_o^\infty \begin{cases} (\text{Srs21})\ \delta\sigma(z)\,dz; & 0 \le z \le d_1 \\ (\text{Srs22})\ \delta\sigma(z)\,dz; & z \ge d_1 \end{cases} \qquad \ldots(4.30)$$

and

$$\delta R_i(t) = -\sqrt{\frac{\pi}{2}}\,\frac{\vartheta_1^2}{2t} \int_o^\infty \begin{cases} (\text{Sri21})\ \delta\sigma(z)\,dz; & 0 \le z \le d_1 \\ (\text{Sri22})\ \delta\sigma(z)\,dz; & z \ge d_1 \end{cases} \qquad \ldots(4.31)$$

where $\vartheta_1 = \sqrt{\frac{2}{\pi}}\,\frac{1}{\delta_{dd}\,\sigma_1}$, $\delta_{dd} = (2t/\mu_o\sigma_1)^{1/2}$, $\zeta_1 = d_1/\delta_{dd}$, Srs2i and Sri2i (i=1,2) are the respective sums of the series involved inside the integration in δR_s and δR_i. These are given as

$$\text{Srs21} = \sum_{n=1}^{\infty} nK_{12}^{n-1}\left[u_1 \exp(-u_1^2/2) + 2K_{12}\,v_1 \exp(-v_1^2/2) + K_{12}^2 w_1 \exp(-w_1^2/2)\right] \qquad \ldots(4.32)$$

$$\text{Srs22} = \sum_{n=1}^{\infty} nK_{12}^{n-1}\left[(1+K_{12})^2\,u_2 \exp(-u_2^2/2)\right] \qquad \ldots(4.33)$$

$$\text{Sri21} = \sum_{n=1}^{\infty} nK_{12}^{n-1}\left[(u_1^2-3)\,u_1 \exp(-u_1^2/2) + 2K_{12}(v_1^2-3)\,v_1 \exp(-v_1^2/2) + K_{12}^2(w_1^2-3)\,w_1 \exp(-w_1^2/2)\right] \qquad \ldots(4.34)$$

$$Sri22=\sum_{n=1}^{\infty} nK_{12}^{n-1}\left[(1+K_{12})^2\, u_2(u_2^2-3)\exp(-u_2^2/2)\right] \qquad ...(4.35)$$

The auxiliary functions u_1, v_1, w_1 and u_2 appeared in equations 3.34-3.37 are

$$u_1 = \frac{2[(n-1)d_1 + z]}{\delta_{dd}}\ ;\ v_1 = 2\left[\frac{nd_1}{\delta_{dd}}\right];\ v_1 = 2\left[\frac{(n+1)d_1 - z}{\delta_{dd}}\right];\quad \text{and}$$

$$u_2 = 2\left[\frac{nh_1 + (z-d_1)\sqrt{\sigma_2/\sigma_1}}{\delta_{dd}}\right]$$

ii) Three-layer Earth Model

The expressions and method of derivation for step and impulse response functions for three layer model are derived in Chapter II, section 2.4.2 ii). The expressions for small perturbations, δR_s and δR_i, in step and impulse response functions can be derived by the same way as response functions themselves have been. These are given as

$$\delta R_s(t) = -\sqrt{\frac{\pi}{4t}}\,\vartheta_1^2 \int_o^{\infty} \begin{cases} (Srs31)\ \delta\sigma(z)\,dz; & 0 \le z \le d_1 \\ (Srs32)\ \delta\sigma(z)\,dz; & d_1 \le z \le H_2 \\ (Srs33)\ \delta\sigma(z)\,dz; & z \ge H_2 \end{cases} \qquad ...(4.36)$$

and

$$\delta R_i(t) = -\sqrt{\frac{\pi}{4t}}\,\frac{\vartheta_1^2}{2t} \int^{\infty} \begin{cases} (Sri31)\ \delta\sigma(z)\,dz; & 0 \le z \le d_1 \\ (Sri32)\ \delta\sigma(z)\,dz; & d_1 \le z \le H_2 \\ (Sri33)\ \delta\sigma(z)\,dz; & z \ge H_1 \end{cases} \qquad ...(4.37)$$

where, Srs3i and Sri3i (i=1,2,3) are the respective sums of the series involved inside the integration in δR_s and δR_i. These are

given as

$$Srs31 = n\sum_{n=1}^{\infty}\left[\sum_{r=0}^{n-1}\sum_{s=0}^{\infty} f_{11}\sqrt{\alpha_{11}}\exp(\frac{\alpha_{11}}{4t}) + 2n\sum_{r=0}^{n}\sum_{s=0}^{\infty} f_{12}\sqrt{\alpha_{12}}\right.$$

$$\left.\exp(-\frac{\alpha_{12}}{4t}) + n\sum_{r=0}^{n+1}\sum_{s=0}^{\infty} f_{13}\sqrt{\alpha_{13}}\exp(-\frac{\alpha_{13}}{4t})\right] \quad \ldots(4.38)$$

$$Srs32 = (1+K_{12})^2\sum_{m=1}^{\infty}\sum_{n=1}^{\infty}(-1)^{m+1}\, mn\sum_{r=0}^{n-1}\sum_{s=0}^{\infty} C_1\{(n-1),r\}$$

$$C_2\{-(n-1),s\}\, K_{12}^{m+n-2}\, K_{23}^{m-1}\left[\sqrt{\alpha_{21}}\exp(\frac{\alpha_{21}}{4t}) + \right.$$

$$\left.K_{23}^2\sqrt{\alpha_{22}}\exp(\frac{\alpha_{22}}{4t}) + 2K_{23}\sqrt{\alpha_{23}}\exp(\frac{\alpha_{23}}{4t})\right]; \quad \ldots(4.39)$$

$$Srs33 = (1+K_{12})^2(1+K_{23})^2\sum_{m=1}^{\infty}\sum_{n=1}^{\infty}(-1)^{m+1}\, K_{12}^{m+n-2}\, K_{23}^{m-1}\sum_{r=0}^{n-1}\sum_{s=0}^{\infty}$$

$$\left[C_1\{(n-1),r\}\, C_2\{-(n-1),s\}\sqrt{\alpha_{31}}\exp(\frac{\alpha_{31}}{4t})\right] \quad \ldots(4.40)$$

$$Sri31 = n\sum_{n=1}^{\infty}\left[\sum_{r=0}^{n-1}\sum_{s=0}^{\infty} f'_{11}\sqrt{\alpha_{11}}\exp(\frac{\alpha_{11}}{4t}) + 2n\sum_{r=0}^{n}\sum_{s=0}^{\infty} f'_{12}\sqrt{\alpha_{12}}\right.$$

$$\left.\exp(-\frac{\alpha_{12}}{4t}) + n\sum_{r=0}^{n+1}\sum_{s=0}^{\infty} f'_{13}\sqrt{\alpha_{13}}\exp(-\frac{\alpha_{13}}{4t})\right] \quad \ldots(4.41)$$

$$Sri32 = (1+K_{12})^2\sum_{m=1}^{\infty}\sum_{n=1}^{\infty}(-1)^{m+1}\, mn\sum_{r=0}^{n-1}\sum_{s=0}^{\infty} C_1\{(n-1),r\}$$

$$C_2\{-(n-1),s\}\, K_{12}^{m+n-2}\, K_{23}^{m-1}\left[\sqrt{\alpha_{21}}\exp(\frac{\alpha_{21}}{4t})\,(\frac{\alpha_{21}}{2t}3)+\right.$$

$$\left.K_{23}^2\sqrt{\alpha_{22}}\exp(\frac{\alpha_{22}}{4t})\,(\frac{\alpha_{22}}{2t}3) + 2K_{23}\sqrt{\alpha_{23}}\exp(\frac{\alpha_{23}}{4t})\,(\frac{\alpha_{23}}{2t}-3)\right]$$

$$\ldots(4.42)$$

$$Sr133 = (1+K_{12})^2(1+K_{23})^2 \sum_{m=1}^{\infty} \sum_{n=1}^{\infty} (-1)^{m+1} K_{12}^{m+n-2} K_{23}^{m-1}$$

$$\sum_{r=0}^{n-1} \sum_{s=0}^{\infty} \left[C_1\{(n-1),r\}\, C_2\{-(n-1),s\}\, \sqrt{\alpha_{31}}\, \exp\left(\frac{\alpha_{31}}{4t}\right) \left(\frac{\alpha_{31}}{2t} - 3\right) \right]$$

...(4.43)

The auxiliary functions, appeared in equations 3.38-3.44, are given as

$$f_{11} = K_{12}^{n-1}\, C_1((n-1),r)\, C_2(-(n-1),s);$$

$$f_{12} = K_{12}^{n-1}\, C_1((n-1),r)\, C_2(-(n-1),s);$$

$$f_{13} = K_{12}^{n-1}\, C_1((n-1),r)\, C_2(-(n-1),s);$$

$$f'_{11} = K_{12}^{n-1}\, C_1((n-1),r)\, C_2(-(n-1),s)\, \left(\frac{\alpha_{11}}{2t} - 3\right);$$

$$f'_{12} = K_{12}^{n-1}\, C_1((n-1),r)\, C_2(-(n-1),s)\, \left(\frac{\alpha_{12}}{2t} - 3\right);$$

$$f'_{13} = K_{12}^{n-1}\, C_1((n-1),r)\, C_2(-(n-1),s)\, \left(\frac{\alpha_{13}}{2t} - 3\right);$$

$$\alpha_{11} = \left[2\sqrt{\mu_o \sigma_1} \left\{ (n-1)d_1 + z + (r+s)\, d_2 \sqrt{\sigma_2/\sigma_1} \right\} \right]^2;$$

$$\alpha_{12} = \left[2\sqrt{\mu_o \sigma_1} \left\{ nd_1 + z + (r+s)\, d_2 \sqrt{\sigma_2/\sigma_1} \right\} \right]^2$$

$$\alpha_{13} = \left[2\sqrt{\mu_o \sigma_1} \left\{ (n+1)d_1 + z + (r+s)\, d_2 \sqrt{\sigma_2/\sigma_1} \right\} \right]^2;$$

$$\alpha_{21} = \left[2\sqrt{\mu_o \sigma_1} \left\{ (m+r+s-1)d_2\sqrt{\sigma_2/\sigma_1} + nd_1 - (z-d_1) \sqrt{\sigma_2/\sigma_1} \right\} \right]^2;$$

$$\alpha_{22} = \left[2\sqrt{\mu_o \sigma_1} \left\{ (m+r+s+1)d_2\sqrt{\sigma_2/\sigma_1} + nd_1 - (z-d_1) \sqrt{\sigma_2/\sigma_1} \right\} \right]^2;$$

$$\alpha_{23} = \left[2\sqrt{\mu_o \sigma_1} \left\{ (m+r+s)d_2\sqrt{\sigma_2/\sigma_1} + nd_1 \right\} \right]^2; \text{ and}$$

$$\alpha_{31} = \left[2\sqrt{\mu_o \sigma_1} \left\{ (m+r+s)d_2\sqrt{\sigma_2/\sigma_1} + nd_1 + (z-d_1-d_2\sqrt{\sigma_3/\sigma_1} \right\} \right]^2;$$

iii) Exponentially Increasing Vertical Conductivity profile

The determination of small perturbation in terms of $\delta R_s(t)$ and $\delta R_i(t)$ have been accomplished by numerical means, for exponentially increasing conductivity models. The method of numerical determination for both step and impulse response functions or perturbation in them have been described in Chapter II. Numerically determined values of response functions and perturbations in thereof, when substituted in corresponding equations 4.28 and 4.29 give the desired sensitivity functions for exponentially decreasing conductivity models.

iv) Exponentially Decreasing Vertical Conductivity profile

For this case also, the determination of response functions and perturbations in them have been carried out numerically. Numerically determined values of response functions and perturbations in thereof, when substituted in corresponding equations 4.28 and 4.29 give the desired sensitivity functions for exponentially decreasing conductivity models.

4.4 Results and Discussion

The behaviour of sensitivity functions inside and on the surface of the Earth is important in understanding the conductivity variations. In order to understand the behaviour of the sensitivity functions, detailed sensitivity analysis have been carried out over various Earth models in both frequency and time-domains. The fractional and normalized sensitivity functions have been computed using equations 4.14 and 4.15.

The skin depth or diffused depth (scaled by $1/\sqrt{2\pi}$), which is (nearly 1590 m) in each domain, have been used to serve as the factor of normalization. Both of them have been computed, for all stratified Earth models, in a layer of uniform resistivity 100 Ω-m at period T=0.1 sec or delay-time t=0.1 sec, respectively. The fractional sensitivity functions with real depth, and normalized sensitivity functions with normalized depth are illustrated graphically. The value of sensitivity function (normalized or fractional) at any depth have been referred as 'sensitivity' in following sections. The effect of resistivity and thickness of layers on sensitivity functions has been studied for various Earth models.

4.4.1 Two-layer Models

The normalized sensitivity functions over two-layer Earth models; for real, imaginary and amplitude parts in frequency-domain; and for step and impulse responses in time-domain are shown with normalized depth in Figures 4.1, 4.2 (for frequency-domain) and in Figure 4.3 (for time-domain), respectively. These sensitivity functions have been compared with the model of homogeneous half-space of uniform resistivity 100 Ω-m. The Figures 4.1a-4.1c (frequency-domain) and 4.3a-4.3b (time-domain) show sensitivity functions for variable overburden resistivity (ρ_1 = 25, 50, 200 and 1000 Ω-m) at constant thickness (d_1 = 6000 m). The Figures 4.1d-4.1f (frequency-domain) and 4.3c-4.3d (time-domain) show sensitivity functions for variable thickness (d_1 = 6000, 3000, 750 and 150 m) of conductive overburden at constant resistivity (ρ_1 = 25 Ω-m). The conductance values of overburden, for models with varying overburden resistivity at constant thickness (Figures 4.1a-4.1c and 4.3a-4.3b) and for models with varying thickness

of conductive overburden at constant resistivity (Figures 4.1d-4.1f and 4.3c-4.3d) respectively are 240, 120, 30 and 6 mhos. The Figures 4.2a-4.2c show the real, imaginary and amplitude parts of sensitivity functions, respectively, for variable thickness (d_1) of resistive overburden at constant resistivity 1000 Ω-m.

i) Frequency-domain

In general, each curve in Figures 4.1 and 4.2 show the maximum sensitivity on the Earth surface and minimum inside the Earth. In particular, the real parts of sensitivity functions for conductive overburden having thickness greater than 3000 m (Figures 4.1a and 4.1d) show the maximum sensitivity at depths close to the surface of the Earth; and characteristically the imaginary parts show minimum sensitivity (negative side lobes) at intermediate depths.

The effect of variations in resistivity of overburden on sensitivity functions is shown in Figures 4.1a-4.3c. On increasing overburden resistivity from 25 to 1000 Ω-m, two features are noticed. First- the sensitivity is found to decrease on and near the surface of the Earth. Second- the flattening of sensitivity functions along the depth is seen. Both the features are pronounced as long as overburden is more conductive than lower half-space. Moreover, the comparison of sensitivity functions for two-layer Earth models (shown by dotted curves in Figures 4.1a-4.1c) with the homogeneous half-space model (shown by solid curves in Figures 4.1a-4.1c) shows that from the surface of the Earth to shallow depths, the sensitivity function for conductive overburden is always higher than the homogeneous half-space model whereas, for resistive overburden it is always lower than the homogeneous half-space model.

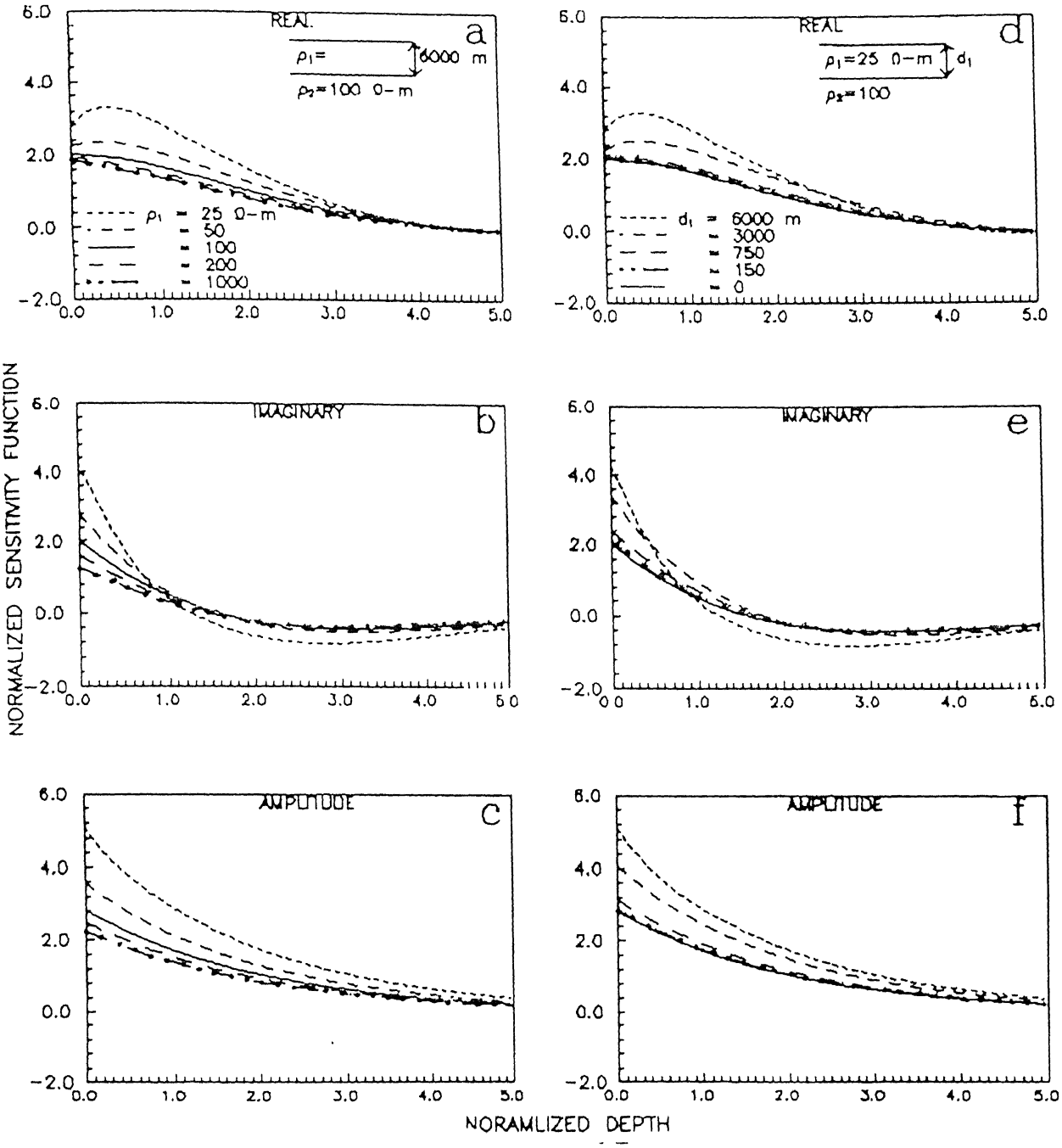

Figure 4.1 The behaviour of normalized sensitivity functions over two-layer models in frequency-domain i) for variable overburden resistivity at constant thickness (a, b and c); and ii) for variable thickness of conductive overburden at constant resistivity (d, e and f).

The effect of variations in overburden thickness on sensitivity functions when overburden is conductive, is shown in Figures 4.1d-4.1f. On decreasing the overburden thickness from 6000 to 150 m the sensitivity decreases on and near the surface of the Earth. The sensitivity for overburden thickness 150 m is almost similar to that of homogeneous half-space. The nature of sensitivity functions along the normalized depth for variable overburden thickness (Figures 4.1d-4.1f) is found almost similar to the sensitivity functions for variable overburden resistivity (Figures 4.1a-4.1c). The effect of resistivity variations in overburden show high resolution on and near the Earth surface whereas, the thickness variations in overburden show poor resolution.

The effect of variations in the overburden thickness on sensitivity functions for resistive overburden is shown in Figure 4.2. The decrease in the overburden thickness from 6000 to 150 m shows the increase in sensitivity functions from Earth surface to larger depths. However, at deeper places the increase is not highly pronounced. The sensitivity functions for overburden thickness of 750 and 150 m show almost no difference with the sensitivity function for homogeneous half-space Earth model.

It has been found that the sensitivity functions (real, imaginary and amplitude) show characteristic behaviour along the depth. The nature of variations in sensitivity functions reflects the physical properties of the model. The lower resistivity (than the half-space) of the overburden gives rise to an increase in sensitivity on and near the Earth's surface due to strong attenuation of magnetic field in conductive overburden. Locally induced currents in conductive overburden flow parallel to the boundary (between overburden and half-space) which

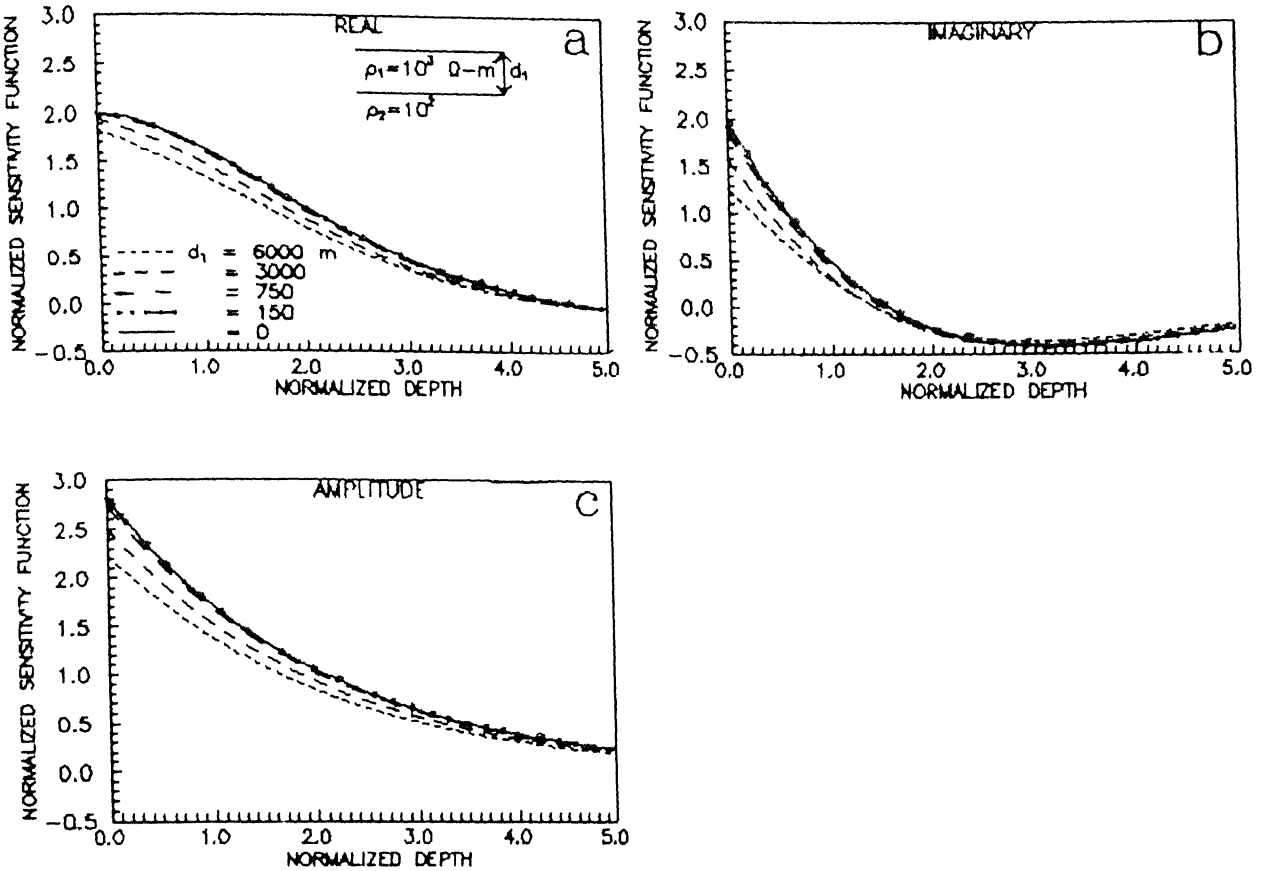

Figure 4.2 The behaviour of normalized sensitivity functions over two-layer models in frequency-domain for variable thickness of resistive overburden at constant resistivity.

results in a higher sensitivity within conductive overburden. Strongly induced current within the conductive overburden reduces the current density in lower half-space and as a result the sensitivity decreases in deeper regions. The presence of resistive overburden induces very little current as the magnetic field is not significantly attenuated within it, which results in a poor sensitivity within resistive overburden. This is shown by variations in sensitivity functions for resistive overburden. The resistive overburden shows lower sensitivity on Earth's surface but the advantage of it is felt by deeper structures, having higher sensitivities than those in case of highly conductive overburden. The effect of decreasing overburden thickness, such that the conductance of overburden attains the same values as they are in case of increasing overburden resistivity, is similar in nature to those of increasing overburden resistivity i.e. a change in overburden thickness is related to a change in resistivity of the overburden. This feature is clearly illustrated in the Figures 4.1d-4.1f and Figure 4.2 which shows that even for smaller thicknesses of conductive and resistive overburden, their sensitivity is always different from the homogeneous half-space model.

ii) Time-domain

The sensitivity variations inside the Earth for two-layer case are shown in Figure 4.3, for both step and impulse responses. The zones of maximum sensitivity function for step response (Figures 4.3a and 4.3c) are observed located inside the Earth. The successive increasing resistivity of overburden is aimed at achieving the larger diffusion depth into subsurface and hence allow more concentration of current to focus at successive larger depths. On the surface of the Earth, the

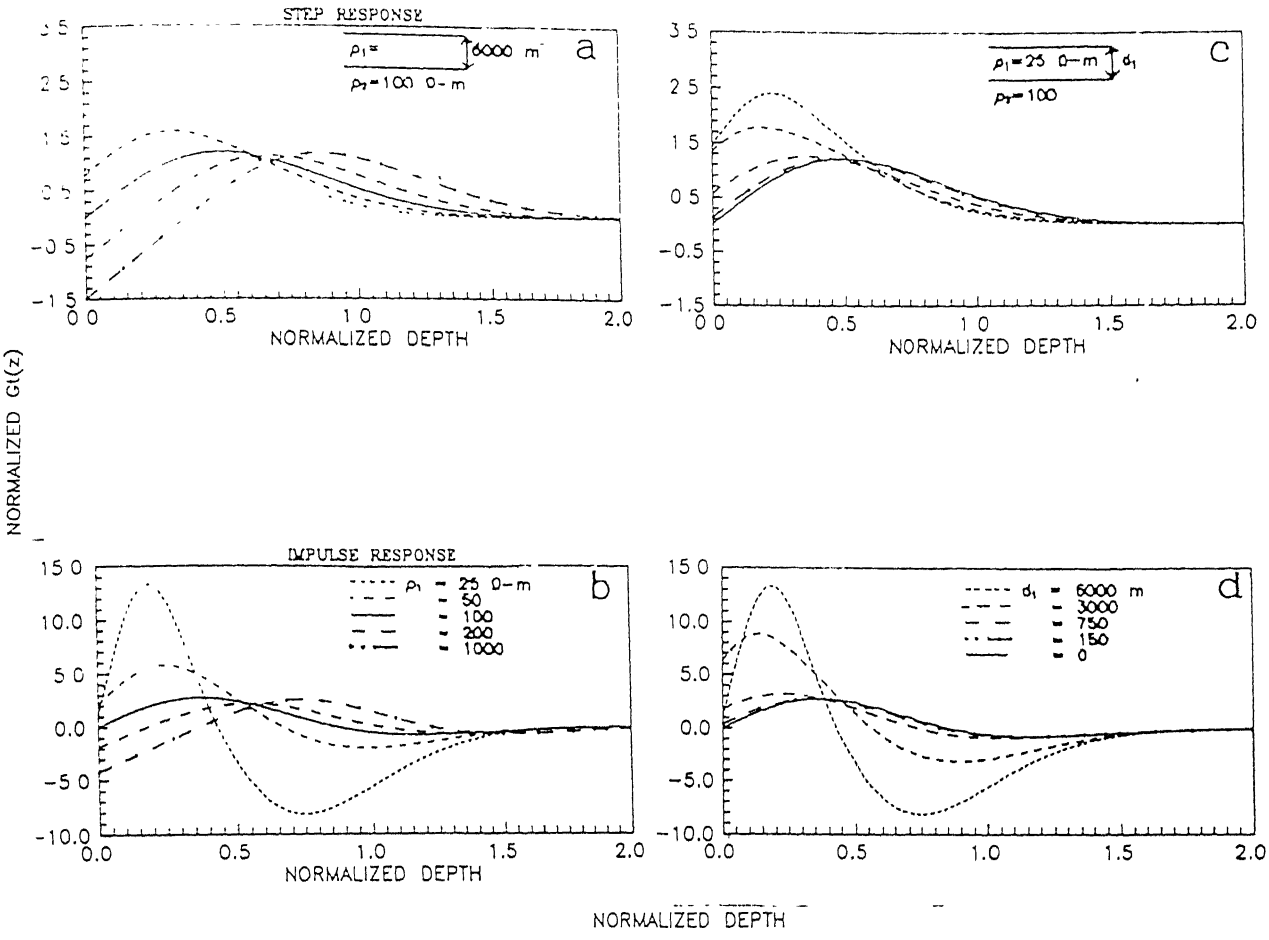

Figure 4.3 The behaviour of normalized sensitivity functions over two-layer models in time-domain i) for variable overburden resistivity at constant thickness (a and b); and ii) for variable thickness of conductive overburden at constant resistivity (c, and d).

sensitivity falls below zero for resistive overburden. The sensitivity functions starting from negative values on the surface of the Earth, for resistive overburden, attain the positive maximum values (which are higher than the value for homogeneous half-space) at certain depth before approaching to zero at larger depth (Figure 4.3a). The decrease in the thickness of conductive overburden (in Figure 4.3c, such that the conductance of the overburden could attain the same values as in case of increasing resistivity) forces more of the induced current to be detained into the overburden, as long as the conductive overburden is quite thick, which causes surfaceward movement of the maximum sensitivity zones and enhances the sensitivity on the surface of the Earth (Figure 4.3c, for d_1= 6000 and 3000 m) compared to their counterpart (Figure 4.3a, for ρ_1=25 and 50 Ω-m). On further decreasing the conductive overburden thickness, the maximum sensitivity moves downward as thinning overburden can not hold the entire induced current which leaks into lower half space. However, the sensitivity decreases on the surface of the Earth on decreasing the thickness of the conductive overburden because the thin conductive layer can not hold the entire induced current and leaks into lower half-space.

In Figures 4.3b and 4.3d, the sensitivity functions associated with impulse response are shown. These sensitivity functions have the same characteristic and demonstrate the mechanism of migration of maximum sensitivity surfaceward and downward as shown in case of step response. The negative side lobes for conductive overburden associated with these functions at depths below the zones of maximum sensitivity, makes it insensitive at those depths and from which it never recovers.

The above discussion suggests that the sensitivity analysis of two-layer Earth models provides a tool to understand its physical

properties and contrasts the electromagnetic responses (i.e. surface impedance, step responses impulse response). The depth dependence of sensitivity functions makes it feasible to see underneath explicitly, and gives a global information of subsurface for the chosen resistivity distribution which is not directly available from comparison of electromagnetic responses.

4.4.2 Three-layer models

The computation of normalized sensitivity (and fractional) functions along the normalized depth (and real depth) for three-layer Earth models have been carried out. A three-layer model is characterized by five parameters: namely ρ_1, d_1, ρ_2, d_2 and ρ_3. Depending upon the resistivity contrast of the layers, four different types of models have been considered:

* K-type models ($\rho_1 < \rho_2 > \rho_3$),
* H-type models ($\rho_1 > \rho_2 < \rho_3$),
* Q-type models ($\rho_1 > \rho_2 > \rho_3$), and
* A-type models ($\rho_1 < \rho_2 < \rho_3$)

The Figures 4.4-4.15 show the behaviour of sensitivity functions (normalized and fractional) in frequency and time-domain. Two cases for each type of model have been considered to study the effect of i) resistivity of intermediate layer and ii) thickness of intermediate layer on normalized sensitivity functions (or fractional sensitivity functions for resistive/conductive thin layer embedding in homogeneous half-space) along the normalized/real depths. The first layer resistivity (ρ_1) and thickness (d_1) are taken to be 100 Ω-m and 500 m,

respectively, for all models. The effects of top layer parameters on the underlying structure have already been analysed in two-layer Earth models. The similar effects have been observed for three-layer Earth models. Therefore, the resistivity and thickness of first layer have not been changed for either model.

4.4.2.1 K-type Models ($\rho_1 < \rho_2 > \rho_3$)

i) Frequency-domain

In Figure 4.4, the behaviour and characteristics of real, imaginary and amplitude parts of normalized sensitivity functions along the normalized depth over K-type of models have been shown. The model consists of first layer parameters as ρ_1= 100 Ω-m and d_1= 500 m; the intermediate layer is taken as 2000 m thick with variable resistivity (ρ_2) of 200, 400 and 800 Ω-m in one case, and resistivity of 200 Ω-m with variable thickness(d_2) 2000, 1000 and 500 m in second case; and the half-space resistivity is taken as 50 Ω-m. The resistivity and thickness parameters of the intermediate layer are varied such that the consecutive conductances of the intermediate layer in both the cases carry the same values. The consecutive conductances of the intermediate layer for both the cases are 10, 5 and 2.5 mhos.

The variations in intermediate layer resistivity is found to have the significant effect on the real, imaginary and amplitude parts (Figure 4.4a-4.4c) of normalized sensitivity functions. This effect on real part is found to be very pronounced and produces maximum sensitivity near the Earth surface. The sensitivity for all parts, in general, decreases on and near the Earth's surface with the increase of resistivity of the intermediate layer. On and near the Earth surface, the imaginary parts of the sensitivity functions do not show much effect

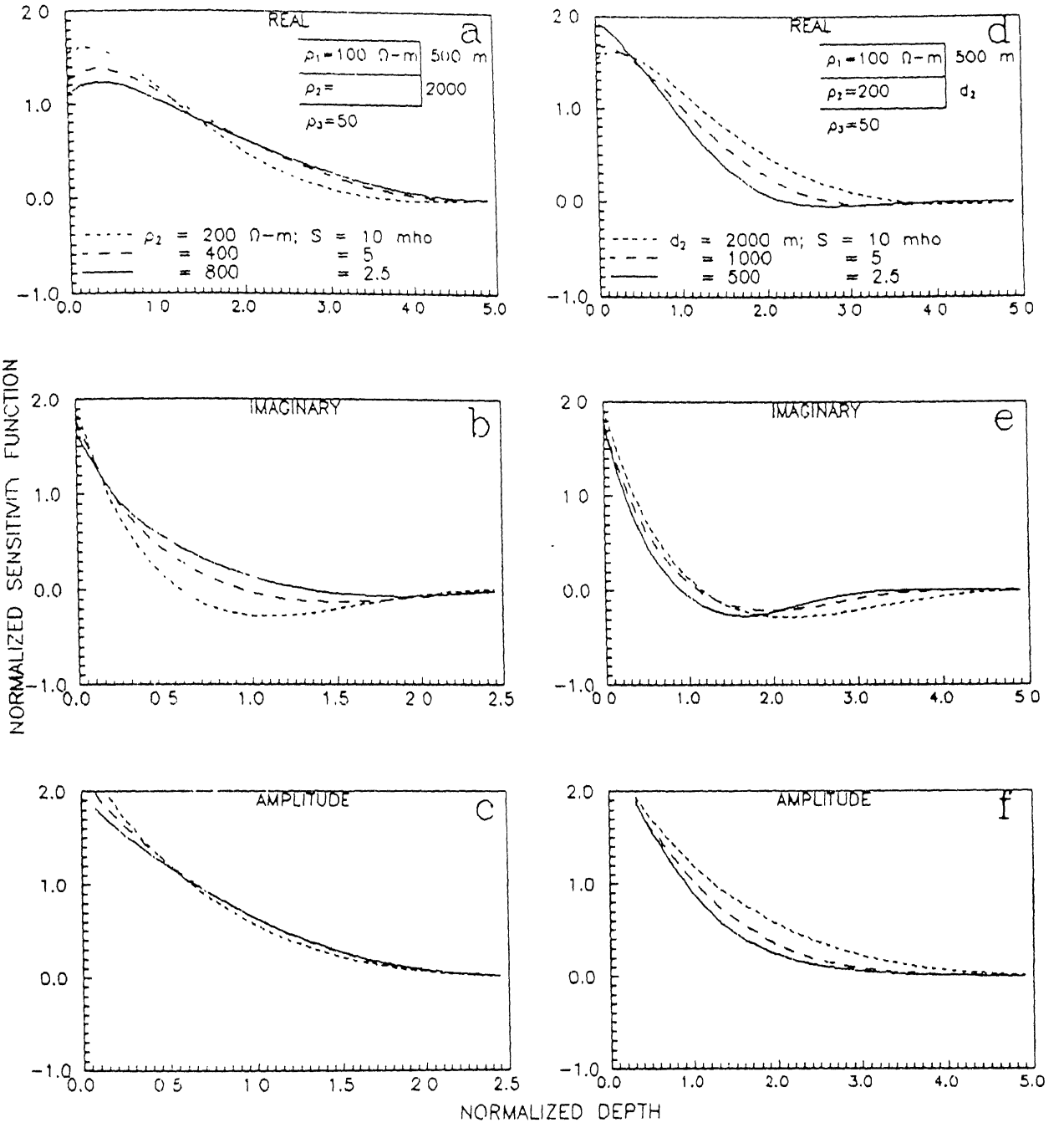

Figure 4.4 The behaviour of normalized sensitivity functions for K-type models in frequency-domain i) for variable intermediate layer resistivity at constant thickness (a, b and c); and ii) for variable intermediate layer thickness at constant resistivity (d, e and f).

for resistivity variations of intermediate layer. At intermediate depths (roughly from 0.7-2.0 skin depth) the sensitivity increases with the increase of resistivity of intermediate layer. The pronounced effect at intermediate depth for the variations of resistivity in intermediate layer is shown by the real and imaginary parts of normalized sensitivity functions. The effect is insignificant in amplitude of normalized sensitivity functions. The imaginary parts of the sensitivity functions show negative lobes characteristically at intermediate depths and are observed prominent only if the resistivity of the intermediate layer is small i.e. resistivity contrast of the three layers is low. At great depths the sensitivity approaches to zero for all variations given to intermediate layer resistivity.

Similar effects of thickness variations in intermediate layer are observed on real (Figure 4.4d), imaginary (Figure 4.4e) and amplitude (Figure 4.4f) parts of normalized sensitivity functions. The values of sensitivity functions on the surface of the Earth are higher for smaller thicknesses of intermediate layer, and smaller at intermediate depths. The variations of imaginary parts of sensitivity functions are quite different than those of real and amplitude parts with negative lobes at intermediate depths. In all the cases, the sensitivity functions approach to zero at great depth (nearly after 2 skin depth). The effect of thickness variations is significantly shown only by real and amplitude parts of sensitivity functions.

Comparison between the two cases suggests that decrease in resistivity of intermediate layer has the same impact on sensitivity characteristics along the depth as the increase in thickness of intermediate layer. On and near the Earth's surface, the sensitivity functions for a set of values for resistivity of intermediate layer are

lower than for a set of values for thickness. The contrast in the sensitivity functions in the former case is more pronounced. However, at intermediate depths the sensitivity functions for a set of values for thickness of intermediate layer have more resolution than for a set of values for resistivity. Moreover, the sensitivity functions for thickness values decays faster than for resistivity values of intermediate layer. Therefore, contribution made by variations in thickness of intermediate layer to electromagnetic response comes more from shallower depths in comparison to variations in resistivity of intermediate layer values.

The variation of real, imaginary and amplitude parts of fractional sensitivity functions along the depth axis are shown in Figure 4.5 over a model that consists of a 80 m thin resistive layer, embedded at 400 m depth in a homogeneous half-space of uniform resistivity 100 Ω-m. The fractional sensitivity functions for two resistivity values of thin layer (the dotted curves) are compared with homogeneous half-space model (solid curves). The dotted curves in Figure 4.5 show the effect on sensitivity functions for increase in resistivity values of thin layer when compared with half-space Earth model (shown by solid curves). The successive falls, within the thin layer, in fractional sensitivity of real and amplitude parts are observed when the resistivity of the thin layer is increased from 300 to 600 Ω-m. However, imaginary parts of sensitivity functions show a slight increase inside the layer which is insignificant. Moreover, an increase in fractional sensitivity at depths above and below the embedded thin resistive layer is observed in real, imaginary and amplitude parts.

Each curve shows a fractional change in electric field due to a set of conductive sources distributed at each depth in host and embedded

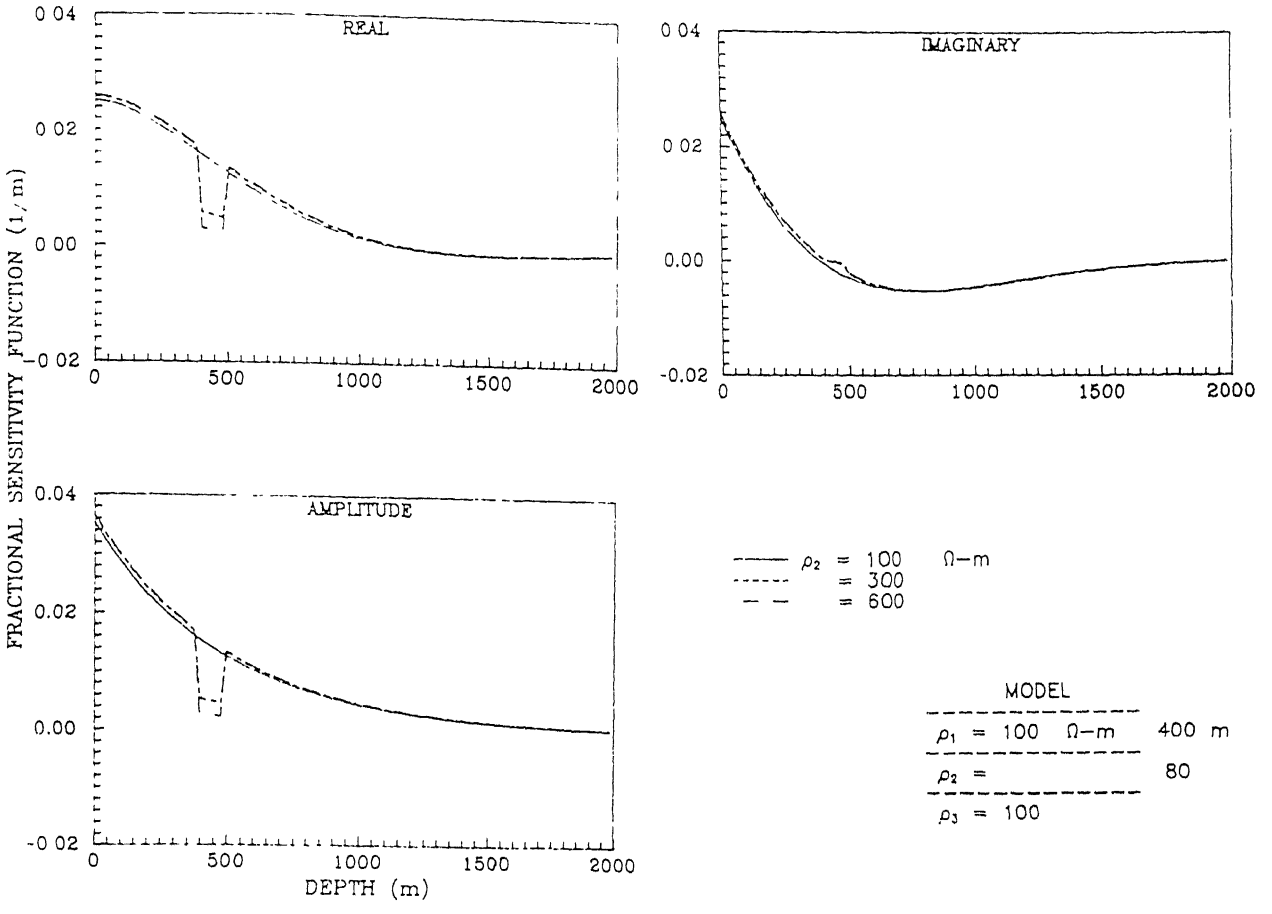

Figure 4.5 The behaviour of fractional sensitivity functions in frequency-domain over a model which consists a thin resistive layer embedded in conducting half-space of uniform resistivity.

media. The electric field over any finite thickness ΔZ is directly proportional to the magnetic field attenuation over ΔZ. The attenuation of magnetic field across the thin layer is inversely proportional to resistivity distribution inside it. Consequently, this results in poor attenuation of magnetic field when the resistivity of thin layer is increased and vice-versa. This implies a low strength electric field which is responsible for a sudden fall in fractional sensitivity.

The regions outside the resistive thin layer become relatively conductive which attract currents from thin layer. This causes the redistribution of current density in such a way that thin layer as carry lower current density than what actually have been induced; and regions outside it carry current density higher than what have actually been induced in these regions. This consequently gives a secondary decrease in fractional sensitivity within the layer and an increase in outside regions. This is in full agreement what have been observed in Figure 4.4.

ii) Time-domain

The variations in normalized sensitivity functions along the normalized depth for both step and impulse responses for various resistivity and thickness values of intermediate layer are shown in Figure 4.6. The characteristics of sensitivity functions for both step and impulse responses below the depth of maxima are similar to the real and imaginary parts of sensitivity functions (Figure 4.4) in frequency-domain.

The maximum sensitivity which occurs inside the Earth, shifts towards the surface and decreases when resistivity of the intermediate layer increases from 200 to 800 ohm-m, however, on the surface of the

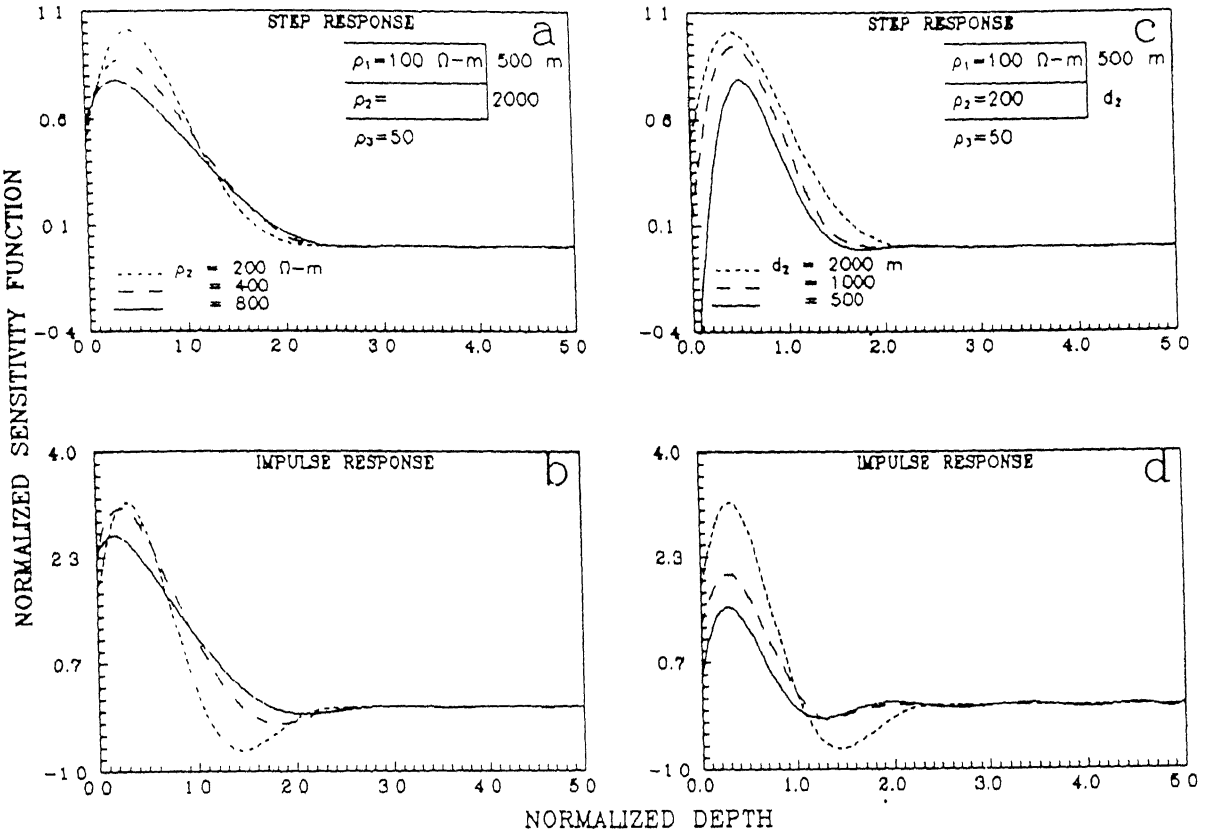

Figure 4.6 The behaviour of normalized sensitivity functions for K-type models in time-domain i) for variable intermediate layer resistivity at constant thickness (a, and b); and ii) for variable intermediate layer thickness at constant resistivity (c and d).

Earth it increases marginally. The successive curves for sensitivity functions, on decreasing thickness of intermediate layer from 2000 m to 500 m, attain lower amplitude at each depth such that a parallel translation is observed. However, migration of maximum sensitivity towards surface for impulse response is observed clearly as the thickness of the intermediate layer decreases. The corresponding sensitivity functions for each conductance (S = 10, 5 and 2.5 mhos in right and left panels, Figure 4.6) exhibit different levels of variations in sensitivity function.

The variations of fractional sensitivity functions with depth for the step and impulse responses are shown in Figure 4.7 for the model which consist a thin resistive layer embedded in the homogeneous half-space of uniform resistivity 100 Ω-m from z = 400 to 480 m. Three curves are plotted in this Figure- dotted curves represent fractional sensitivity for two different resistivities higher than the host half-space (solid) to illustrate the effect of increasing resistivity of thin layer. Two successive increasing values of resistivity of thin layer show that fractional sensitivity functions along the depth for both step and impulse responses exhibit the similar characteristics. The rapid falls in amplitude of sensitivity functions above and within the layer and small rise below it, are observed when compared with host half-space.

The time varying magnetic field which varies in steps and impulses for corresponding step and impulse responses, induces almost no current in resistive thin layer. Therefore, the fall in sensitivity is observed within the thin layer in both step and impulse responses. The characteristics of time-domain response functions which emphasizes the sensitivity, minimum (zero) on Earth's surface and maximum inside the

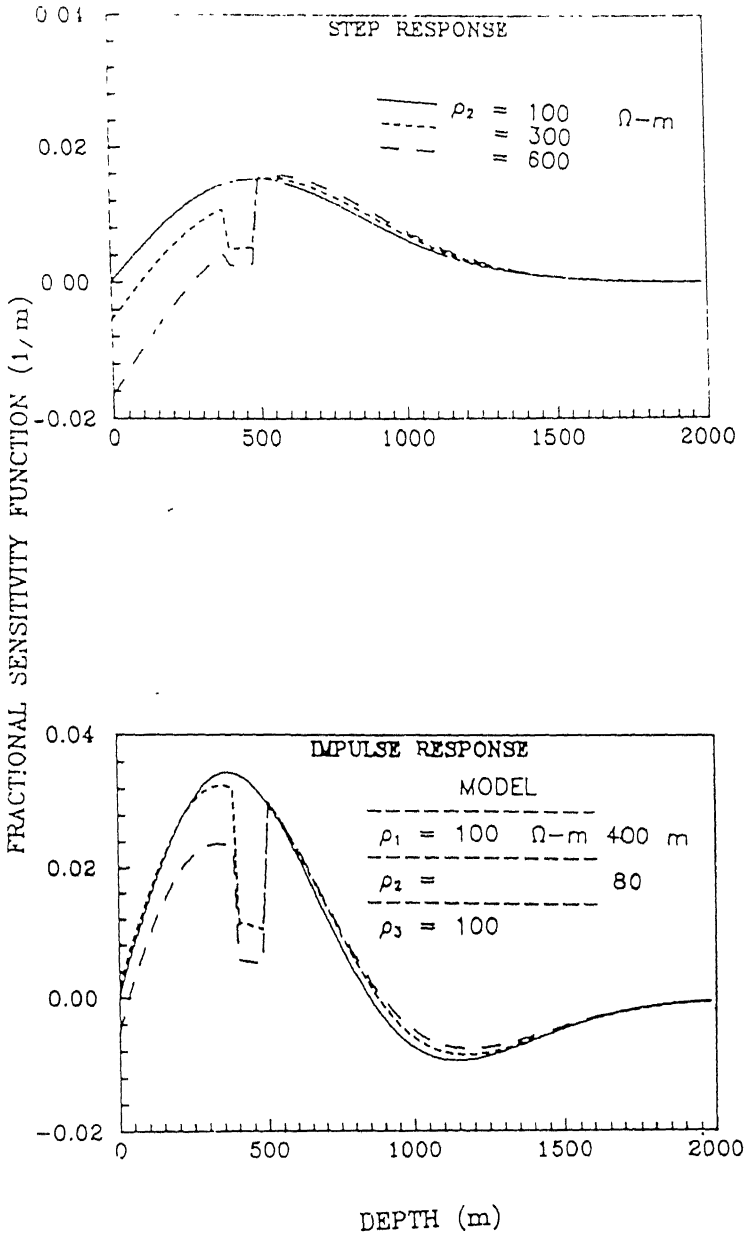

Figure 4.7 The behaviour of fractional sensitivity functions in time-domain over a model which consists a thin resistive layer embedded in conductive half-space of uniform resistivity.

Earth (solid curves for half-space in Figure 4.7) turns out to be more striking in the presence of resistive layer by showing reduction in sensitivity above the layer and increase below the layer. This feature is even more prominent in step response where sensitivity above the layer shows negative values. Thus, the region above thin layer is more transparent to host half-space in case of step response than the case of impulse response.

4.4.2.2 H-Type Models ($\rho_1 < \rho_2 < \rho_3$)

i) Frequency-domain

The effect of resistivity and thickness variations in intermediate layer on normalized sensitivity functions for H - type models are shown in Figure 4.8. The resistivity and thickness of the first layer are taken as 100 Ω-m and 500 m respectively, and the resistivity of the third layer as 200 Ω-m. To study the effect of variations in intermediate layer resistivity and thickness variation, two cases have been considered. In one case variable intermediate layer resistivity of 20, 40 and 80 Ω-m with 2000 m thick and in second case constant resistivity of 20 Ω-m with variable thickness of 500, 1000 and 2000 m have been taken. Under the variations in ρ_2 or d_2, for case first or second, the values of intermediate layer conductance are 100, 50 and 25 mhos.

The maximum sensitivity for both the cases is found on the surface of the Earth for real, imaginary and amplitude parts of normalized sensitivity functions. The effect of the resistivity and thickness variations in intermediate layer is not very well resolved on the surface of the Earth. However, the real part of normalized sensitivity functions show marginally resolved values on changing the resistivity

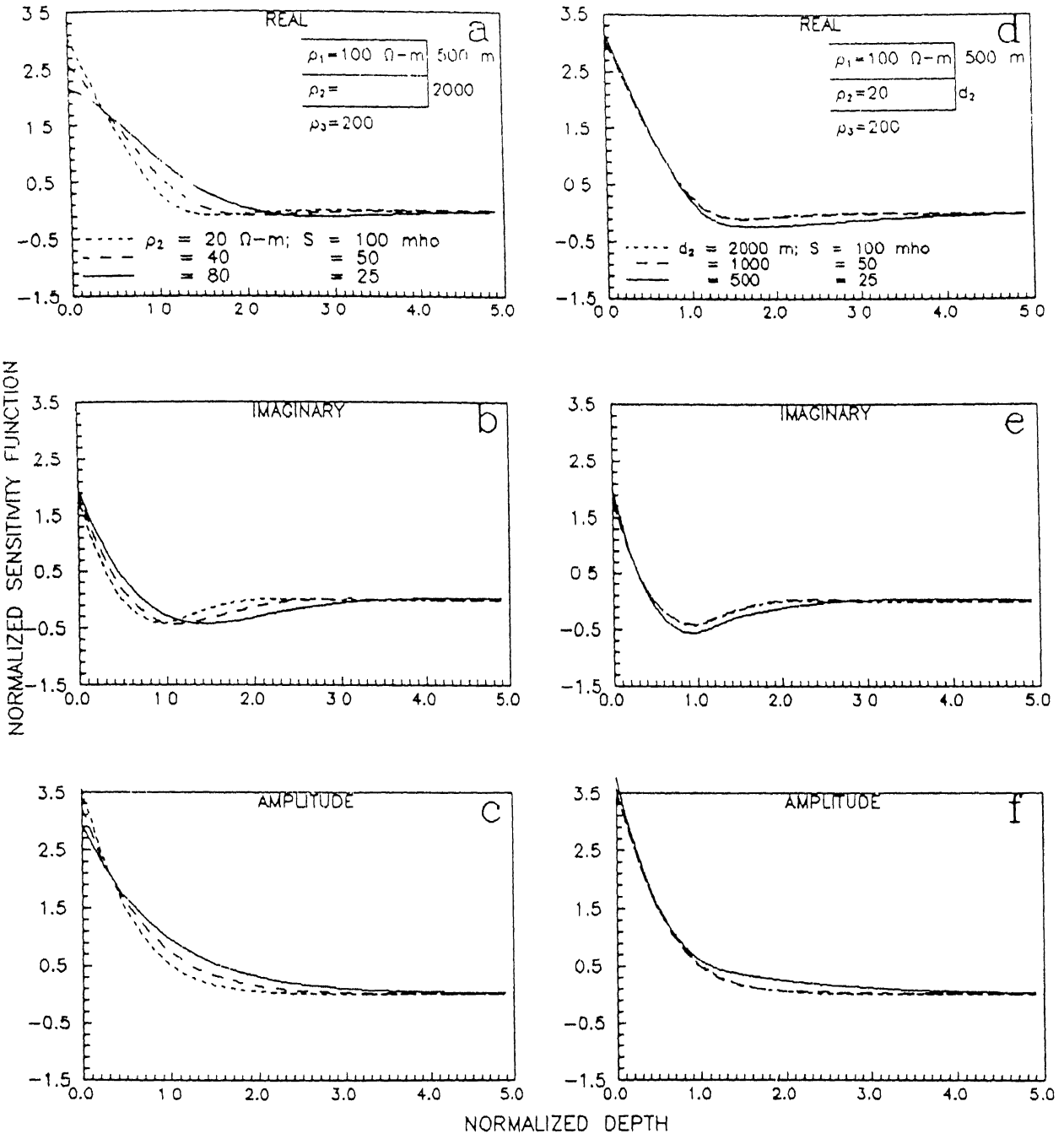

Figure 4.8 The behaviour of normalized sensitivity functions for H-type models in frequency-domain i) for variable intermediate layer resistivity at constant thickness (a, b and c); and ii) for variable intermediate layer thickness at constant resistivity (d, e and f).

of intermediate layer (Figure 4.8a). At intermediate depth the effect of resistivity variation is pronounced in the case of real, imaginary and amplitude parts of sensitivity functions, whereas the effect of thickness variations is not very well pronounced (Figures 4.8d-4.8f). The characteristic negative lobes are observed in the imaginary parts of normalized sensitivity functions. The sensitivity functions are found to fall steeply (Figures 4.8a-4.8c) along the depth with the decrease of resistivity in intermediate layer. The curves for second layer conductance 100, 50 and 25 mho in Figures 4.8a-4.8c have sensitivity different and distinguished from the curves shown in Figures 4.8d-4.8f. On comparison with K-type of models, it has been found that the rate of decrease of sensitivity function is higher for H-type of models i.e. sensitivity decreasing faster in models for intervening conductive layers than the models for intervening resistive layers. It is in full agreement with the fact that the resistive structures show up delaying effect on the signal attenuation when passed through them. This slowness of the magnetic field attenuation in resistive structures allows the corresponding vortex electric field to die at greater depths as compared to conductive structures at a fixed frequency. As far as vertical resolution is concerned on Earth surface, H-type of model show up better, however, followed by the faster rate of fall in sensitivity functions afterward. Therefore, the contribution to the electromagnetic response is made only by limited depths for H-type of models which is generally increased using lower frequency signal. In present case, it is obvious that the layer thickness under consideration is of secondary importance not only due to negligible vertical resolution on the Earth surface but also due to poor vertical resolution at all depths.

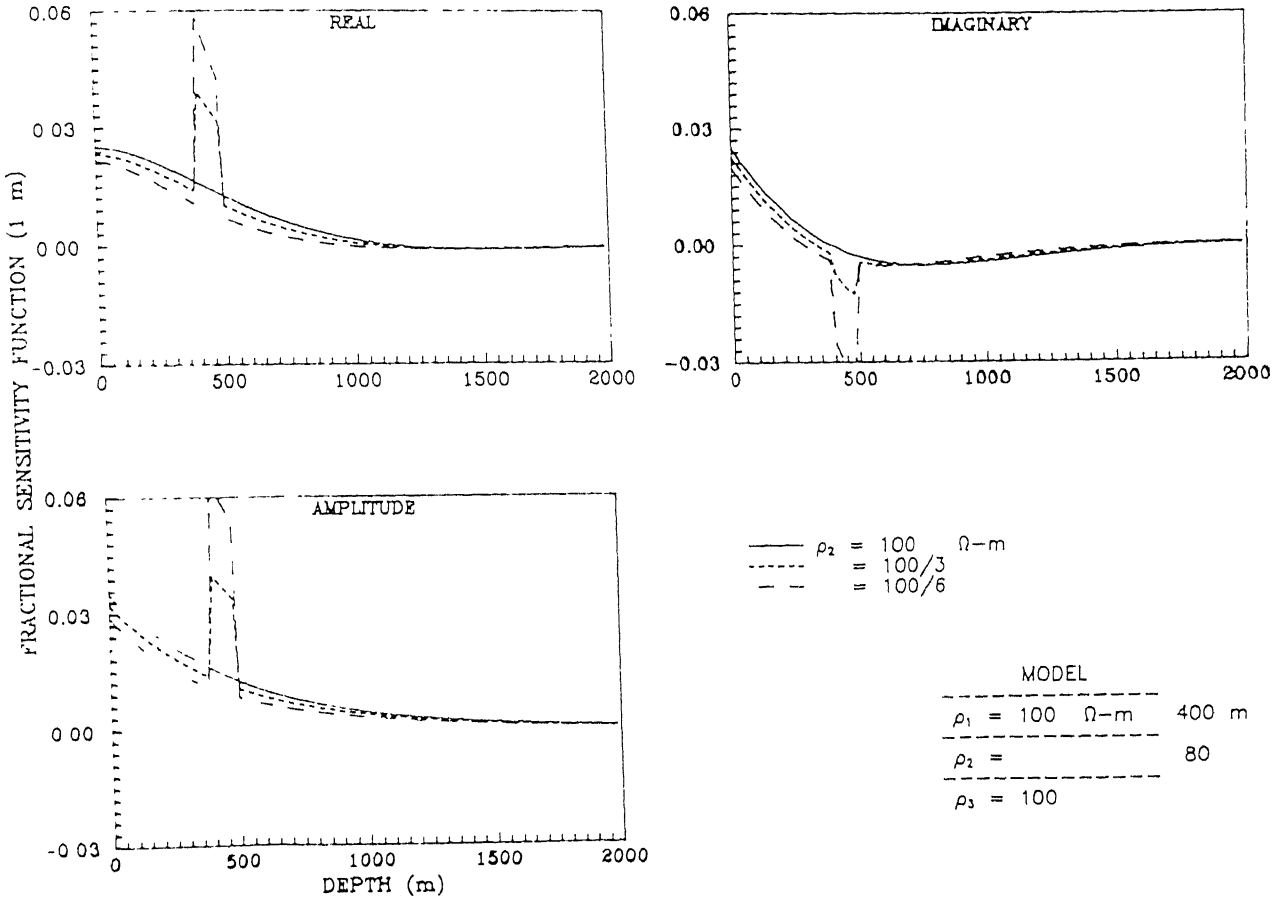

Figure 4.9 The behaviour of fractional sensitivity functions in frequency-domain over a model which consists a thin conductive layer embedded in resistive half-space of uniform resistivity.

Figure 4.9 shows the fractional sensitivity functions along the depth axis for a model in which thin conductive layer is embedded in homogeneous half-space. The fractional sensitivity functions for this case have been computed for conductive thin layer which is 3 and 6 times conductive than those of the host medium. The successive rise in real and amplitude parts of fractional sensitivity functions is observed within the thin layer when resistivity of thin layer decreases from 100 to 100/3 and 100/6 Ω-m, respectively. However, imaginary part shows an increasing trend in the negative direction. A decrease in fractional sensitivity functions at depths above and below the embedded layer is observed in all parts, except in imaginary part of sensitivity function below 750 m depth.

ii) Time-domain

The variations in normalized sensitivity functions with normalized depth for various values intermediate layer resistivity (20, 40 and 80 ohm-m) at fixed thickness (2000 meters) are shown in Figures 4.10a and 4.10b; and for various values of intermediate layer thickness (2000, 1000 and 500 m) at fixed resistivity (20 ohm-m) are shown in Figure 4.10c and 4.10d. On the Earth surface, sensitivity functions show decreasing negative values for both step and impulse responses when resistivity of the intermediate layer increases. The sharp peak of maximum sensitivity function inside the Earth becomes wider and lower in amplitude for step response whereas, it attains higher amplitude for impulse response. The effect of variation of thickness of intermediate layer is almost insignificant for step and impulse responses. It is seen from the Figures 4.10a-4.10d that the curves for the same intermediate layer conductance value have the lower sensitivity when subjected to

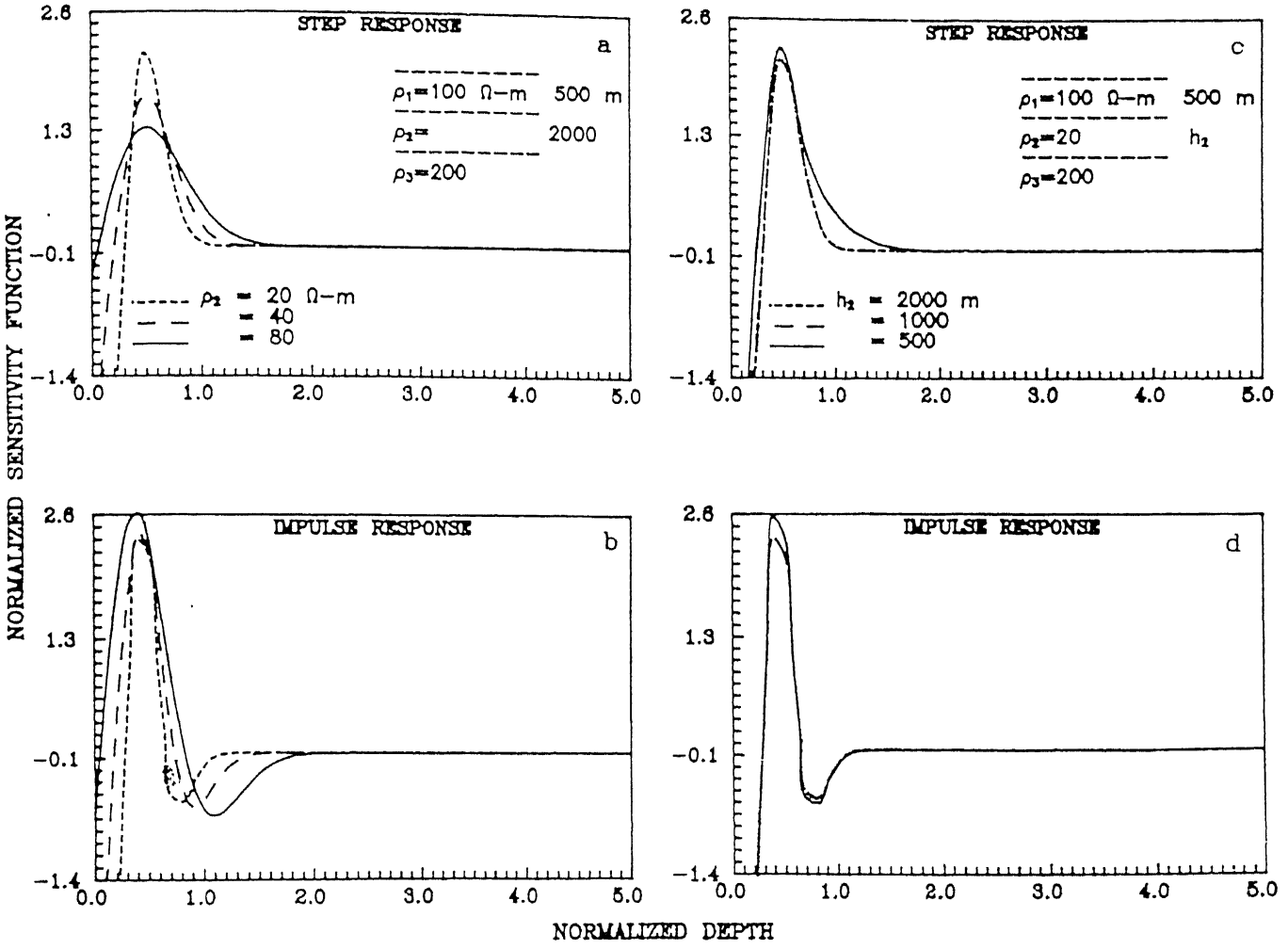

Figure 4.10 The behaviour of normalized sensitivity functions for H-type models in time-domain i) for variable intermediate layer resistivity at constant thickness (a, and b); and ii) for variable thickness of intermediate layer at constant resistivity (c, and d).

changes in resistivity compared to changes in thickness.

The variations of fractional sensitivity functions with the depth for step and impulse responses are shown in Figure 4.11. On decreasing the resistivity of sandwiched layer from 100 Ω-m to 100/3 and to 100/6, an sudden increase in fractional sensitivity within the thin layer is observed in both step and impulse responses, followed by the decrease below the thin layer in both the responses and increase above the thin layer in impulse response only. Therefore, on the surface of the Earth a better vertical resolution is achieved by the conductive intervening layer for impulse response which is not achieved by other response functions under study.

4.4.2.3 Q-Type Models ($\rho_1 > \rho_2 > \rho_3$)

i) Frequency-domain

Two cases of Q-types of models have been considered to study the effect of changes in resistivity and thickness of intermediate layer on the sensitivity function. The model consists of top layer of 100 Ω-m with 500 m thick, the last layer resistivity of 10 Ω-m. The intermediate layer resistivity is varied as 20, 40 and 80 Ω-m with constant thickness of 2000 m in first case, and in the second case the intermediate resistivity is kept constant (20 Ω-m) with variable thickness of 2000, 1000 and 500 m. The corresponding conductance values of intermediate layer is same for the two cases.

The effect of resistivity variations in intermediate layer is seen clearly on the real, imaginary and amplitude parts of sensitivity functions (Figures 4.12a-4.12c). The sensitivity functions are found to be pronounced on the surface of the Earth for real and amplitude parts. All the sensitivity functions show the effect of variations of

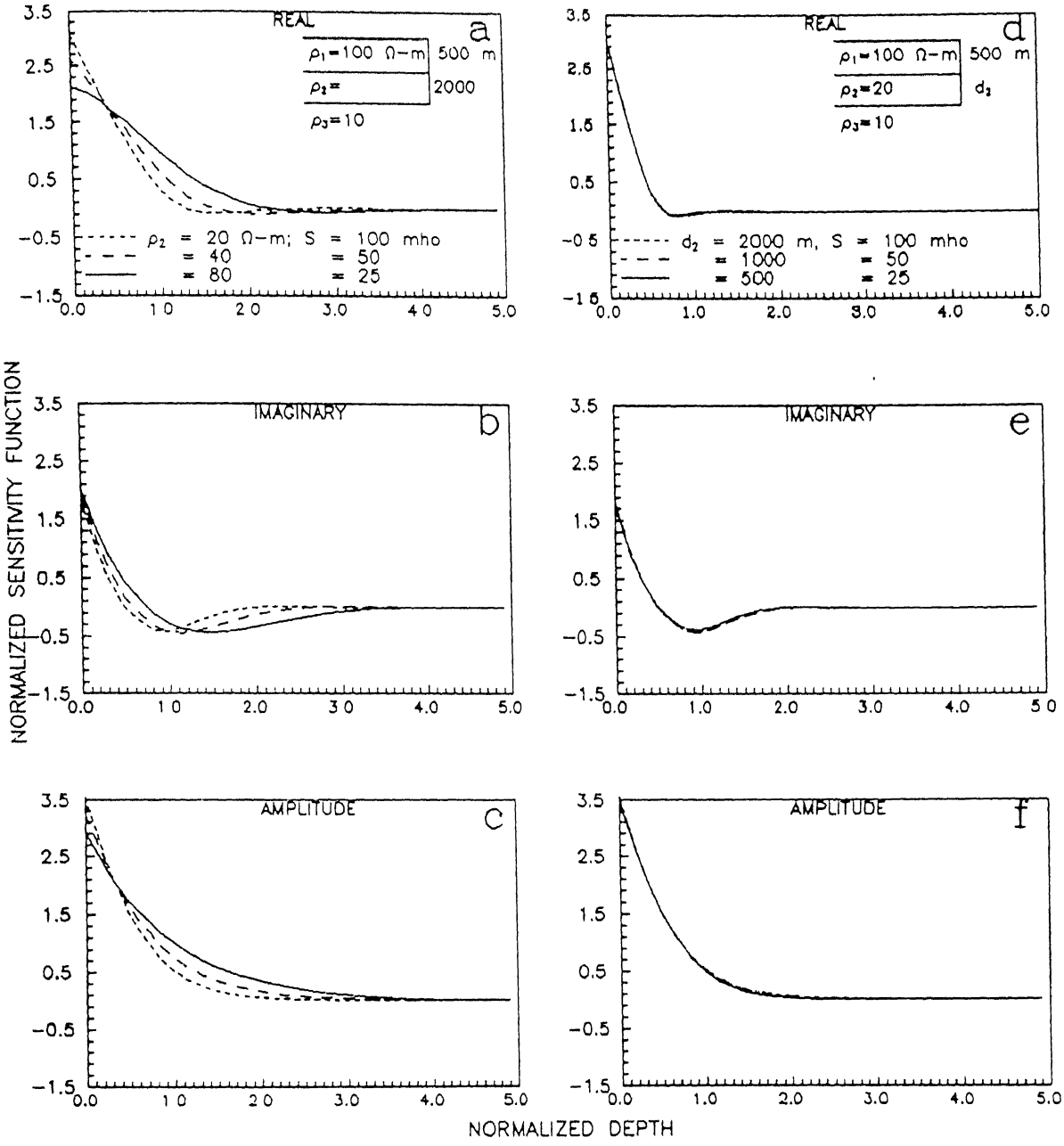

Figure 4.12 The behaviour of normalized sensitivity functions for Q-type models in frequency-domain i) for variable intermediate layer resistivity at constant thickness (a, b and c); and ii) for variable thickness of intermediate layer at constant resistivity (d, e and f).

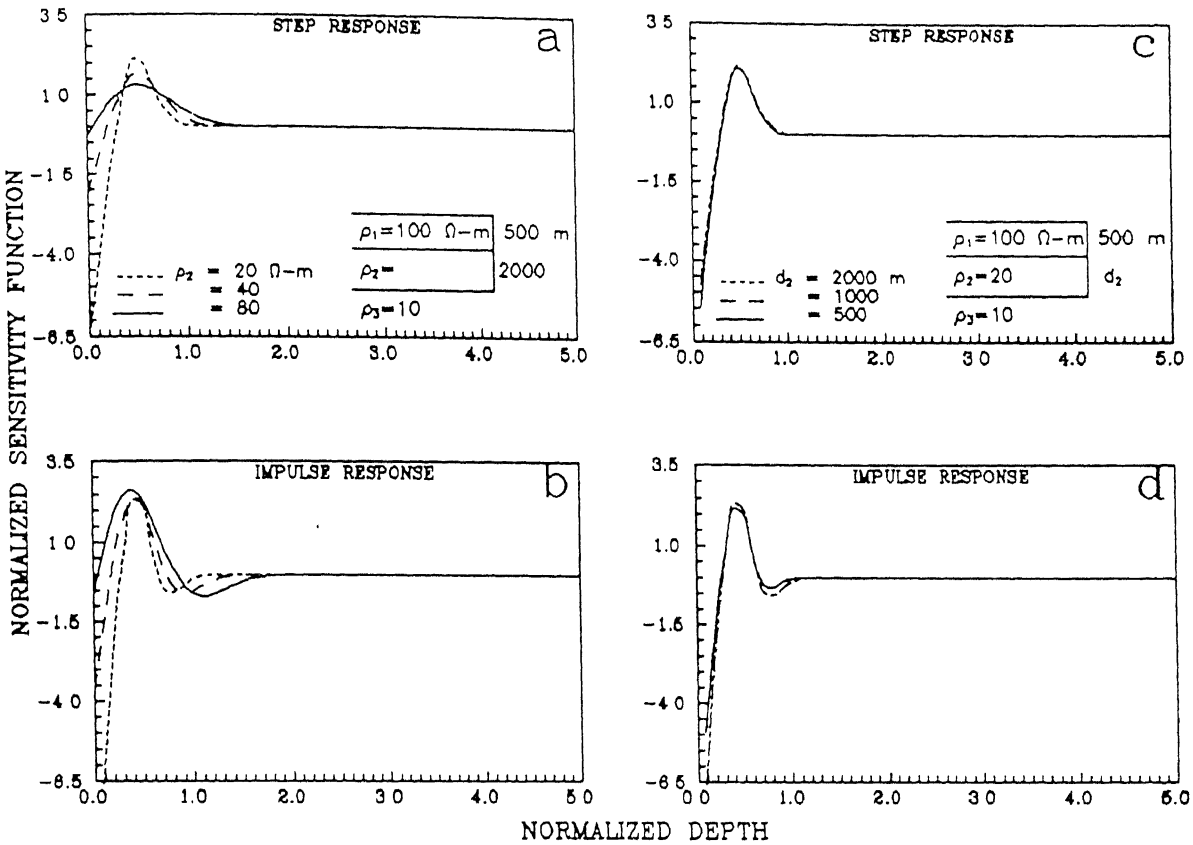

Figure 4.13 The behaviour of normalized sensitivity functions for Q-type models in time-domain i) for variable intermediate layer resistivity at constant thickness (a, and b); and ii) for variable thickness of intermediate layer at constant resistivity (c, and d).

resistivity at intermediate depth. The imaginary parts show the characteristic negative lobes for variations. In second case (Figures 4.12d-4.12f) the sensitivity functions do not show any effect of the thickness variations in intermediate layer. Therefore, the sensitivity functions (Figures 4.12a-4.12c) give information about the changes in resistivity while they do not give any information about the changes in thickness (Figures 4.12d-4.12f).

ii) Time-domain

The effect of resistivity and thickness variation of the intermediate layer on sensitivity function is shown in Figure 4.13. Four features are observed on increasing second layer resistivity. First- on the surface of the Earth, negative sensitivity values approaches toward positive values for both step and impulse responses. Second- the sharp peak of maximum sensitivity functions becomes more wider in step response than those in impulse response. Third- the peaks of maximum sensitivity attain lower values for step response and higher values for impulse response. Fourth and last, the Figure 4.13b shows that impulse response function has better resolution of underneath for Q-type models when intermediate layer has maximum possible resistivity. The effect of the change in thickness of the intermediate layer on sensitivity functions is insignificant (Figures 4.13c and 4.13d).

4.4.2.4 A-Type Models ($\rho_1 < \rho_2 < \rho_3$)

i) Frequency-domain

The sensitivity functions for A-type models are shown in Figure 4.14. The first layer resistivity is 100 Ω-m with thickness of 500 m and the last layer resistivity is taken as 1000 Ω-m. The second layer

resistivity is considered to be variable as 200, 400 and 800 Ω-m with constant thickness of 2000 m to study the effect of variations in intermediate layer resistivity on sensitivity functions. To study the effect of intermediate layer thickness on sensitivity functions, the thickness of this layer has been varied as 2000, 1000 and 500 m with constant resistivity of 200 Ω-m. The corresponding conductances values of the intermediate layer in the two cases are same i.e. 10, 5 and 2.5 mhos.

Figure 4.14 shows the variations of sensitivity functions along the depth with varying resistivity of the intermediate layer in one case and varying thickness of the intermediate layer in second case. The effect of resistivity and thickness of the intermediate layer is found significant on the sensitivity functions. The maximum sensitivity is observed on the surface of the Earth in case of imaginary and amplitude parts, whereas in the case of real part it is observed near the surface of the Earth. The imaginary parts show characteristic negative lobes at the intermediate depth. The negative lobes are found to increase with decrease in resistivity and thickness of the intermediate layer. From the graphical display, it is observed that the sensitivity functions for the changes in resistivity and thickness of the intermediate layer are quite similar in real and amplitude parts, whereas imaginary part show difference in behaviour near the Earth surface. The resolution in sensitivity functions for real and amplitude parts is higher on the surface of the Earth for variations in resistivity of intermediate layer, whereas it is poor for variations in thickness of intermediate layer.

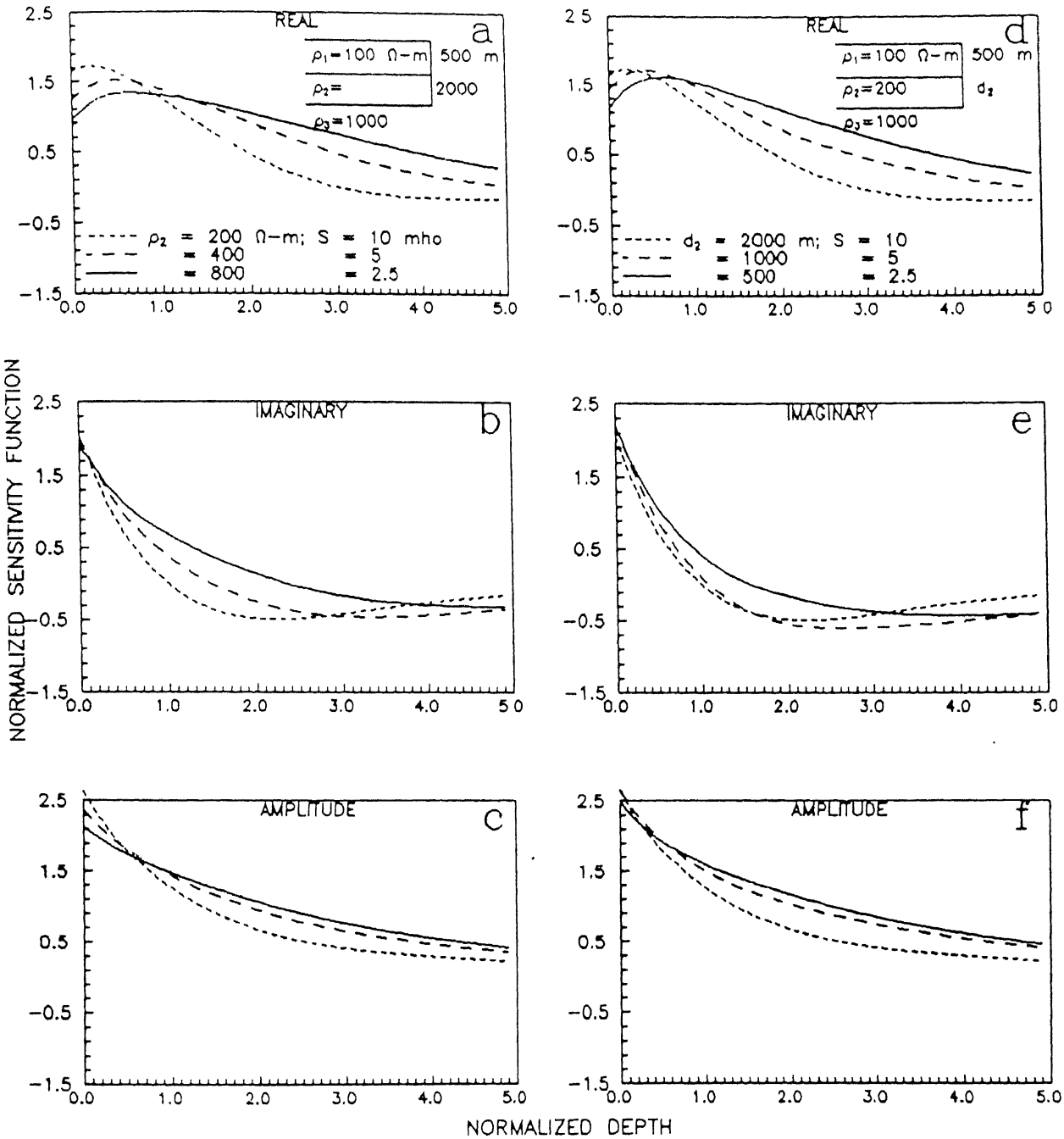

Figure 4.14 The behaviour of normalized sensitivity functions for Q-type models in frequency-domain i) for variable intermediate layer resistivity at constant thickness (a, b and c); and ii) for variable thickness of intermediate layer at constant resistivity (d, e and f).

ii) Time-domain

Variation of sensitivity functions along depth for step and impulse response functions are shown in Figure 4.15. Figures 4.15a and 4.15b show the sensitivity functions for various values of resistivity of intermediate layer at fixed thickness. Figures 4.15c and 4.15d show the sensitivity for various values of thickness of intermediate layer for constant resistivity of the intermediate layer. Three points are observed, when the resistivity of the intermediate layer increases. First- on the surface of the Earth the sensitivity increases marginally with the increase of resistivity of intermediate layer for step response, whereas it significantly decreases for impulse response. The maximum values of sensitivity functions are higher for impulse response compared to step response. On and near the surface of the Earth, impulse response shows positive values of sensitivity function followed by negative values (side lobes) at greater depth. The negative values for this case contribute negatively to the electromagnetic response.

Similar features of sensitivity functions are observed when the second layer thickness (d_2) decreases. The difference lies with impulse response which shows large negative side lobes at depths and sharp maxima peaks of sensitivity at shallower depths. The sensitivities for step response are not much different from the sensitivities obtained by the variations in resistivity values of the intermediate layer, whereas sensitivities for impulse response show contrast difference. Therefore, for various values of the thickness of intermediate layer contribute as much as the various values of resistivity of the intermediate layer i.e. the effect of changes in resistivity and thickness of the intermediate layer are similar to each other.

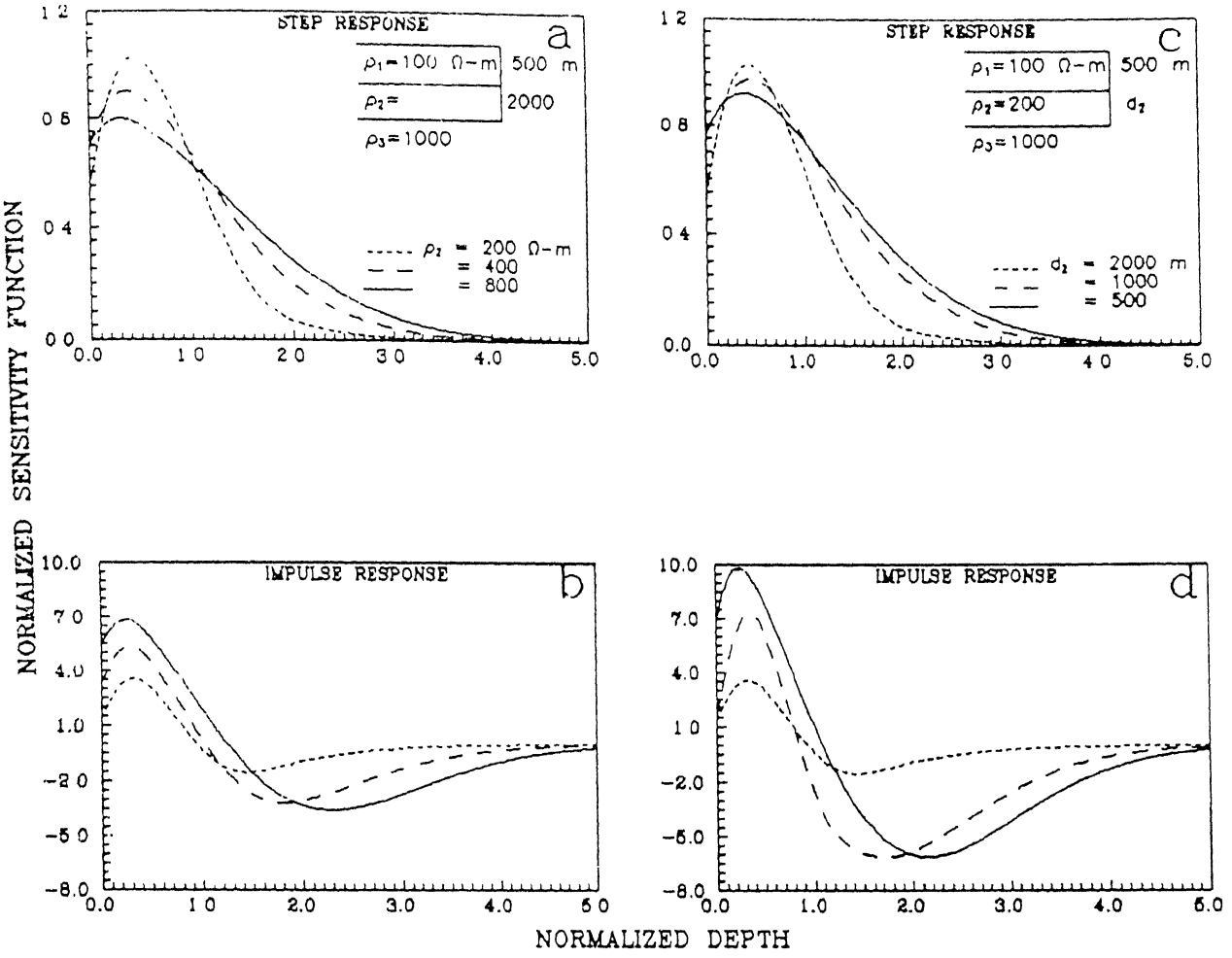

Figure 4.15 The behaviour of normalized sensitivity functions for Q-type models in time-domain i) for variable intermediate layer resistivity at constant thickness (a, and b); and ii) for variable thickness of intermediate layer at constant resistivity (c, and d).

The observations of sensitivity functions reveal that often thickness of the layer is of secondary importance. This is because a change in thickness is not truly a change in conductivity distribution. This can be verified on considering the role of thickness in terms of Frechet derivatives.

There are geological environments or geological complexities (i.e. problem equivalence) where magnetotelluric response (complex apparent conductivity $\sigma_a(\omega)$) remains constant for a product of a pair of layer parameters i.e. product of thickness (d) with conductivity (σ), under variations in layer parameters remains constant. Under such conditions, one can write

$$\sigma_a\,[\sigma(z),\ d] = \text{Constant},$$

On applying differential theorem, one gets

$$\sigma_a\,[\sigma(z) \pm \delta\sigma,\ d \mp \delta d] - \sigma_a\,[\sigma(z),\ d]$$

$$= \left(\frac{\partial \sigma_a}{\partial \sigma}\right)_d \delta\sigma + \left(\frac{\partial \sigma_a}{\partial d}\right)_\sigma \delta d + 0\,(\delta\sigma^2,\ \delta d^2)$$

For small change in conductivity ($\delta\sigma$) and small change in thickness (δd) in a layer such that new configuration allows the layer conductance to be constant i.e. $(\sigma \pm \delta\sigma)\,(d \mp \delta d) = \text{Constant}$. Thus,

$$0 = \left(\frac{\partial \sigma_a}{\partial \sigma}\right)_d \left(\frac{\delta\sigma}{\delta d}\right)_{\sigma_a} + \left(\frac{\partial \sigma_a}{\partial d}\right)_\sigma + 0\,(\delta\sigma^2,\ \delta d^2) \,/\, \delta d$$

As δd and $\delta\sigma \longrightarrow 0$, the second order term approaches to zero faster than first order perturbations i.e. $0(\delta\sigma^2,\ \delta d^2)/\ \delta d$ approaches to zero

faster than δd and $\delta\sigma$. Moreover, $\lim_{\substack{\delta d \to 0 \\ \delta\sigma \to 0}} \frac{\delta\sigma}{\delta d} \longrightarrow \frac{\partial\sigma}{\partial h}$. Thus,

$$\left(\frac{\partial \sigma_a}{\partial d} \right)_\sigma = - \left(\frac{\partial \sigma_a}{\partial \sigma} \right)_d \left(\frac{\partial \sigma}{\partial d} \right)_{\sigma_a}$$

or

$$\left(\frac{\partial \sigma_a}{\partial d} \right)_\sigma = - \left(\frac{\partial \sigma_a}{\partial \sigma} \right)_d \left(\frac{\partial \sigma}{\partial d} \right)_{\sigma_a}$$

or on logarithmic scale, it is written as

$$\left(\frac{\partial \ln\sigma_a}{\partial \ln d} \right)_\sigma = - \left(\frac{\partial \ln\sigma_a}{\partial \ln\sigma} \right)_d \left(\frac{\partial \ln\sigma}{\partial \ln d} \right)_{\sigma_a}$$

where the subscripts denote that the variable held constant for the partial derivative operation. This equation explains that the derivative with respect to thickness of the layer is the scaled derivative with respect to conductivity. The scaling factor, which is constant if the electromagnetic field response is constant and is negative of logarithmic derivative of conductivity with respect to logarithmic thickness of the layer. This shows that derivatives for both, with respect to layer thickness and conductivity are linearly dependent. This is the particular case for a layer of conductivity (σ) and thickness (d) which describes the relationship between derivatives. On generalization, the relationship between Frechet derivative with respect to conductivity profile and derivative with respect to layer thickness are more complicated and not easily described.

4.4.3 Exponentially Increasing Vertical Conductivity Profiles

i) Frequency-domain

The exponentially increasing vertical conductivity Earth model is expressed as follows:

$$\sigma(z) = \sigma_0 e^{pz}$$

where σ_0 is the surface conductivity at z = 0, and p is the positive scalar number. Variations in normalized sensitivity functions with normalized depth for various surface conductivities (0.0032, .0008 and .0002 mhos/m) at fixed p (0.006), and for various p values (0.006, 0.003 and 0.001) at fixed surface conductivity (0.0032 mho/m) are shown in Figure 4.16. The normalization factor is taken (skin depth) is taken to be 890 meters in surface layer of conductivity (σ_0) 0.0032 mho/m at period 0.01 sec.

The sensitivity functions for various surface conductivities at fixed p are shown in Figures 4.16a-4.16c. The maximum sensitivity values are observed to occur inside the Earth due to stronger induction at deeper zones of high conductivity. The maxima of the sensitivity functions shift downward as the surface conductivity decreases. The real, imaginary and amplitude parts of sensitivity functions more or less show the same characteristic behaviour along depth. The real and imaginary parts sensitivity functions show a maxima followed by negative side lobes before functions approach to zero at great depth. The variations in amplitude sensitivity functions are always positive.

The real, imaginary and amplitude parts of normalized sensitivity functions for various values of p at fixed surface conductivity are shown in Figures 4.16d-4.16f. Different values of p allow to increase the inside the Earth with different rates. The nature of the real and imaginary parts of sensitivity function is same for different values of

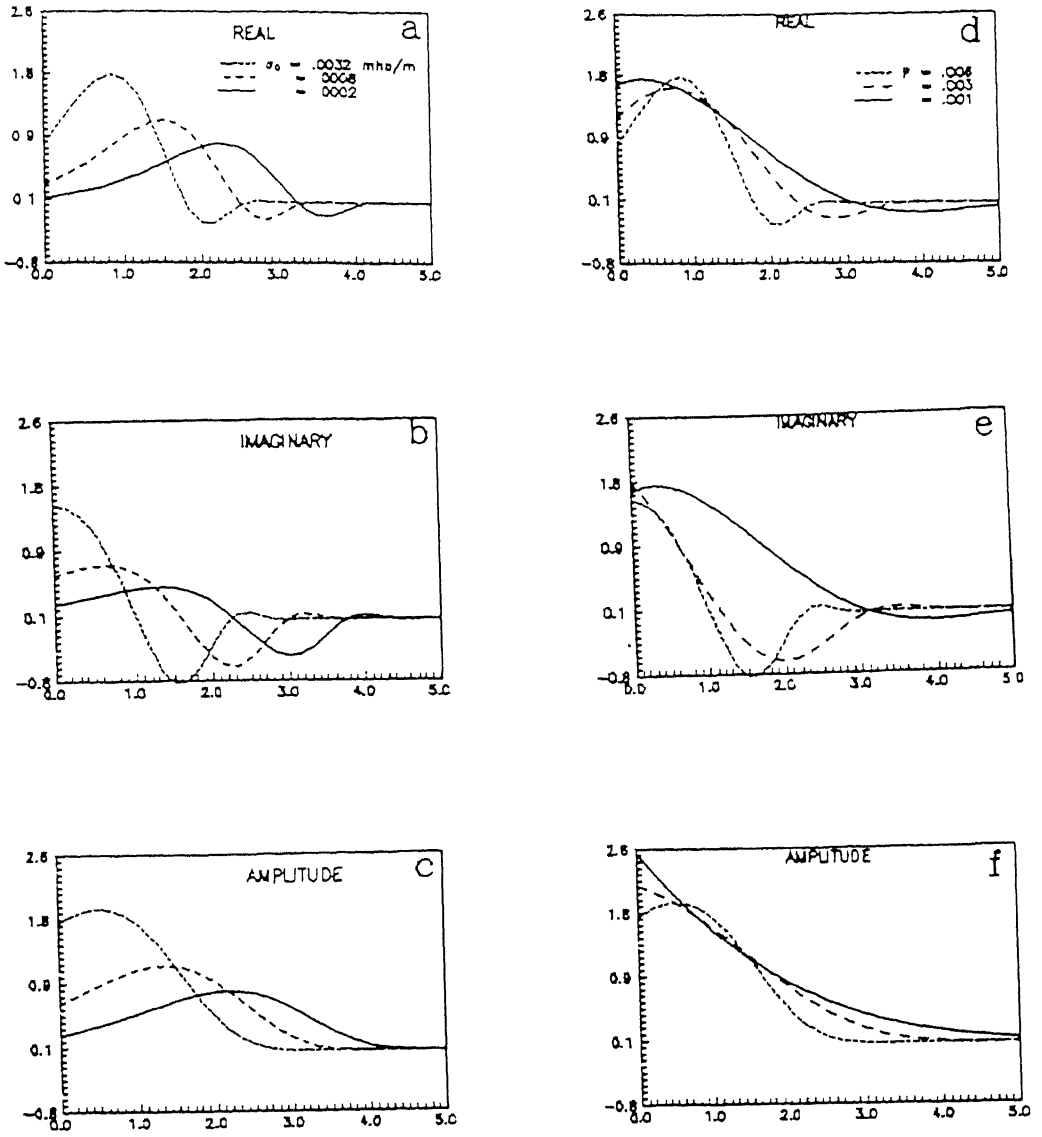

Figure 4.16 The behaviour of normalized sensitivity functions for exponentially increasing vertical conductivity models in frequency-domain i) for variable surface layer resistivity at constant value of p (a, b and c); and ii) for variable values of p at constant surface layer resistivity (d, e and f).

p. For real parts, the maximum sensitivity occurs near the surface of the Earth, and on the surface of the Earth for imaginary parts (Figure 4.16e). Along the depth, increases the sensitivity functions decrease and show negative lobes before approaching to zero. The normalized sensitivity functions show maximum sensitivity near the surface of the Earth for lower values of p and seems to decrease linearly. For higher value of p the sensitivity functions show maxima inside the Earth.

ii) Time-domain

The sensitivity functions for the Earth model when conductivity increases exponentially inside the Earth have been computed using numerical method for the same parameters as in frequency domain. Variations in normalized sensitivity functions, corresponding to step and impulse responses, along normalized depth for various surface conductivities (0.0032, .0008 and .0002 mhos/m) at fixed p (0.006), and for various p values (0.006, 0.003 and 0.001) at fixed surface conductivity (0.0032 mho/m) are shown in Figure 4.17. The normalization factor is taken (diffused depth) is taken to be 890 meters in surface layer of conductivity (σ_0) 0.0032 mho/m at delay-time 0.01 msec. The sensitivity functions shown in Figure 4.17 contain different levels of error even for computation of the same model at second time if the discretization is carried differently.

The sensitivity functions for various surface conductivities at fixed p are shown in Figures 4.17a-4.17b. The sensitivity functions for both step and impulse responses have been observed to have high negative values on and near the surface of the Earth with maximum sensitivity deep inside the Earth. On decreasing the surface conductivity, sensitivity functions for step and impulse responses show three

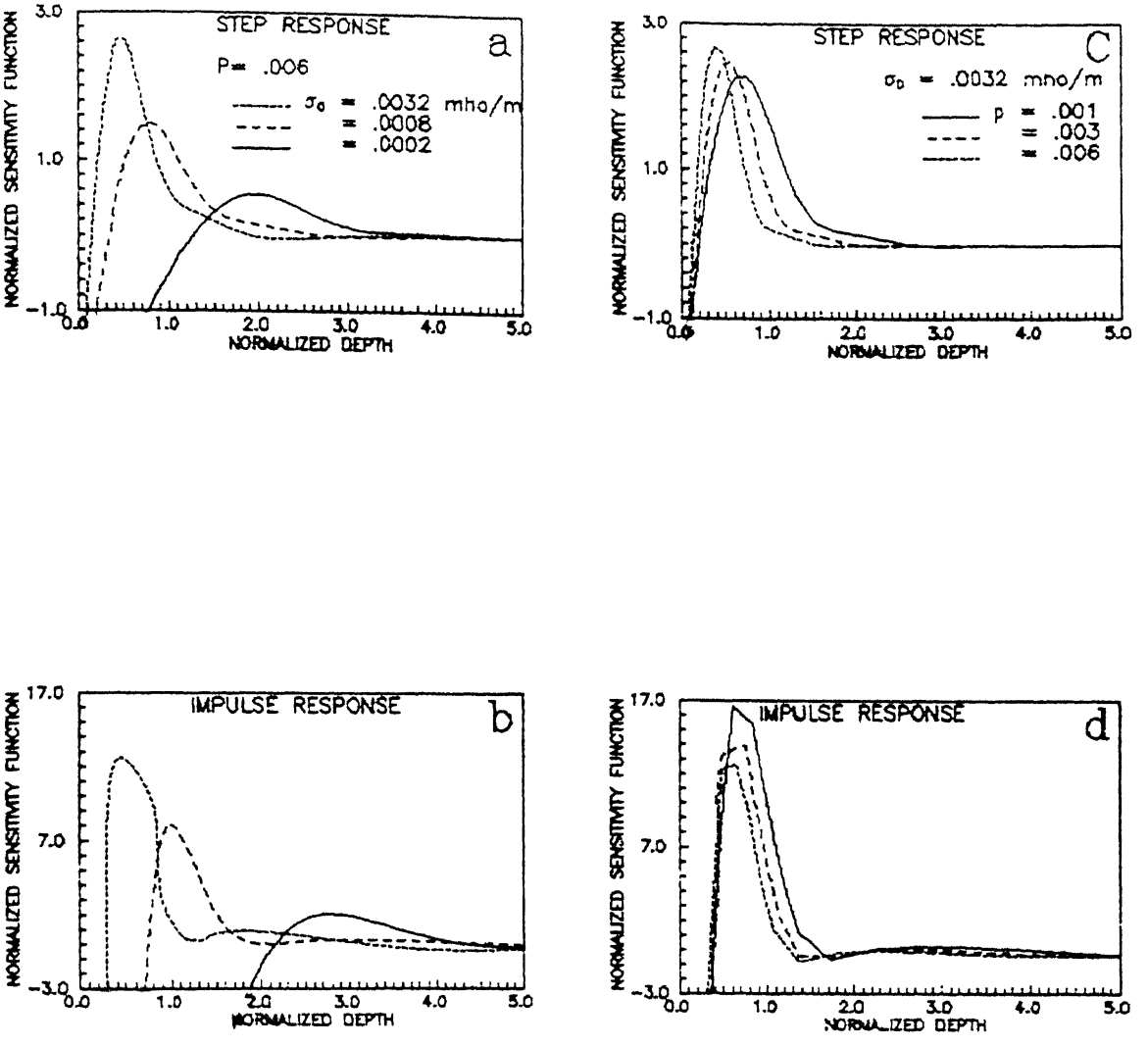

Figure 4.17 The behaviour of normalized sensitivity functions for exponentially increasing vertical conductivity models in time-domain i) for variable surface layer resistivity at constant value of p (a, and b); and ii) for variable values of p at constant surface layer resistivity (c and d).

features. First- the zones of maximum sensitivity move downward. Second- the maximum sensitivity achieve lower values. Third and last- the width of the sensitivity functions becomes broader, which is indicative of reduction in resolution of the subsurface.

The normalized sensitivity functions for various values of p at fixed surface conductivity are shown in Figures 4.17c-4.17d. On decreasing the p values three features are observed associated with sensitivity functions for step and impulse responses. First- the zones of maximum sensitivity move downward for step response and surfaceward for impulse response. Second- the sensitivity functions for both step and impulse responses attain lower values. Third and last- the sensitivity functions become wider for response and narrower for impulse response function.

The comparison of sensitivity functions for step and impulse responses show that for they behave similarly for variations in surface conductivity and differently for variations in p values. This feature of sensitivity functions for step and impulse responses associated with different p values make them comlimentary in nature.

4.4.4 Exponentially Decreasing Vertical Conductivity Profiles

i) Frequency-domain

The exponentially decreasing vertical conductivity Earth model is expressed as follows:

$$\sigma(z) = \sigma_0 \, e^{-pz}$$

where σ_0 is the surface conductivity at z = 0, and p is the positive scalar number. Variations in normalized sensitivity functions with normalized depth for various surface conductivities (0.32, .08 and .02 mhos/m) at fixed p (0.001), and for various p values (0.0018, 0.0014 and

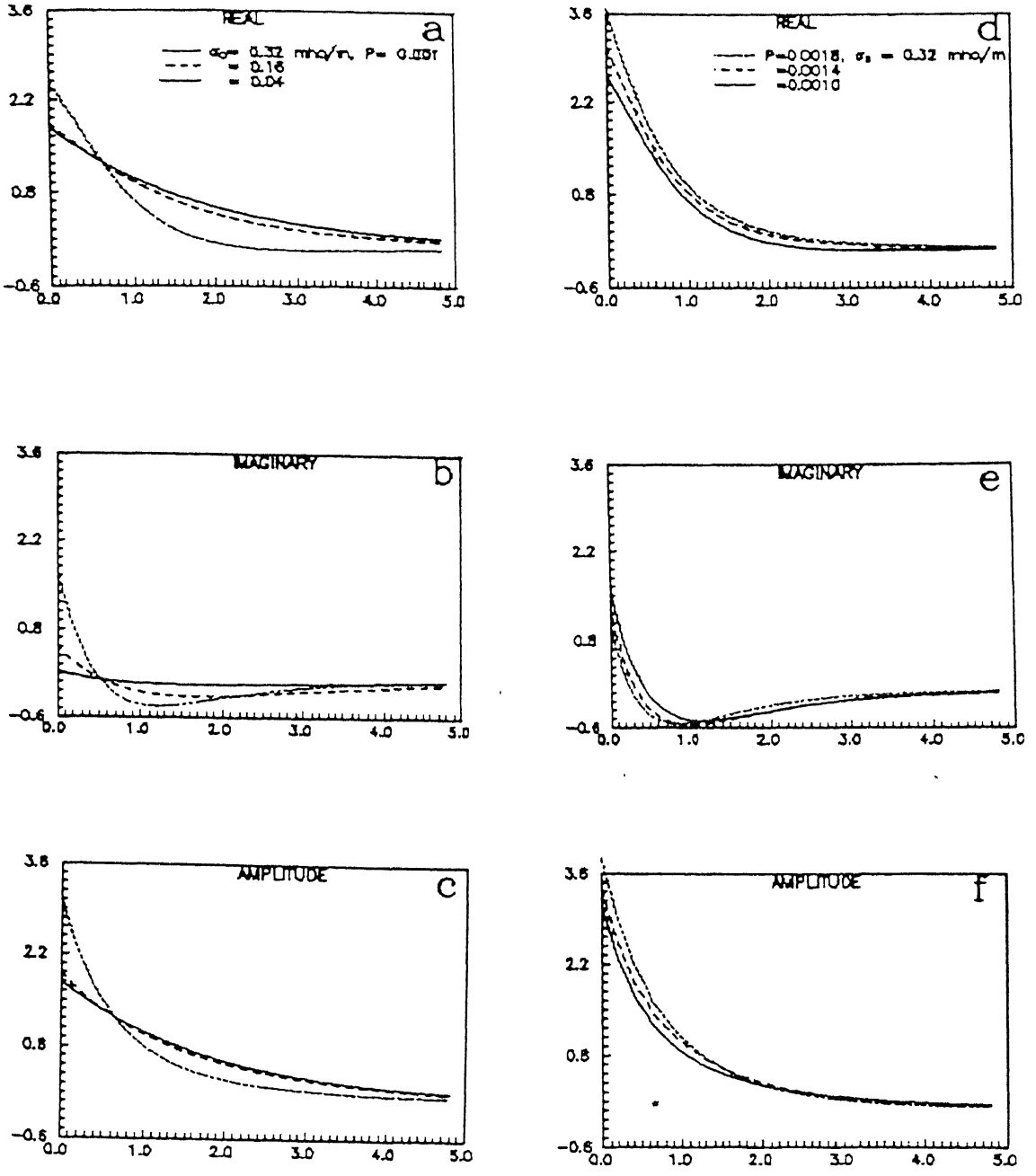

Figure 4.18 The behaviour of normalized sensitivity functions for exponentially decreasing vertical conductivity models in frequency-domain i) for variable surface layer resistivity at constant value of p (a, b and c); and ii) for variable values of p at constant surface layer resistivity (d, e and f).

0.001) at fixed surface conductivity (0.32 mho/m) are shown in Figure 4.18. The normalization factor is taken (skin depth) is taken to be 890 meters in surface layer of conductivity (σ_0) 0.32 mho/m at period 1.0 sec.

The sensitivity functions for various surface conductivities at fixed p are shown in Figures 4.18a-4.18c. The maximum sensitivity for real, imaginary and amplitude parts is observed on the Earth surface for all surface conductivity values. It has been found that on the surface of the Earth the sensitivity increase with the increases of surface conductivity (Figures 4.18a-4.18c). The sensitivity function decreases along the depth for all parts (real imaginary and amplitude), and the rate of decrease is faster in imaginary parts and slower in amplitude parts at a given surface conductivity (σ_0). The imaginary parts show negative side lobes before approaching to zero at great depth. The contribution made by different parts of the subsurface to magnetotelluric measurements is affected on chosen value of surface conductivity. About 80% contribution, for highest value of surface conductivity (0.32 mho/m), is made by the structures lying within the one and a half skin depth and marginally made by the structures below to one and a half skin depth. For lowest surface conductivity (0.02 mhos/m), structures within one and a half skin depth contributes nearly 65% and another 35% is made by the structures below the one and a half skin depth.

Variation of normalized sensitivity functions along normalized depth for a surface conductivity 0.32 mho/m for various values of p have been shown in Figures 4.18d-4.18d. The models with decreasing rate of conductivity inside the Earth, when value of p is increased from 0.001 to 0.0018, show increase in sensitivity all along the depth. The higher

values of p contributes relatively less negatively to the observation.

ii) Time-domain

The sensitivity functions for the Earth model when conductivity decreases exponentially inside the Earth have been computed using numerical method for the same parameters as in frequency domain. As have been observed in frequency domain that the sensitivity functions often for the present case do not have much resolution, especially inside the Earth. The similar situations with worsen resolution at all depths have been observed, and it is found not worthy to display them graphically and to analyse. The values of these sensitivity functions were found so close that it was not possible to make out any thing out of these.

4.5. Conclusions

The sensitivity functions analysed for electromagnetic responses, in frequency and time-domains, demonstrate some of the useful physical concepts and characteristics associated with each response. The graphical visualization of sensitivity functions for underground resistivity distribution provides the inherent nature of how individual responses sample the resistivity distribution. Moreover, the sensitivity functions pave the way for relative merits of responses in each domain, and different responses (step and impulse) within the same domain. Though, sensitivity functions have been analyzed for very simple various one-dimensional vertical conductivity profiles , but to a certain extent these give sufficient understanding and explanation, qualitatively, for relative variations in sensitivity functions when subjected to change(s) in model parameter(s). However, the explanations given are relative with respect to reference model undergone a change.

The maximum sensitivity of the response functions in frequency-domain, in general, is on the surface of the Earth whereas, and in time-domain it is very well localized deep inside the Earth. In cases- when the surface layer is many more times conductive than the reference model or when the conductivity inside the Earth increases exponentially; the maximum sensitivity occurs just below the Earth surface for former case, and deep inside the Earth for later case.

The sensitivity functions in either domain explain that the relatively conductive surface layers act to mask the information from deeper structures, owing to higher magnitude of sensitivity functions on the Earth surface. Relatively resistive surface layers are transparent to deeper structures with reduced vertical resolution as opposed to conductive surface layers. Moreover, to a given fractional change, in the resistivity of the surface layer of the reference model such that surface layer alternatively becomes resistive and conductive- the response function in frequency-domain reveals stronger sensitivity on the surface of the Earth for conductive surface layer compared to resistive surface layer; and the response functions in time-domain, step and impulse both, reveal no such severity as they have their sensitive zones deep inside the Earth.

The significant point to notice is that- the frequency-domain response functions (the measurements) might still be sensitive on the surface of the Earth if the currents are flowing deep inside the Earth; contrary to it, the time-domain response functions have the property of focusing their maximum sensitivity deep inside the Earth even if the current is flowing near the surface of the Earth. The only condition, to have maximum sensitivity inside the Earth in frequency-domain, is to have a favourable Earth structure such that the conductivity might be

increasing continuously with depth.

The response functions in both the domains are sensitive to conductive sandwiched layer and insensitive to resistive sandwiched layer. The sensitivity and vertical resolution at each depth out side the conductive sandwiched layer is poor in case of frequency-domain, and in case of step response function in time-domain. However, impulse response function has more sensitivity and good vertical resolution only above the sandwiched layer. The sensitivity and vertical resolution at each depth out side the resistive sandwiched layer is higher in case of frequency-domain, and in case of time-domain it is higher only below the resistive sandwiched layer.

CHAPTER V

RESISTIVITY STRUCTURE OF INDO-GANGETIC PLAINS

5.1 General

The magnetotelluric method is widely used for the deeper subsurface mapping and exploration of oil and gas in USA, Canada, Australia and European countries (Hermance and Neumann, 1988; Jones and Craven, 1990; Hjelt, 1984; Gupta and Jones, 1990). The magnetotelluric method has been successfully employed for the mapping of hydrocarbon deposits in the Basaltic provinces. In India, the seismic method has been widely used for the mapping of hydrocarbon deposits. In the geologically complex areas such as Deccan Trap, Himalayan foothills and in the densely populated area such as Indo-Gangetic basin, the seismic method has been failed to reveal information about the deeper subsurface structure. The need of magnetotelluric method in such complex areas have been stressed by various workers.

Deeper subsurface information, as deduced by using gravity, magnetic, seismic and magnetotelluric methods has paramount importance in understanding the physics of tectonic movements of plates. In India, seismic methods have been widely used for mapping hydrocarbon resources. The magnetotelluric method is new in India and has only been recently employed to obtain information about deep structures. During 1989, magnetotelluric soundings were carried out in the Indo-Gangetic basin and in Indian peninsular region under a collaborative project between the Indian Institute of Technology, Kanpur, India and the University of Uppsala, Sweden.

5.2 Indo-Gangetic Basin and Himalayan Foothills

The Indo-Gangetic plains extends over the area of about 250,000 square kilometers lying approximately within longitudes 77^{o} to 88^{o} E and latitudes 24^{o} to 30^{o} N. It lies between the Himalayan mountains to the north and the Indian Peninsular shield to the south (Figure 5.1). The southern boundary of the basin is shown by thick dashed line in Figure 5.1.

The Indo-Gangetic basin has attracted the attentions of the geoscientific community ever since Burrard (Oldham, 1917) suggested, on the basis of geodetic observations, that the Himalayan folds were the result of underthrusting of the Indian sub-crust below the land mass of central Asia. Burrard believed that this observation explained the mass deficiency of the Indo-Gangetic and Himalayan regions. After the Burrard observations, efforts were made to study the subsurface structure of the Indo-Gangetic and Himalayan foothills region (Wadia, 1931; Auden, 1934; Gansser, 1964).

The Himalayas extend over a length of about 2400 kilometers and are 225 to 375 kilometers wide. This area is one of the active tectonic areas where frequent earthquakes are being recorded. The earthquake data observed in this region have been analyzed, which indicate that the Indian plate is subducting beneath the Tibetan plate (McKenzie and Sclater, 1971). Dewey and Bird (1970) model suggested the birth of Himalaya as a result of collision between Indian and Eurasian plates. The low density continental crust and its large thickness prevented further subduction of the Indian lithosphere (Isacks et al., 1968; McKenzie,1969). The rate of subduction is about 5-6 cm/year (Powell and Conagham, 1973). The Main Boundary Fault (MBF) which separates the Tertiary from the pre-Tertiary represents the appropriate northern limit

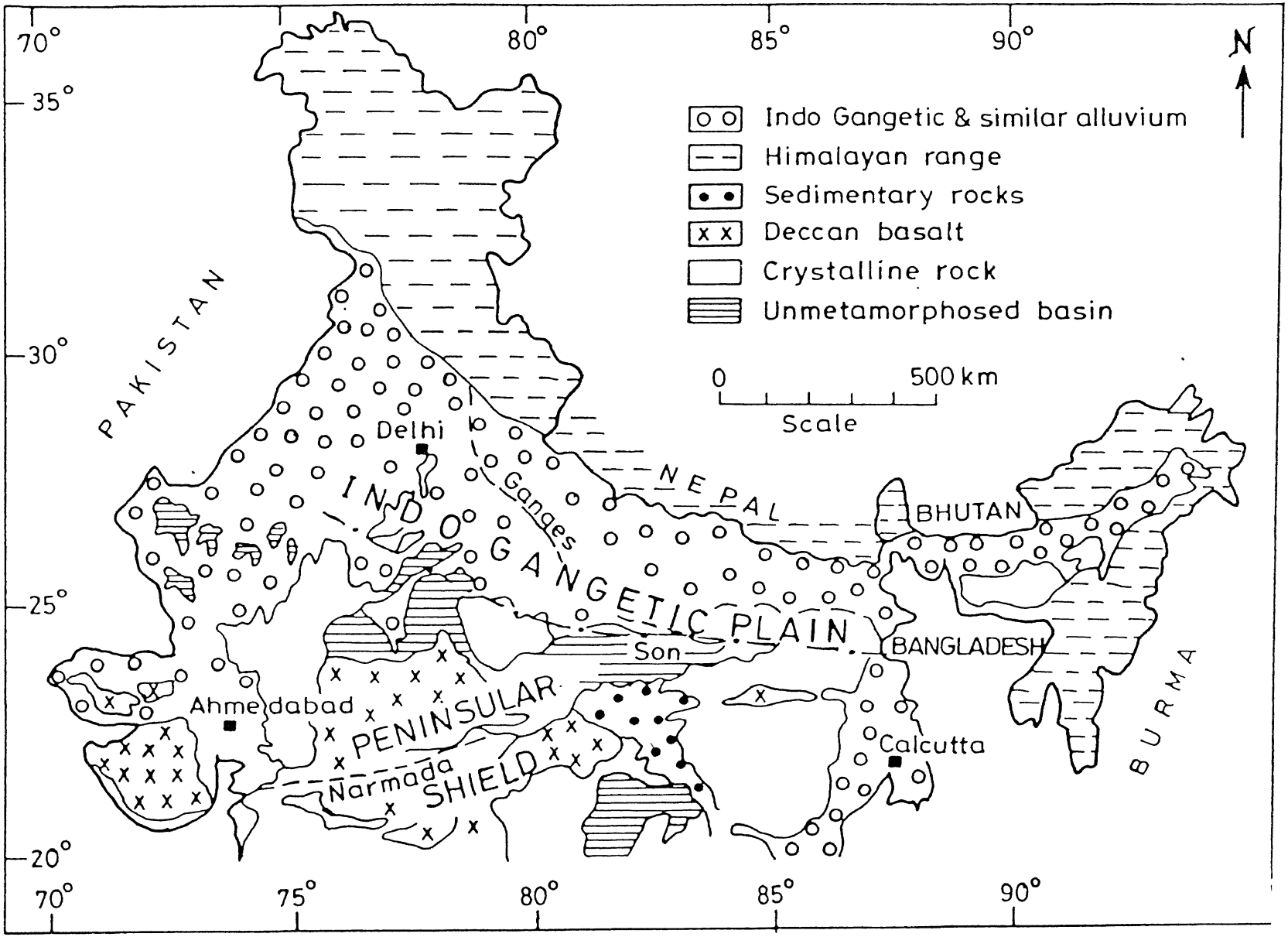

Figure 5.1 The coverage of Indo-Gangetic plains.

(Raiverman et al., 1983).

5.3 Results of Earlier Investigations

The geophysical data base in Himalaya and Indo-Gangetic basin includes seismotectonic, seismic, gravity and magnetic studies. Detailed gravity and magnetic data are available for the Indo-Gangetic basin. The data base show substantial variations in the thickness of the sedimentary overburden and an uneven basement topography (Sastri et al., 1971; Sengupta, 1977) throughout the basin. The crustal structure, obtained from the analysis of earthquake and gravity data, generally indicates the thickening of the crust beneath the Himalaya. This result is consistent with the Airy-Heiskanen's hypothesis of isostasy. On the basis of positive Airy-Heiskanen anomaly over the Himalaya, which can be attributed to the densification and thickening of the lower part of the crust beneath the Himalaya, the crustal thickness of 81 Km was obtained in the Himalayan region (Qureshy, 1969, 1971; Qureshy and Midha, 1986). This finding further has been supplemented by the crustal thickness of 65-70 Km estimated from analysis of Bouguer anomaly profiles in the same region (Choudhury, 1975). On the basis of gravity and aeromagnetic data, the Indo-Gangetic basin has been divided into four different parts separated by basement highs. Gupta (1971) while interpreting the residual gravity anomalies has divided plains into several tectonic blocks on the basis of the trends of the anomalies.

A number of transverse folds of mesoscopic and macroscopic dimensions have been mapped. A deep seismic sounding (DSS) (Beloussov et al., 1980) in the north-west of the Indo-Gangetic plains, underneath the southern part of the high Himalayan range Nanga Parbat, has also indicated a crustal thickness of 65-70 Km in the extreme part of the

basin. Deeper information about the basin is available only from earthquake generated body-wave (Kaila et al., 1968; Tandon and Dubey, 1973) and surface-wave studies (Choudhury, 1966; Gupta and Narain, 1967; Gupta et al., 1977; Bhattacharya, 1981, 1991; Chun, 1986). Extension of the Indian shield under the Indo-Gangetic plains and close relationship between the shield and the Himalayan rocks has been inferred from geological studies (Gansser, 1974; Valdiya, 1976). Gupta et al. (1977) have summarized results of the various investigations and have estimated physical properties and velocity substructure of the Indo-Gangetic plains. The lack of deeper information has led to controversy exist about the extension of shield type structure beneath the Indo-Gangetic basin. The use of extensive deep seismic sounding and magnetotelluric surveys (Srivastav et al., 1984) has been stressed to investigate the subsurface structure of the Indo-Gangetic basin.

5.4 Magnetotelluric Data Acquisition

The magnetotelluric soundings were carried out at 18 locations (Figure 5.2) along nearly two perpendicular profiles AA' and BB' (SW-NE and ES-WN) simultaneously, covering a part of the Indo-Gangetic basin. At each location, two horizontal and orthogonal components H_x and H_y of the time varying magnetic field and two components E_x and E_y of the electric field were measured, independently. The attempt to measure the vertical component H_z of the magnetic field vector was made but unfortunately due to the hard nature of the top soil it was difficult to erect the induction coil for recording the vertical component. Induction coils were used for measuring the magnetic intensity H and electrodes of $Pb\text{-}PbCl_2$ type with a separation of 100-150 m were used for measuring the electric field E. Three filters, which subdivide the broad-band

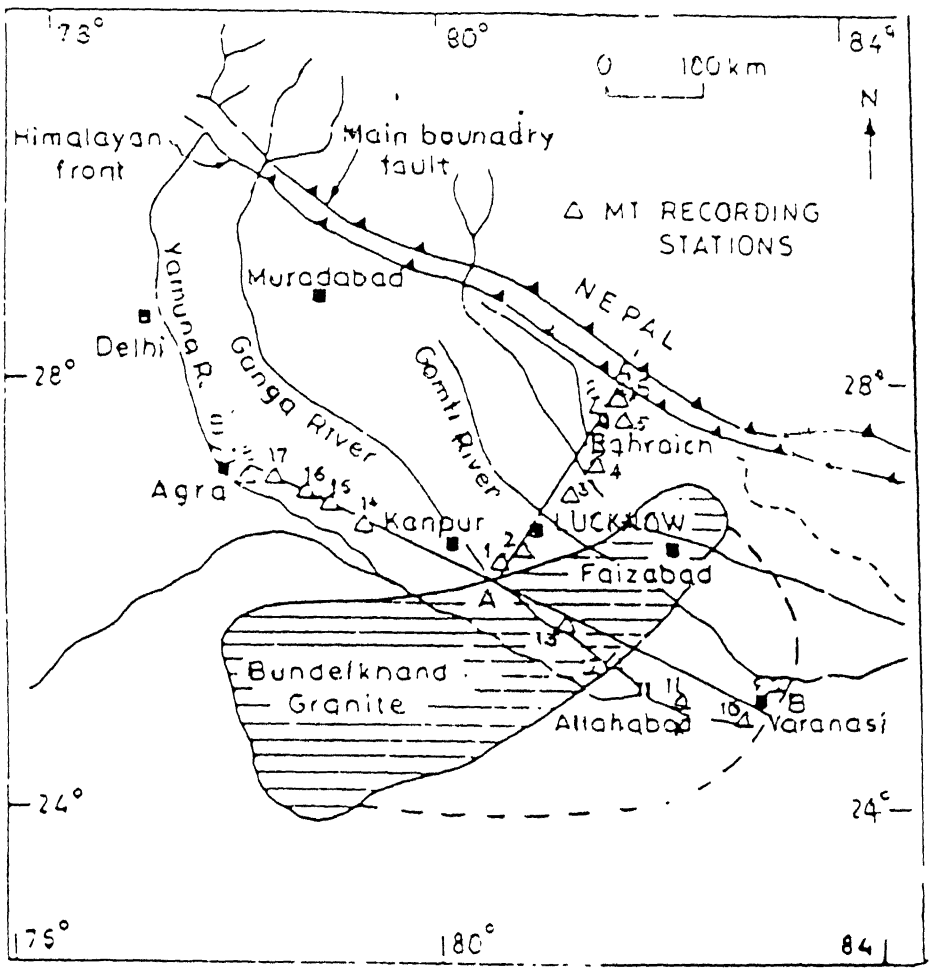

Figure 5.2 The location of magnetotelluric recording stations.

frequency spectrum of the signal ranging from 1/3600 to 0.5Hz, 1/500 to 0.5 Hz, and 0.1 to 10 Hz were used to record the independent components of electric and magnetic fields of the signal. The recording duration for the above three filter sub-bands were ranging from 8-16 hours (long period), 6-8 hours (medium period) and 30 minutes (short period), respectively. At most of the stations magnetotelluric recordings were carried out in the long and short periods. To record the more number of stations within the stipulated duration for which the magnetotelluric equipment was available, only medium and short period recordings were carried out at few stations. The separation between sites was usually ranging from 25-40 Km, but at few locations the separation was ranging from 50-60 Km due to non-availability of an appropriate site from the point of view to avoid the cultural noise from electrified railway lines, tubewells, power lines, highways; and some times owing to improper road conditions.

The surface impedance tensor elements are estimated using the least square technique (Pedersen, 1982). The measured signal components of electric and magnetic fields (the time series) are transformed into frequency domain by using Discrete Fast Fourier Transform. At each location, the apparent resistivities and phase along two principal directions (ρ_{xy}, ρ_{yx}, ϕ_{xy} and ϕ_{yx}) have been computed using well known relation (Cagniard, 1953) and plotted against period. The averaged estimates of apparent resistivity and phase have been carried out from the determinant average impedance following the approach of Berdichevsky and Dimitriev (1976).

5.5 Interpretation of Magnetotelluric Data Along Profile AA'

5.5.1 Behaviour of Data

Figure 5.3, shows the apparent resistivity (first and second rows with dots) and phase (third and fourth rows with dots) data for stations 1-7 for E- and H-polarizations, respectively, along profile AA'. The data (apparent and phase) at each station for E- and H-polarizations show more or less the same values at shorter periods, whereas at longer periods a large difference between the data for E- and H-polarization is seen (Figure 5.3). This large difference at longer periods may be attributed to the presence of anisotropy, due to the nature of the existing structure. The possible effect of anisotropy may be due to micro- or macro-anisotropy caused by the schistosity and foliation in the rocks. The data show increasing anisotropy at northern stations which can be attributed primarily to neotectonic activities in this seismically active region.

5.5.2 Two-dimensioanl modelling along profile AA'

As mentioned above, the data show anisotropic behavior along the profile AA'. The use of determinant data when modelling the long period part of the response functions allow a simplified representation of the regional structure. In order to start with two-dimensional modelling, one-dimensional inversion of determinant data has been carried out using least-square procedure (Pedersen and Rasmussen, 1989). The data fits very well at each station and yield three to four layered models. The results show the presence of light sedimentary rocks beneath the alluvial sediments. The behaviour of apparent resistivity changes drastically after a certain depth. Hence, it clearly detects the lithospheric-asthenospheric boundary except at the extreme station 6,

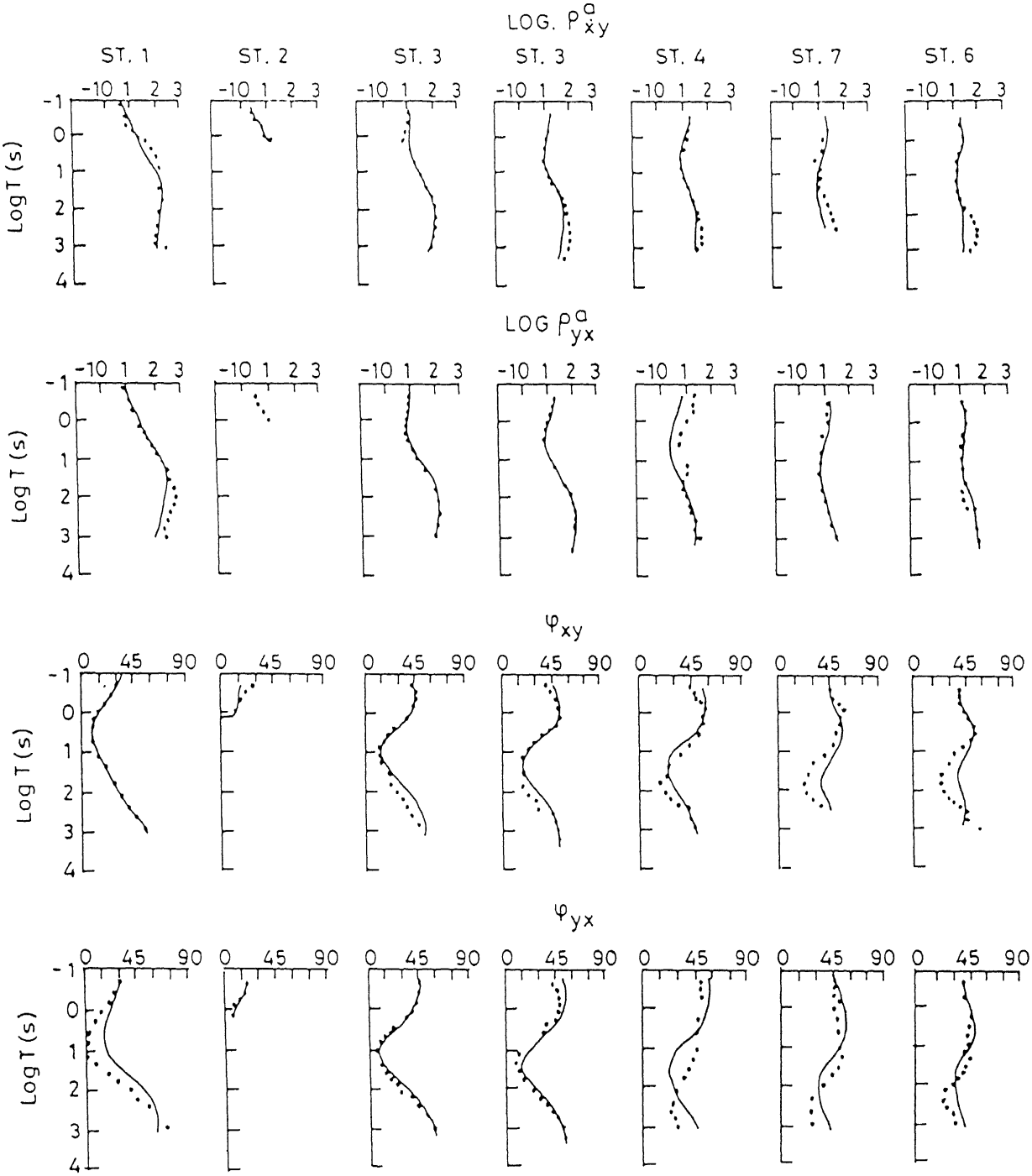

Figure 5.3 The variation of apparent resistivity and phase with periods for recording stations 1-7 along profile AA' in north-south and east-west directions.

While the gravity measurements infer information only about the crustal thickness. As has been mentioned, this exercise is merely a preliminary which has to be incorporated as a starting point with the two-dimensional modelling, the results are not shown.

On the basis of one-dimensional results of deteminant data, two-dimensional modelling exercises have been carried out using the Brewitt-Taylor and Weaver (1976) finite difference algorithm. An appropriate two-dimensional model (shown in Figure 5.4) is obtained which fits the apparent resistivity and phase data (Figure 5.3 , the solid lines represent the modelled results and dots represent the field data) moderately, but to a certain degree of accuracy. The two-dimensional model shows a lithospheric-asthenospheric boundary at a depth about 80-90 Km at Kanpur and at the extreme northern side. At the centre of the profile (AA'), it shows an upwarping of the lithosphere. This is a preliminary result of two-dimensional modelling exercise; and the modelled data do not show good consistency with the field data observed in two measuring directions, especially at longer periods. However, at shorter periods the misfit between observed and modelled data is negligibly small. Therefore, the two-dimensional subsurface resistivity cross-section, shown in Figure 5.4, is more reliable to a depth of 25.0 Km from the surface of the Earth. Along the northern side of the profile (AA') near Bahraich, the modelled result reveals a zone of low resistivity (resistivity 3.0 Ω-m) at a depth of 4.0 Km (Figure 5.4) below the surface of the Earth. This low resistivity zone shows an orientation of N30E-S30W (the orientation of the profile AA') which can be attributed to one or more of the following reasons:

I. may be due to the presence of partial melting at a shallower depth. Similar finding has been observed at Lahsa block in Tibet which is

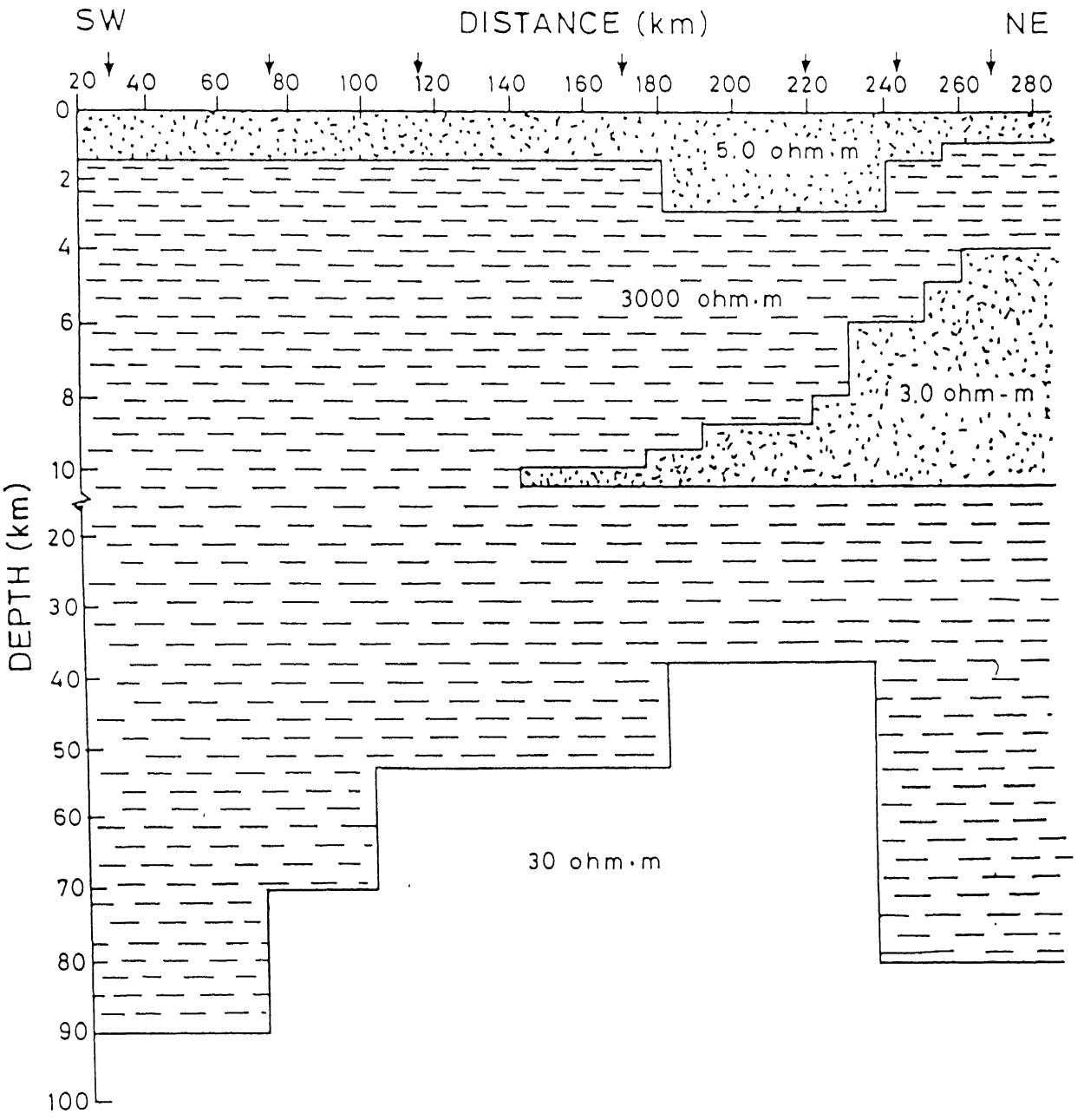

Figure 5.4 The two-dimensional model along profile Kanpur-Nepal border (AA').

about 500 Km. in east (Pham et al., 1986; Menvielle and Mouel, 1990),

II. may be associated with the presence of oil and gas formation. The oil and gas are generally associated with saline water due to which a low resistivity zone can be seen,

III. may be due to the presence of graphite or metasediments. Similar situation has been observed in the foothills of Alps (Adam et al., 1990; Adam et al., 1986; Adam and Verga, 1990), and

IV. may be due to the presence of fluids which may have moved from the Indo-Gangetic plains or from the subducted lithosphere under the Himalaya.

The possibility of partial melt can be ruled out due to the low heat flow (30-45 mW^2/m^2) observed in this region (Shanker, 1988).

5.6 Interpretation of Determinant Data Along the Profile BB': An One-dimensional Inversion

Figure 5.5 shows the apparent resistivity and phase data for the determinant of impedance tenser elements with one-dimensional inversion results for stations 9, 14, 16 and 17 chosen as representative of the profile BB'. The stations east of Kanpur along the profile BB' (stations 9-13) show a high resistivity formation beneath the alluvial sediments (see data at station 9, Figure 5.5). The high resistivity formation is attributed to the presence of granite from the Peninsular shield, and also to the extension of Vindhyan plains (Valdiya, 1976; Gupta et al., 1977). The high resistivity shown by the stations east of Kanpur confirm the presence of a shield-like structure beneath the Indo-Gangetic plains (Gupta et al., 1977). The boundary (shown by the thick line in Figure 5.2) of the subsurface extension of the Bundelkhand granite has been identified as the Bundelkhand-Faizabad ridge (Valdiya, 1976). Based on

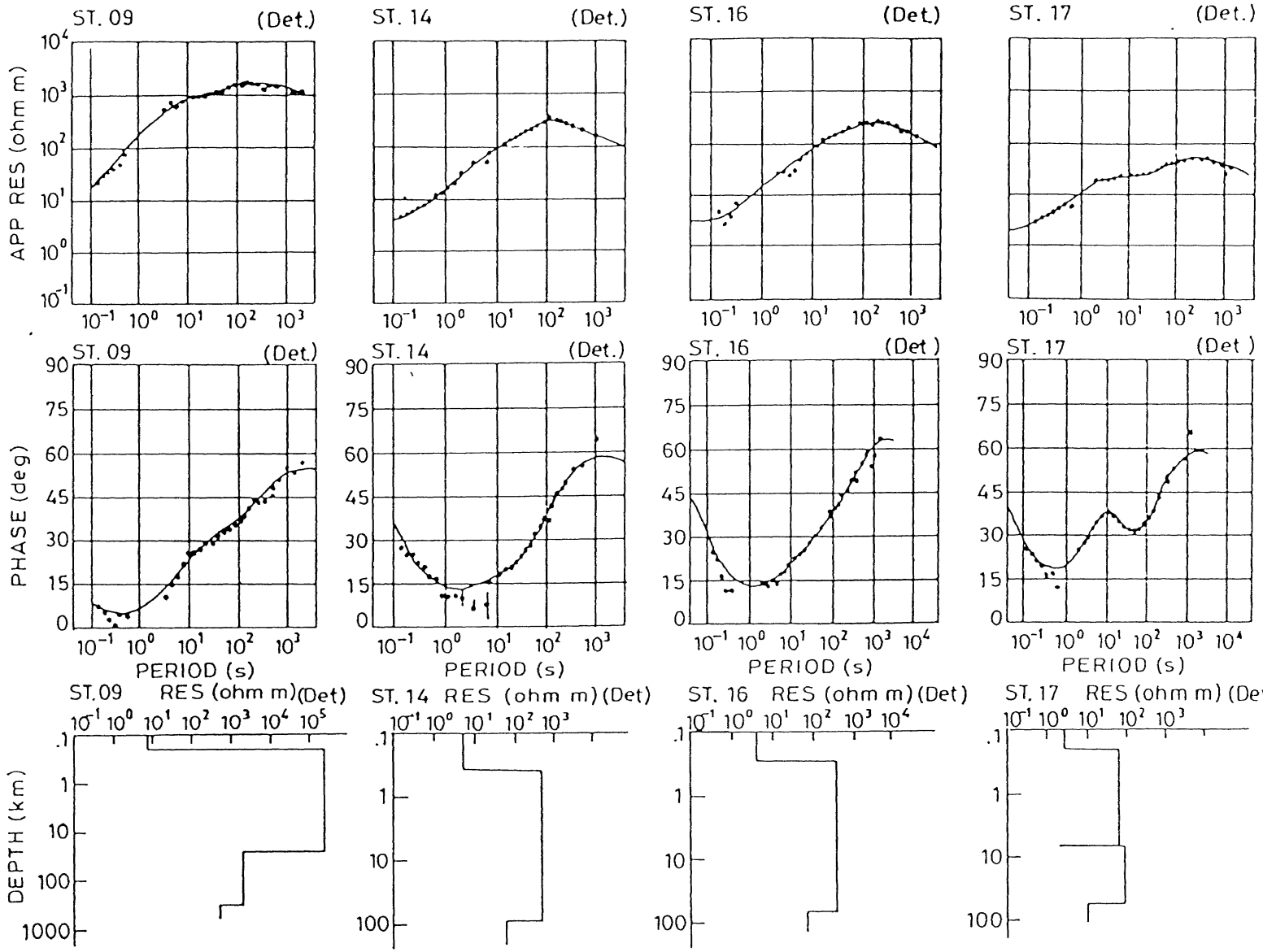

Figure 5.5 The apparent resistivity and phase determinant data and one-dimensional inversion result for the stations 9, 14, 16 and 17

magnetotelluric sounding results, the boundary of this ridge has been proposed to be extended up to Varanasi and beyond (shown by the thick dotted line Figure 5.2). In the western side of Kanpur (stations 14-18) , the top layer resistivity shows a variation of 5-7 Ω-m which corresponds to the resistivity of alluvial sediments. Beneath the alluvial sediments, the second layer resistivity corresponds to very light sediments (sedimentary rocks). Such sediments has also been revealed from the gravity measurements (Choudhury, 1975; Qureshy, 1969; Valdiya, 1976). The resistivity of this layer is found to be of the order of 80-300 Ω-m and extends to a great depth. These data do not reflect the resistivity corresponding to basement, which implies that the basement may be conductive due to the presence of saline water in pore spaces in the rock forming basement (Majorowicz and Gough, 1991). This is confirmed by the litho-logs available from the existing boreholes and the presence of higher salinity of the drinking water in this region. The low resistivity values of the second layer observed at the western stations along the profile (BB') are nearly the lowest resistivity values observed in the continental crust of shields of different regions in the world (Majorowicz and Gough, 1991; Haak and Hutton, 1986).A low conducting anomaly in the upper crust (station 17) at a depth of 8-10 Km is found. Its presence has also been confirmed from the magnetometer array studies (Arora et al., 1982).

Using one-dimensional resistivity variation with depth at each station a resistivity cross-section has been constructed (Figure 5.6) which shows only the alluvial sediments thickness along east-west profile (BB') in the Indo-Gangetic basin. The maximum thickness of alluvium sediments has been found to be of the order of 500 m near Kanpur. This agrees with the lithology obtained from deep boreholes

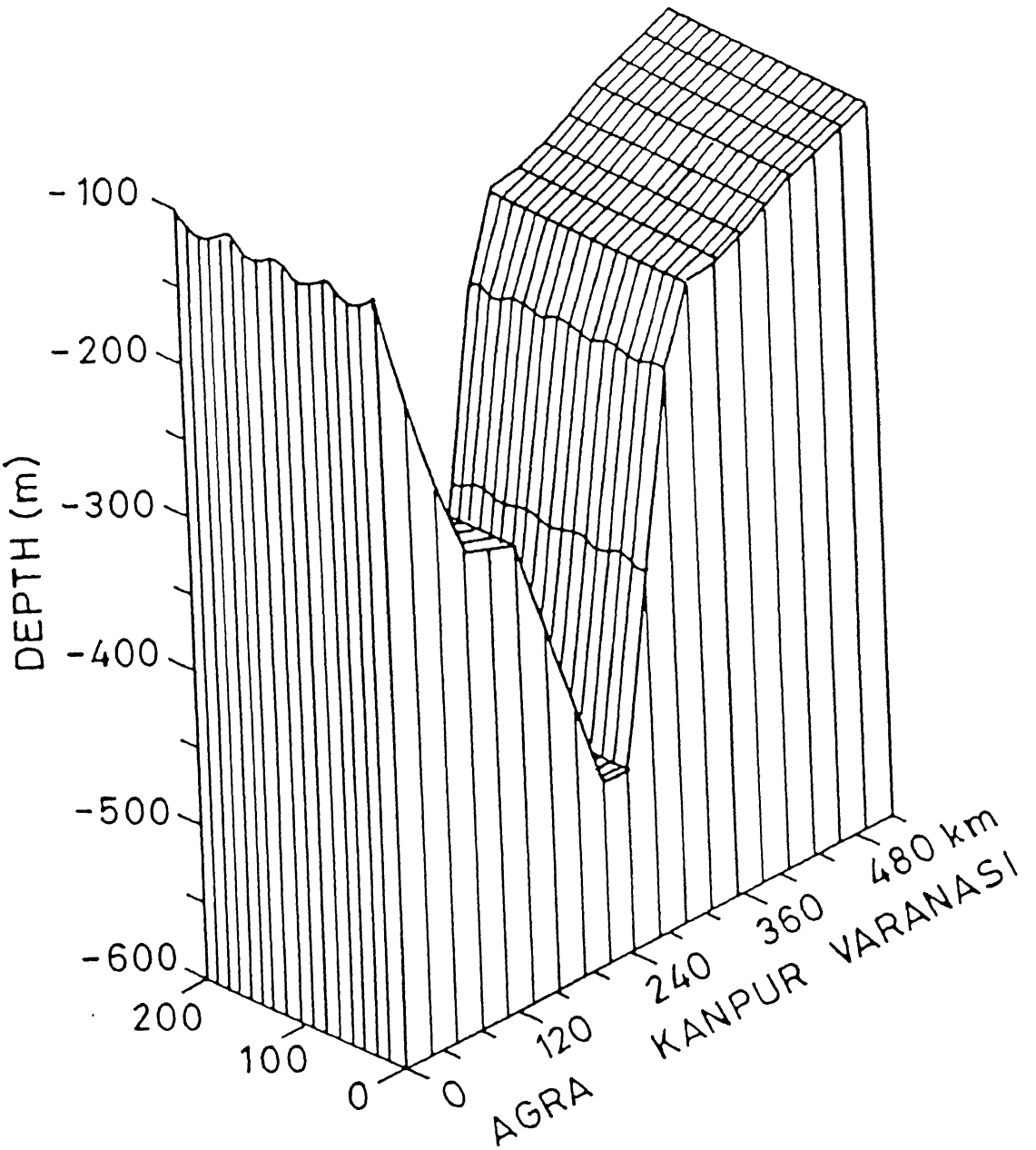

Figure 5.6 The resistivity cross-section along profile Agra-Varanasi (BB') showing the Ganga valley filled with alluvium sediments.

(upto 500 m depth) drilled for drinking water. The rotated impedance elements Z_{xx} and Z_{xy} are further analyzed. The rotated elements show variable strike at each stations along profile BB'. Due to variation in the strike direction and large station intervals, a proper two-dimensional modelling of the data has been found difficult.

5.7 Interpretation of Magnetotelluric Data Along Sub-meridianal Profile CC'

In order to interpret the average regional structure of the Indo-Gangetic basin, all of the representative stations (11, 9, 1, 14, 15, 3, and 4) are projected onto sub-meridianal profile CC' (Figure 5.7).

5.7.1 Behaviour of Polar Diagrams and Conductaces of Top Layer

The impedance tensor elements at each station along the profile CC' for various periods have been computed and analyzed azimuthly thruogh polar plots. The polar diagrams for diagonal element $|Z_{xx}(\omega, \alpha)|$ and off-diagonal element $|Z_{xy}(\omega, \alpha)|$ of impedance tensor, only at a representative period of 500 sec, are shown in Figure 5.8. The period 500 sec is chosen such that all the stations for this period could show interesting azimuthal characteristics of impedance tensor elements. The polar diagrams show three major features:

I. Diagonal components of the impedance tensor suggest more or less two-dimensional structure of the magnetotelluric field with major axes NNE and ESE directions. The later direction coincides with the trend of Indo-Gangetic plains. Therefore, one can conclude that the magnetotelluric field structure depends mainly on the geometry of sedimentary basin.

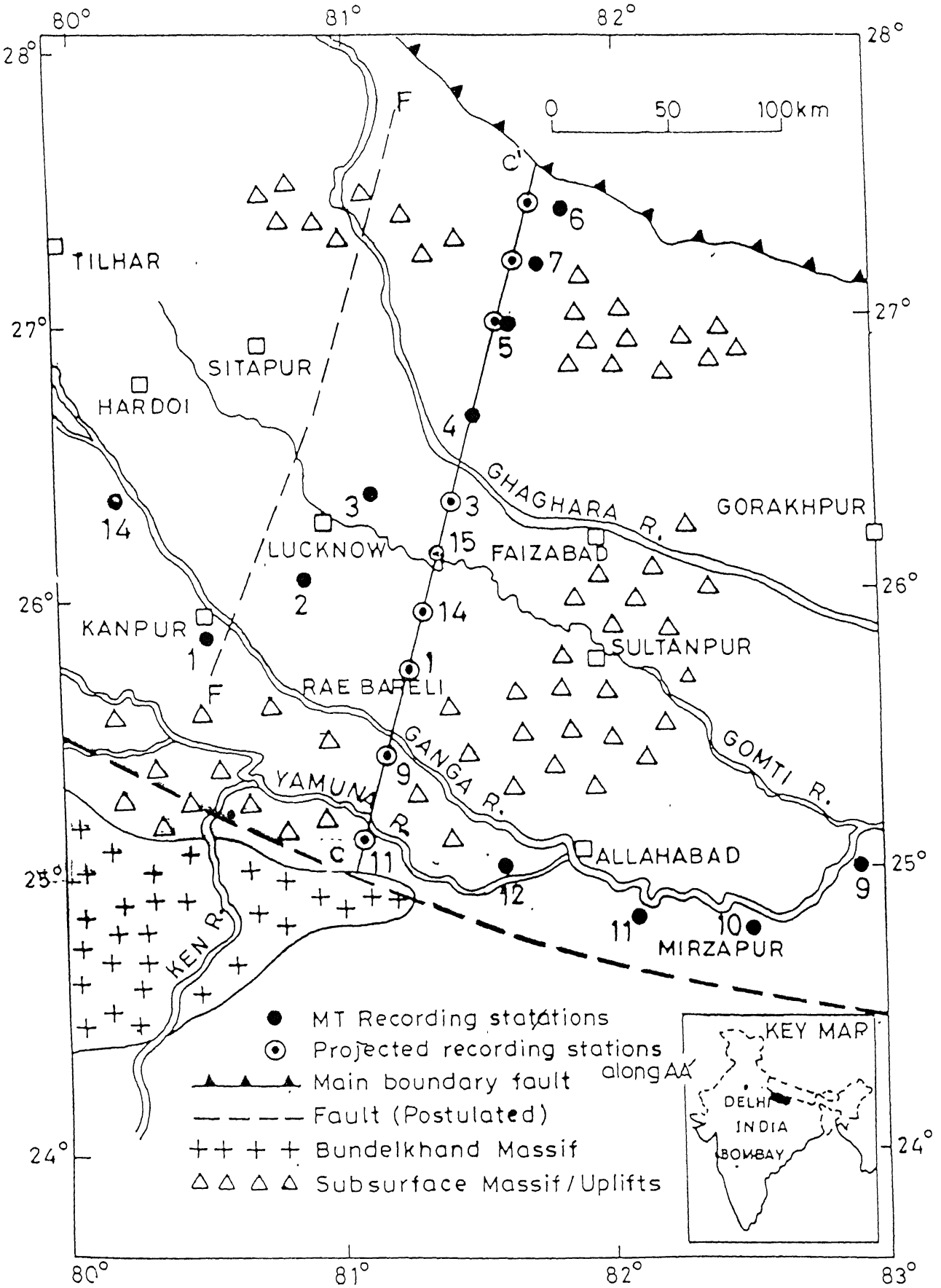

Figure 5.7 Map showing projection of magnetotelluric recording stations along sub-meridian profile CC'.

II The magnitude of the off-diagonal components of the impedance tensor at stations 1, 14, 15, 3 and 4 are three-four times smaller than those at stations 9 and 11. It is in accordance with the behaviour of the sediment conductance (Figure 5.9) estimated from apparent resistivity curves (Figure, 5.10, first row) for H-polarization. The Conductance is estimated by means of routine asymptotic technique (Porstendorfer, 1975)

$$S = 114 \sqrt{T}$$

where T is period corresponding to the point of intersection between asymptote drawn at 45^{o} on the asending branch of ρ_{ayx} and line $\rho_a = 10.0$, only if the length of one decade on period-axis is equal to the length of one decade on ρ_a-axis. The conductance value is found to be about 17 Siemens at the southern end (station 11) of the profile CC', which increases to 60 Siemens at station 1 and reaches 283 Siemens at the northern end of the profile CC' (station 4).

III. The azimuth of major axis of the polar diagrams turns through 90^{o} between stations 9 and 1. The stations 11 and 9 are located over a highly resistive underlying formation which seems to be the extension of Bundelkhand massive. At these stations the azimuth of the major axis is nearly perpendicular to the trend of the Indo-Gangetic basin. For rest of the stations the major axis is more or less parallel to this trend.

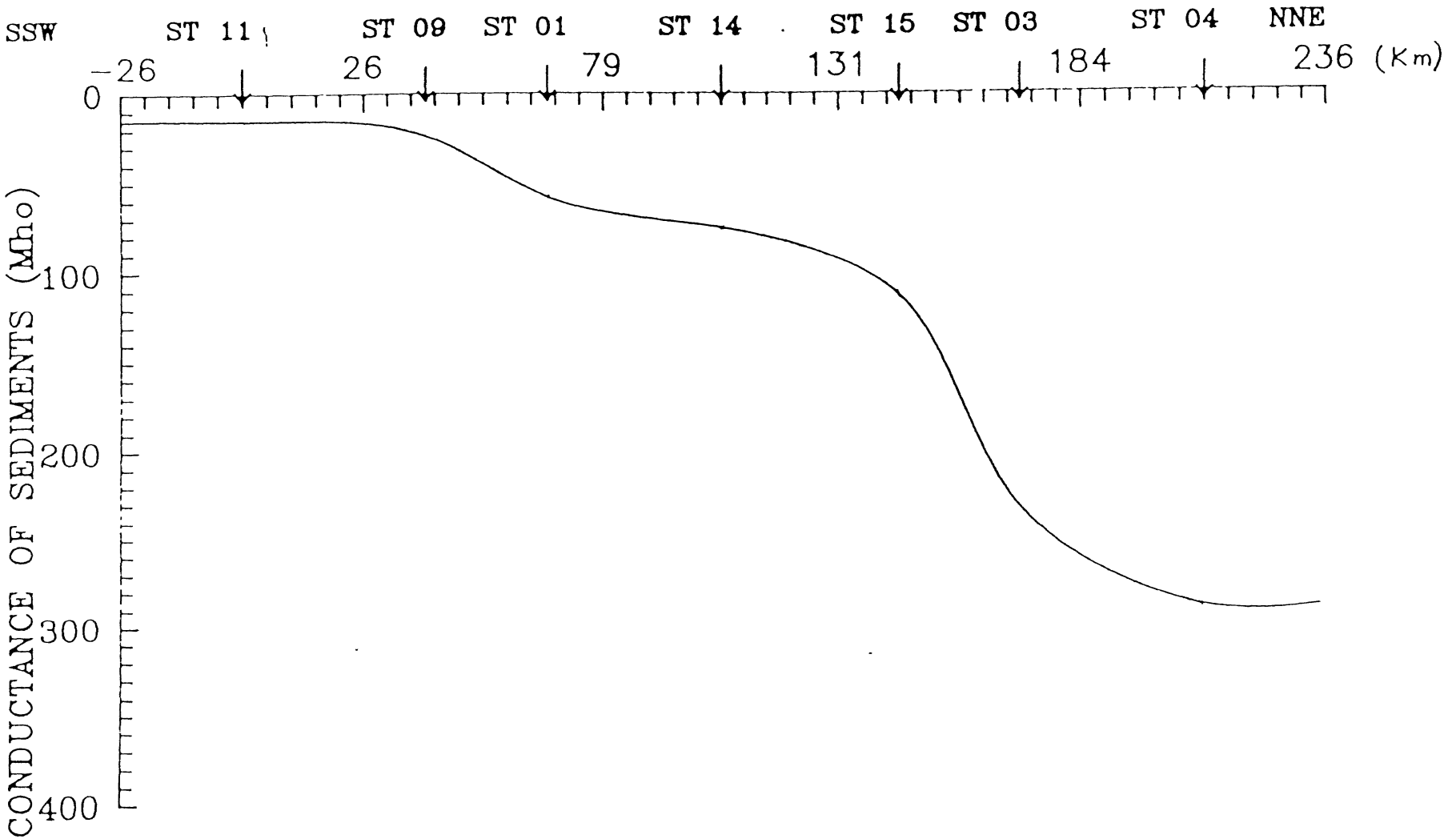

Figure 5.9 Conductance computed from field data shown at recordig stations along profile AA'.

5.7.2 Behaviour of Data

The data along profile CC' (Figure 5.10), suggest that only at long periods, their behaviour have a large difference between E- and H-polarizations at each station, except stations 3 and 4 but these stations (3 and 4) have large values for conductance of top layer compared to other stations. Moreover, from the asymptotic values of apparent resistivities at short periods, it is inferred that near surface ground below each station has differing resistivity, which changes one fold on logrithmic scale between stations 11 and 14. Therefore, posible models to explain the behaviour are to be found in terms of either two-dimensional regional structures or a layered Earth structure for deeper parts together with inhomogeneous surface layer. The former has been tried for profile AA' and is not possible for present profile (CC') due to the very simple reason that it contains projected stations and hence, their interpretation as a two-dimensional regional structure will not warrant a true location of structures below each station. The former is simple in the sense that in actual case, the deeper part of the two-dimensional model is essentially one-dimensional. The two-dimensional modelling, in what follows, is motivated by the above statement which allows the two-dimensional model consist of a layered Earth structure for deeper parts and a surface layer, segmented symmetrically around each station with differing resistivities. It has been tried to prove i) that such a two-dimensional model essentially is one-dimensional for deeper parts, ii) that E-polarization for such two-dimensional model is equivalent to local one-dimensional at each station, iii) that the H-polarization can not be used to deduce information for deeper structures due to distortion by near surface inhomogeneities, and iv) that the E-polarization can be used to deduce

information for deeper structures

5.7.3 Two-dimensional Modelling Along Sub-meridianal Profile CC'

The magnetotelluric field data along the sub-meridianal profile CC' (Figure 5.7) show a magnetotelluric field typical of a two-dimensional structure. Accordingly, two-dimensional modelling was carried out using Brewitt-Taylor and Weaver (1976) algorithm for period range 0.25-4096 seconds. The top layer thickness of two-dimensional model is taken to be 1500 meters in order to fulfill the criteria of thin sheet. The conductance ($S = h/\rho$) of top layer, computed at each station from field data, for H-polarization (Porstendorfer, 1975), has been incorporated to select the resistivity of segments below the each station which is valid for shorter periods and then a tentative one-dimensional model for deeper layers has been considered.

The field data (observed), theoretically computed apparent resistivities, and the two-dimensional model over which they are computed, have been shown in Figure 5.10 (top, middle and bottom row, respectively). Theoretically computed curves for E- and H-polarizations are shown by dashed lines, and for local one-dimensional by solid line. Local one-dimensional model, at a particalar station, is the model which is obtained by replacing the resistivities of top layer throughout with the resistivity of the segment underlying the station for which local one-dimensional response is wanted. It is observed that theoretically computed results for E-polarization and for local one-dimensional are very similar. The apparent resistivities for H-polarization were found to be higher than one-dimensional apparent resistivities at the northern and southern ends of profile CC' (Figure 5.10, stations 11 and 4) and lower than one-dimensional results over the basin. Hence, H-polarization

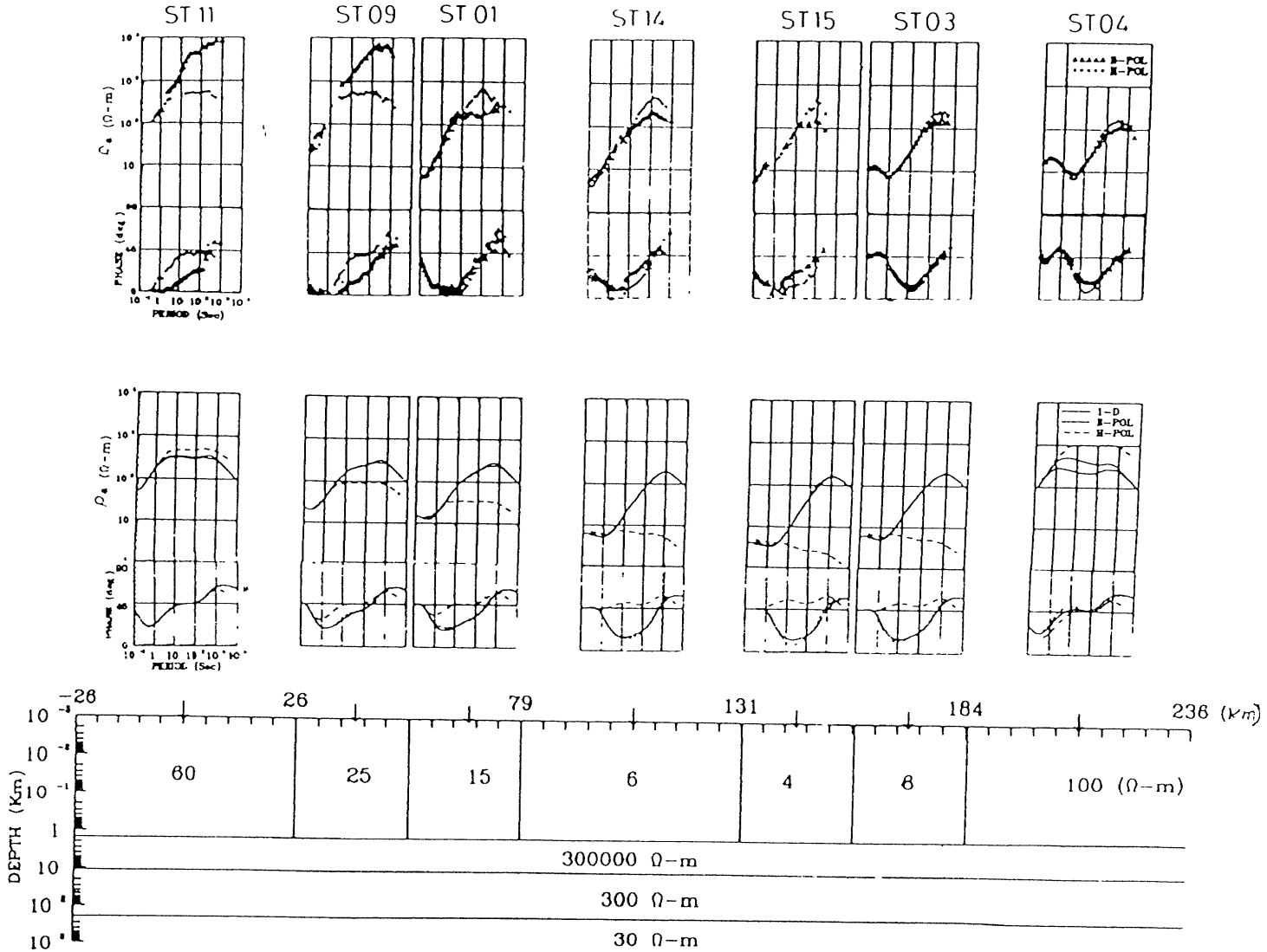

Figure 5.10 Variation of Apparent resistivity at various recording stations along profile AA' (top curves show field data, middle curves show response of model at bottom).

results can not be used for deeper information because of distortion all along the profile CC'. These responses of E- and H-polarizations were found to be in good agreement with the field polar-diagrams shown in Figure 5.8. From the results of numerical modelling, E-polarization data has been selected for the estimation of resistivity structure for deeper parts. The E-polarization corresponds to the ρ_{max} for stations 9 and 11 and to the ρ_{min} for the rest of the stations.

In Figure 5.10, the measured E- and H-polarization apparent resistivities and phase curves are shown. At stations 15, 3 and 4 the apparent resistivity curves show the strong screening effect of thick sediments found in this part of the Indo-Gangetic basin. The apparent resistivity curves shown in Figure 5.11a are similar to the apparent resistivity curves obtained in the western part of the Deccan trap (Gokaran et al. 1992).

For reliable interpretation, apparent resistivity and phase curves free from distortions have been considered. The diagonal components of the impedance tensor suggest more or less two-dimensional structure at stations 11, 9, 1, 14, 15, 3 and 4. These stations are lying in the Indo-Gangetic basin where a layer of highly conducting sediments is present at the top. These sediments can be treated as a conducting thin sheet which can produce distortion on the magnetotelluric sounding curves. Such distortions can be removed using the approach followed by Adam et al. (1982, 1984).

Influence of sediment resistivity on sounding curves is shown in Figure 5.11a. When top layer (sediments) resistivity is 20 Ωm or 40 Ωm, one can hardly infer about the resistivity of layer which is just below the sediments. But after removal of sediments when top layer resistivity becomes 4000 Ωm, correct estimation of first layer can be made from the

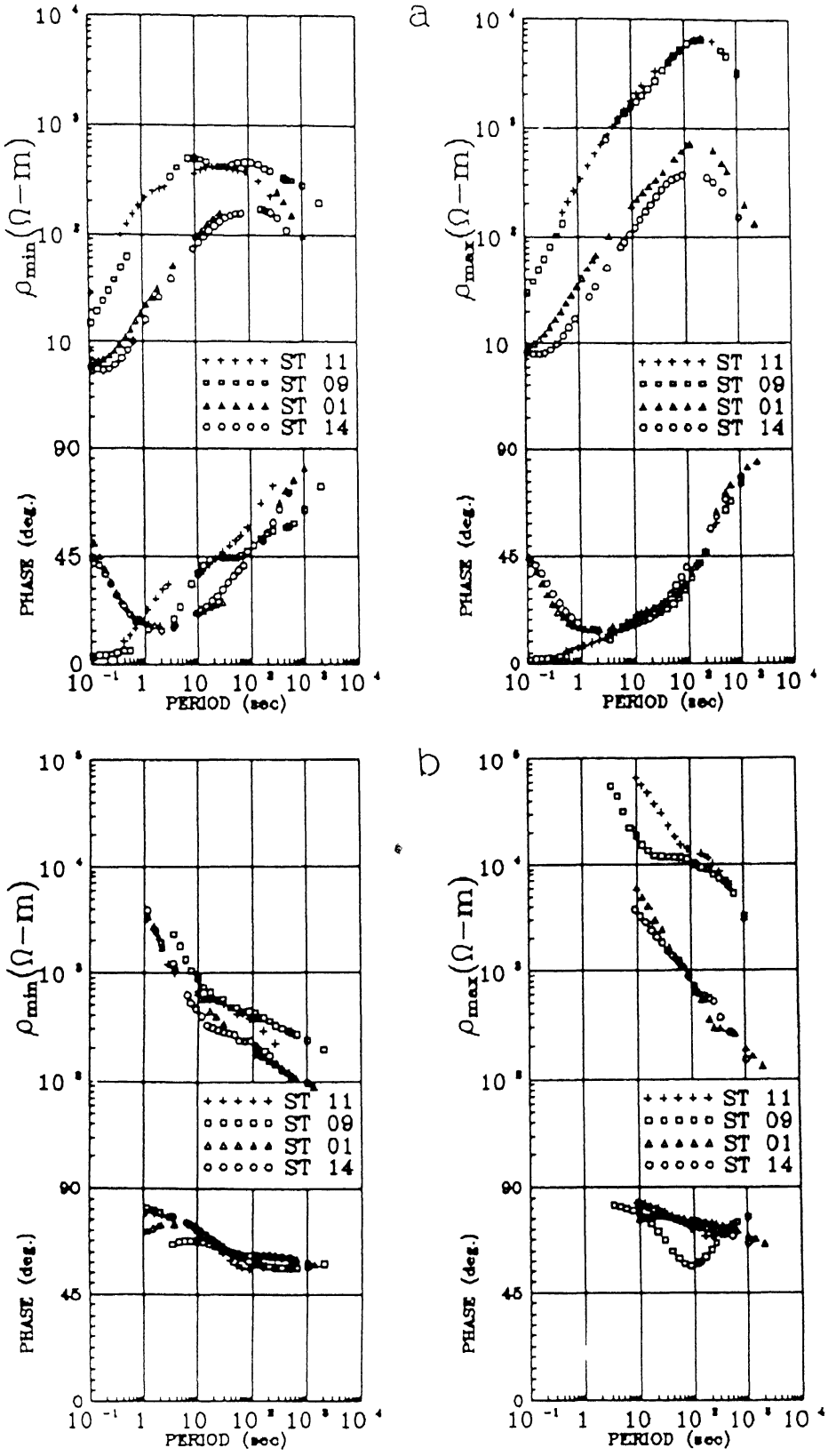

Figure 5.11 ρ_{max} and ρ_{min} variations for Stations 1, 9, 11 and 14 in the case of (a) top layer is covered with sediments and (b) without sediments on the top layer.

sounding curves (Figure 5.11b).

The difference between the two types of curves is mainly due to changes of the near surface conductance (S), so it is better to remove the screening effect present, using the following relation (Adam et al. 1982, 1984)

$$Y = Y_0 - S$$

where, Y_0 is admittance on the surface of the Earth and S is top layer conductance. This allows to obtain an admittance (Y) below the sediments, from the admittance (Y_0) and conductance (S) values estimated from the field data. Y is the admittance without the influence of the conductance S. The E- polarization curves for ρ_{max} from stations 11, 9 and ρ_{min} from stations 1, 14 were then averaged in order to reduce small scale three-dimensional distortions. The average apparent resistivity curves clearly show a resistive upper crust (apparent resistivity upto > 10^4 Ω-m) and a decrease of slope of the apparent resistivity curve in period range 10 to 100 s. This decrease suggests the existence of the crustal conducting layer, although apparent resistivity curves do not show a clear minimum. A similar conducting layer is also seen from the averaged apparent resistivity curves measured in the central part of Siberian platform (Figure 5.12). The apparent resistivity curves of Singhbhum batholith region are also similar to the curves shown in Figure 5.12 (Roy et al., 1989). On the Singhbhum batholith the sediment conductance is only a few Siemens, but the level of the apparent resistivity curves are high due to static shift.

Apparent resistivity and phase curves have been computed over four layered models in order to study their behaviour when the first layer thickness (Figure 5.13a) and second layer resistivity (Figure 5.13b) are varied. The effects of changes in the thickness and resistivity of the

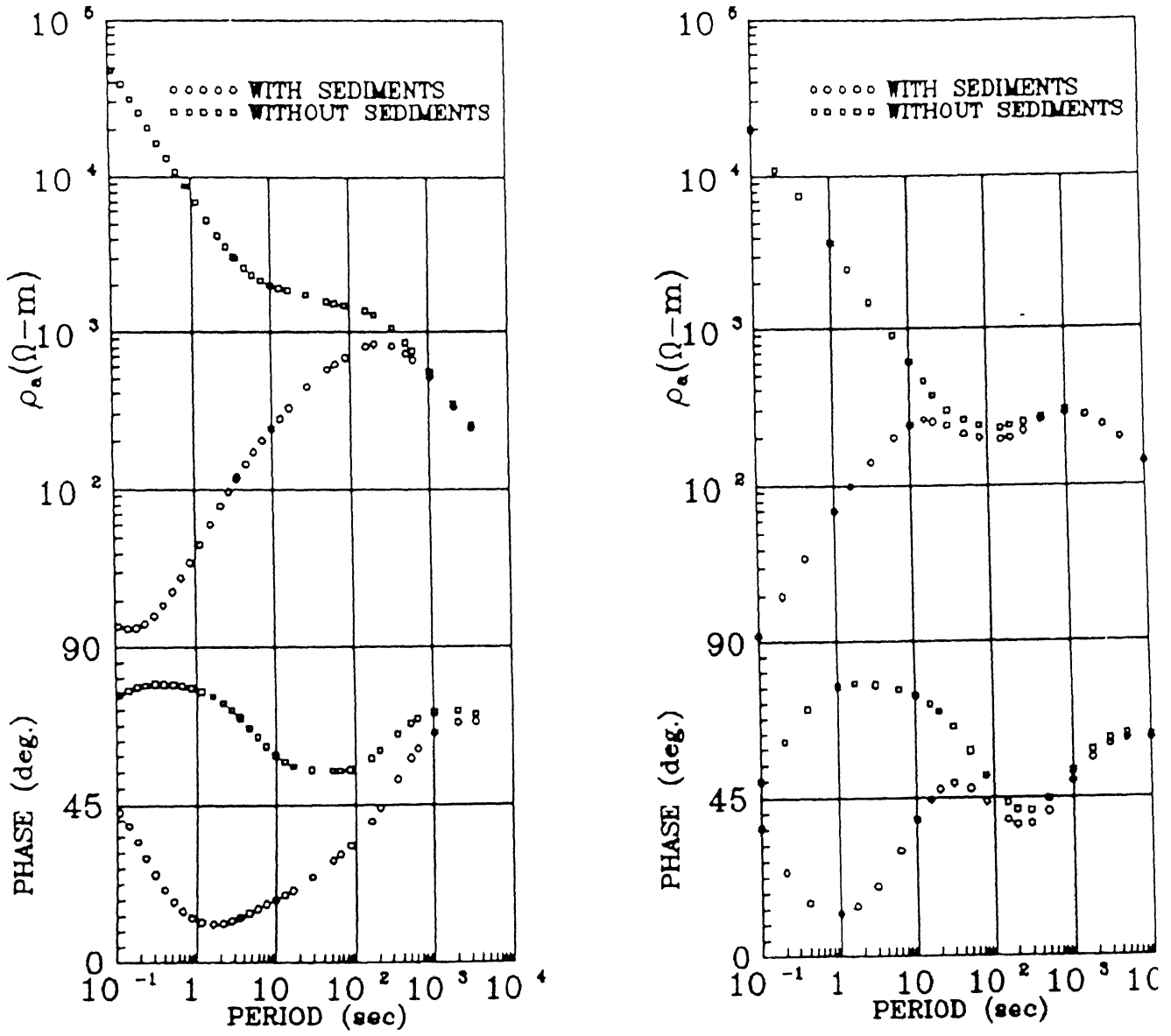

Figure 5.12 Variation of ρ_{av} (average) for Indo-gangetic basin (left part) and Siberian plateform (right part)with and without sediments.

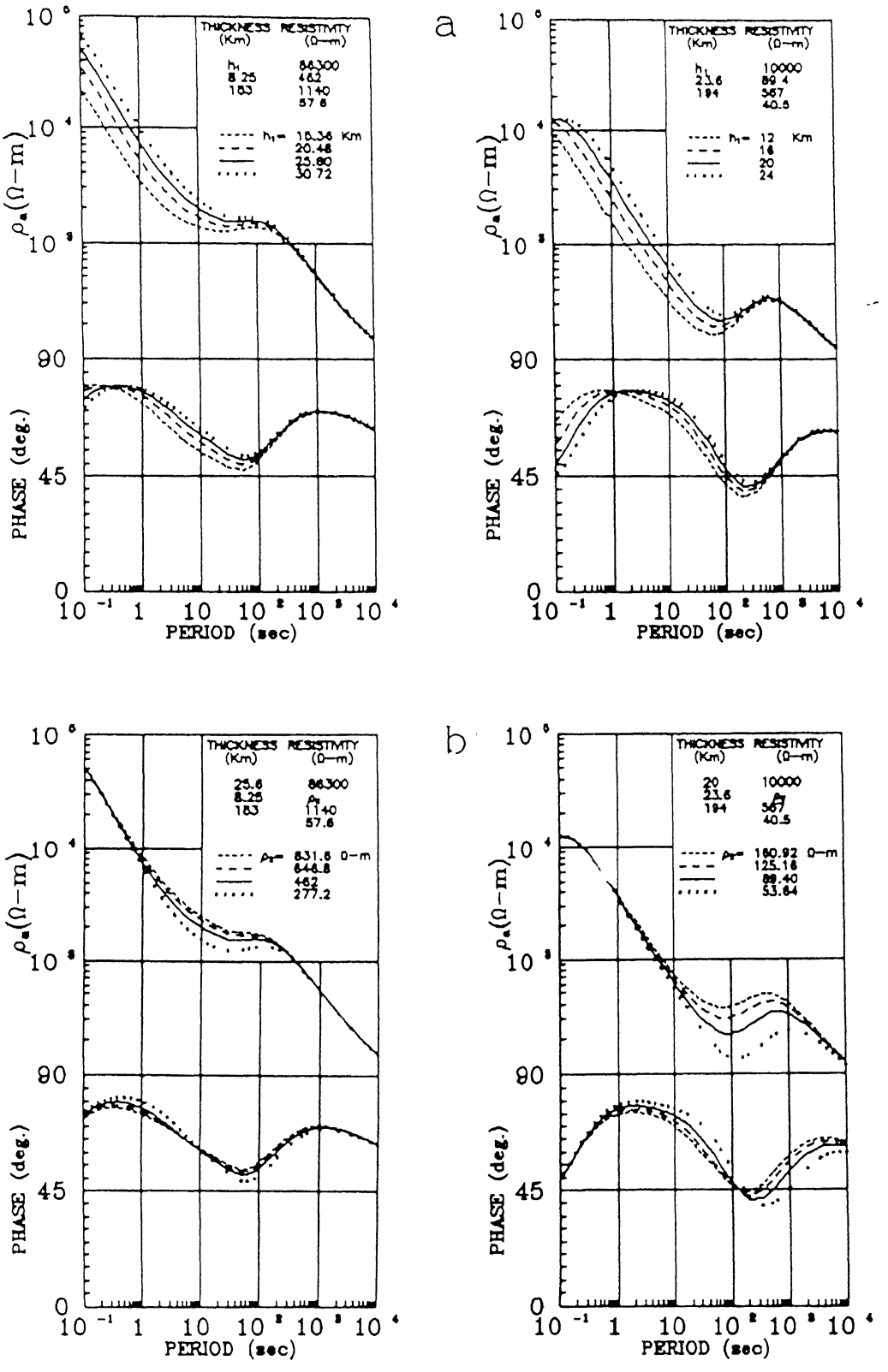

Figure 5.13 Variation of apparent resistivity and phase over four layered models (a)with varying thickness of the top layer and (b) with varying resistivity of the second layer

second layer whilst keeping its conductance ($S=h/\rho$) constant are shown in Figure 5.14. The solid curves shown in Figure 5.13a,b and 5.14 show the best fit model for the corresponding region. The best fit model for Indo-Gangetic basin has a high resistive upper crust ($\simeq$ 25 Km thick), deep crustal conductor ($\simeq$ 8 Km thick) with a resistivity of 462 Ω-m and an upper mantle of high resistivity. The mantle just below the crustal conducting layer has a resistivity value of 1140 Ω-m. For more precise estimation of the upper mantle resistivity long period observations are required.

The best fit model for Siberian platform is shown by a dashed line in Figure 5.15. The thickness and conductivity of the crustal conducting layer of Siberian region are found to be higher than for a similar layer in the model of Indo-Gangetic plains. The maximum resistivity of the upper mantle is almost two times greater than for the Siberian platform, but below 200 Km resistivities for both models are practically the same. The magnetotelluric response parameters have been computed to estimate its sensitivity to changes in parameters of crustal layers. The results show that an increase in the thickness of the upper crust from 20 to 30 Km results in a 100% increase in the apparent resistivity (Figure 5.13a, at short periods). However, the soundings are much less sensitive to the resistivity of the upper crust. The effects on the sounding curves caused by variations of the thickness and resistivity of the deep crustal conductor have been analyzed under the condition that the conductance of this layer remains fixed. Results of this analysis show that an increase of the resistivity of this layer from 231to 924Ω-m causes a change of 50% in the apparent resistivity calculated at a period of 100 seconds. One can thus, conclude that the important features of the model can be resolved using magnetotelluric soundings.

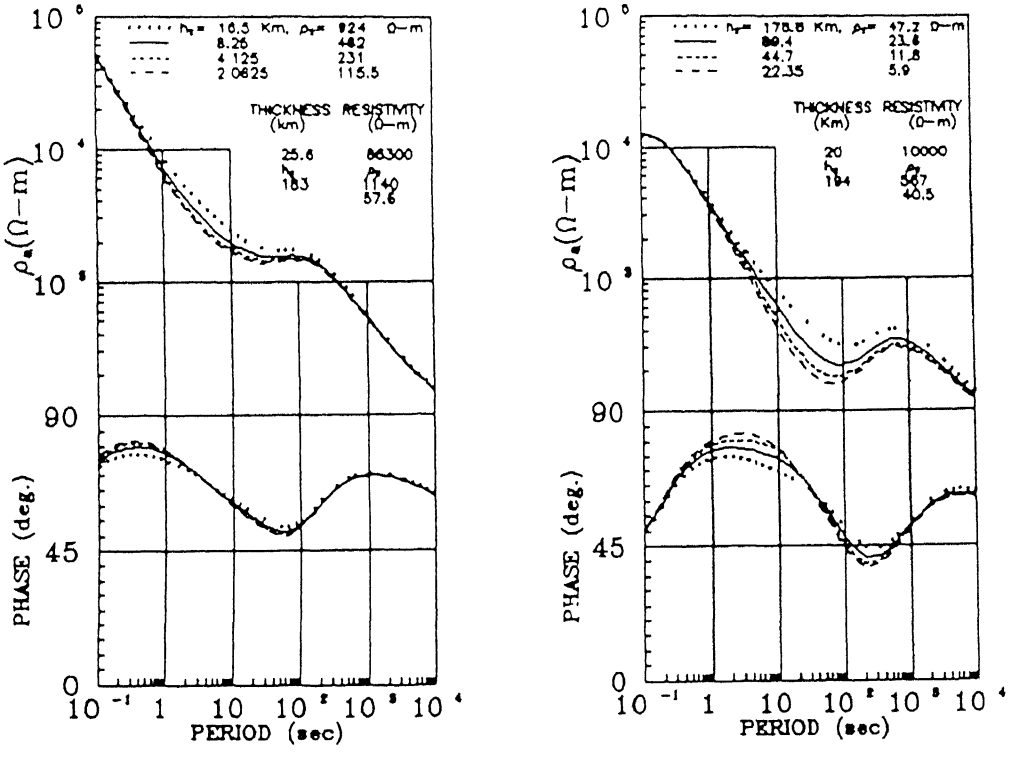

Figure 5.14 Variation of apparent resistivity and phase over four layered models having constant conductance ($S=h/\rho$) of the second layer.

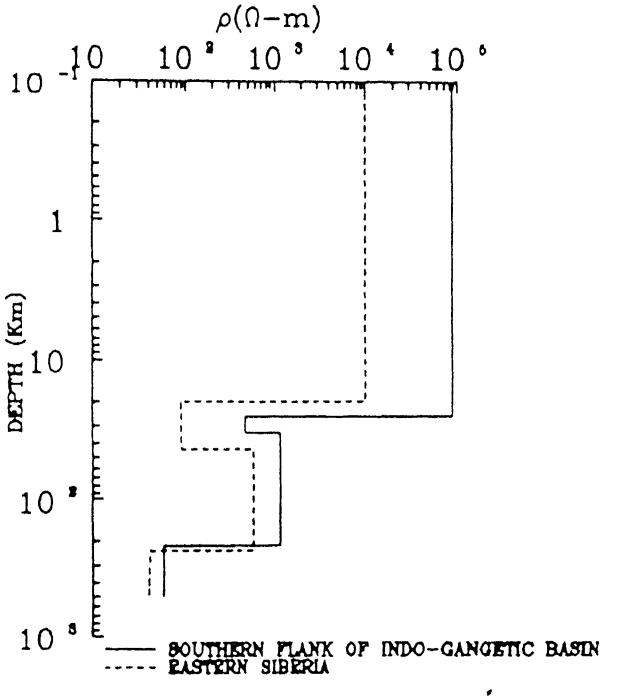

Figure 5.15 Comparison of the best fit of the subsurface resistivity of Indo-gangetic plains with Siberian plateform.

5.8 Conclusions

The southern part of the Indo-Gangetic plains can be considered to have a two-dimensional structure. The high resistivity shown by the stations east of Kanpur confirm the presence of a high resistive structure beneath the Indo-Gangetic plains which could be the subsurface extension of the Bundelkhand granite.

Inversion of the E-polarization apparent resistivity reveals a crustal conducting layer at a depth of 25 Km. This layer is 8 Km thick, with a resistivity of 462 Ω-m, giving the layer a conductance value of 18 Siemens. This conductance value is very less than the conductance of a crustal conductor found beneath the Siberian platform.

The magnetotelluric results show low resistivity zones in the Indo-Gangetic basin. This low resistivity zones at a shallow depth show the possibility of the presence of sediments. The low resistivity sediments show a strong possibility that these sediments may contain hydrocarbon since the presence of hydrocarbon is generally associated with saline water which reduce the resistivity of sediments or rocks. A two-dimensional modelling of data along Kanpur-Nepal show the presence of anticlinal geological structure around Bahraich area. The rotated tensor impedance elements show orientation of this anticlinal structure in $N30^{O}E$-$S30^{O}W$. Thus, the present magnetotelluric studies show promising results in the region under study which deserves further detailed study of the area to obtain more reliable information keeping in mind that present results are perliminary and have high level of errors from 10-20

CHAPTER VI

SUMMARIZED CONCLUSIONS AND SCOPE FOR FUTURE STUDIES

6.1 Conclusions

The conclusions drawn from the problems studied separately in different Chapters are reported at the end of the respective Chapters. The summarized conclusions relevant to specific problems studied are outlined below:

1. Analytical and numerical determination of step and impulse response functions in time domain for various Earth models have been found useful in subsequent stages of study; such as in computing the apparent resistivities., and sensitivity functions.
2. The apparent resistivity definition D7 has been found to show the most efficient transition and succession of subsurface structures followed by D8, D2, D4 and D3, respectively.
3. The apparent resistivity curves D2 and D3 in frequency domain have been found to resemble with the apparent resistivity curves D7 and D8 in time domain, respectively.
4. The magnetotelluric measurements for all models are found to be the most sensitive; on or near the surface of the Earth in frequency domain, except for the case in which conductivity of the Earth continuously increases exponentially with depth; and at depths below the surface of the Earth in time domain.
5. The magnetotelluric measurements, in both the domains, are found to give good resolution for sandwiched narrow regions of high conductivity but not in intervening resistive regions.

6. The sensitivity at depths above the embedded conductive region is found to increase only for impulse response function.
7. The sensitivity at depths above the embedded resistive region is found to increase only for measurements in frequency domain, and below it for measurements in both the domains.
8. Magnetotelluric data suggest a high resistive structure beneath the Indo-Gangetic plains which could be the subsurface extension of the Bundelkhand granite.
9. The magnetotelluric results show low resistivity zones in the Indo-Gangetic basin. This low resistivity zones at a shallow depth show the possibility of the presence of sediments.

6.2 Scope for Future Studies

The results reported for apparent resistivity definitions and sensitivity analysis in this thesis illustrate the basic effects for both the domains which are worth investigating in more complicated situations. Moreover, the interpretation has been carried out only using approaches in frequency domain which can be extended in time domain as well. The following topics are recommended for future studies in both the domains.

1. The comparative study of apparent resistivity definitions in both the domains using present approach and
   a) considering the models containing lateral inhomogeneities near or on the Earth's surface,
   b) considering the models containing continent-ocean boundary, and
   c) considering the models containing conductive or resistive two-dimensional bodies (having infinite length compared to width)

embedded in uniform homogeneous half-space; such as horizontal rectangular parallelepiped with finite but variable width and thickness, horizontal cylinder with finite but variable diameter, faulted slab below the surface of the Earth with finite but variable thickness etc.

2. The sensitivity analysis of the models given under first topic.
3. The comparative study of interpreted results in both the domains using experimental magnetotelluric data as in following stages:
   a) the estimation of the impedance tensor using an adaptive parametric time domain processing approach (Yee et al. 1988),
   b) the inversion of the magnetotelluric data, processed in time domain above,
   c) the inversion of the magnetotelluric data processed in frequency domain,
   d) the inversion of the magnetotelluric data processed in frequency domain and corrected for static effects, and
   e) the two-dimensional modelling of the data for both the domains.

REFERENCES

REFERENCES

Abramovici, F., (1974), "The Forward Magnetotelluric Problem of an Inhomogeneous and Anisotropic Structure", *Geophysics*, 39, 56-68.

Abramowitz, M. and Stefun, I. A., (1964), "Hand Book of Mathematical Function With Formulas, Graphs, and Mathematical Tables", *National Bureau of standards, Applied Mathematics series*, 55.

Adam, A., Vanyan, L. L., Varlamov, D. A., Yegorov, I. V., Shilovski, A. P. and Shilovski, P. P., (1982), "Depth of Crustal Conducting Layer and Asthenospheric in the Pannonian Basin Determined by Magnetotellurics", *Physics of the Earth and Planetary Interior*, 28, 251-260.

Adam, A., et. al., (1984), "On Deep Electrical Conductivity of the Pannonian Basin", *Fizika Zemli*, No. 6, 100-102.

Adam, A., Duma, G., Gutdeutsch, R., Vero, J. and Wallner, A., (1986), "Periadriatic Lineaments in the Alps Studied by Magnetotellurics", *Journal of Geophysics*, 59, 103-111.

Adam, A., Duma, G. and Horvath, J., (1990), "A New Approach to the Electrical Conductivity Anomalies in the Drauzug-Bakony Geological Unit", *Physics of the Earth and Planetary Interior*, 60, 155-162.

Adam, A. and Verga, G., (1990), "Distortions of the Electromagnetic Field by Shallow Basins and by Resistive Outcrops", *Physics of the Earth and Planetary Interior*, 60, 80-88.

Anderssen, R. S., (1975), "On the Inversion of Global Electromagnetic Induction Data", *Physics of the Earth and Planetary Interior*, 10, 292-298.

Arora, B. R., Lilley, F. E. M., Sloane, M. N., Singh, B. P., Srivastava, B. J. and Prasad, S. N., (1982), "Geomagnetic Induction and Conductive Structures in Northwest India", *Geophysical Journal of Royal Astronomical Society*, 69, 459-475.

Auden, J. B., (1934), "The Geology of the Krol. Belt.", *Rec. Geol. Surv. Ind*, 67, 357-454.

Backus, G. E. and Gilbert, F., (1967), "Numerical Applications of a Formalism for Geophysical Inverse Problem", *Geophysical Journal of the Royal Astronomical Society*, 13, 247-276.

Backus, G. and Gilbert, F., (1968), "The Resolving Power of Grass Earth Data", *Geophysical Journal of the Royal Astronomical Society*, 16, 169-205.

Banerjee, B., Sengupta, B. J. and Pal, B. P., (1980), "Apparent Resistivity of a Multilayered Earth With a Layer Having Exponentially Varying Conductivity", *Geophysical Prospecting*, 28, 435-452.

Beloussov, N. A., Belyaevsky, A. A., Borison, B. S., Volvovsky, B. S., Volovsky, I. S., Resvoy, D. P., Tal-Virsky, B. B., Khamrabaev, I. Kh., Kaila, K. L., Narain, H., Marussi, A. and Finetti, J., (1980), "Structure of the Lithosphere Along the Deep Seismic Sounding Profile: Tien Shan - Pamirs - Karakorum - Himalayas", *Tectonophysics*, 70, 193-221.

Berdichevsky, M. N. and Dmitriev, V. I., (1976a), "Basic principles of Interpretation of Magnetotelluric Sounding Curves, in: Geoelectric and Geothermal Studies", *KAPG Geoph. Mon. Adam A. (ed.), Budapest: Akademiai Kiado*, 165-221.

Berdichevsky, M. N. and Dmitriev, V. I., (1976b), "Distortion of Magnetic and Electric Fields by Near Surface Lateral Inhomogeneities", *Acta Geod. Geophys. Mont. Hung*, 11, 447-483.

Berdichevsky, M. N., Dubrovskiy, K. I., Soloklov, V. V. and Faynberg, E. B., (1970), "Geoelectric Characteristics of the Earth's Crust and Upper Mantle in Turkmenia", Izv., *Earth Physics*, 11, 86-91.

Berdichevsky, M. N., Vanyan, L. L., Kuznetsov, V. A., Levadny, V. T., Mandelbaum, M. M., Nechaeva, G. P., Okulssky, B. A., Shilovsky P. P. and Shpak, I. P., (1980), "Geoelectric Model of the Baikal Region", *Physics of the Earth and Planetary Interior*, 22, 1-11.

Bhattacharya, S. N., (1981), "Observation and Inversion of Surface Wave Group Velocity Across Central India", *Bull. Seismol. Soc. Am.* 71, 1489-1501.

Bhattacharya, S. N., (1991), "Surface Wave and Lithosphere Structure Across the Northwestern Part of the Indian Peninsula", *Pure Applied Geophysics*, 135, 53-59.

Boerner, D. E. and Holladay, J. S., (1990), "Approximate Fréchet Derivatives in Inductive Electromagnetic Soundings", *Geophysics*, 55, 1589-1595.

Boerner, D. E. and West, G. F., (1989a), A Generalized Representation of Electromagnetic fields in a Layered Earth", *Geophysical Journal of the Royal Astronomical Society*, 97, 529-547.

Boerner, D. E. and West, G. F., (1989b), A Spatial and Spectral Analysis of Electromagnetic Sensitivity in a Layered Earth", *Geophysical Journal International*, 98, 11-21.

Boerner, D. E. and West, G. F., (1989c), "Fréchet Derivative and Single Scattering Theory", *Geophysical Journal International*, 98, 385-390.

Brewitt-Taylor, C. R. and Weaver, J. T., (1976), "On the Finite Difference Solution of Two-Dimensional Induction Problems", *Geophysical Journal of the Royal Astronomical Society*, 47, 375-396.

Cagniard, L., (1953), "Basic Theory of the Magnetotelluric Method of Geophysical Prospecting", *Geophysics*, 18, 605-635.

Cantwell, T., (1960), "Detection and Analysis of Low Frequency Magnetotelluric Signals, Ph.D. Thesis, Geology and Geophysics", *Massachusetts Institute of Technology*.

Chave, A. D., (1984), "The Fréchet Derivatives of Electromagnetic Induction", *Journal of Geophysical Research*, 89, 3373-3380.

Chave, A. D. and Cox, C. S., (1982), "Controlled Electromagnetic Sources for Measuring Electrical Conductivity Beneath the Oceans, Forward Problem and Model Study", *Journal of Geophysical Research*, 87, 5327-5338.

Chaudhury, S. K., (1966), "Seismic Surface Wave Dispersion and the Crust Across the Gangetic Basin", *Ind. J. Met. Geophysics*, 17, 385-394.

Choudhury, S. K., (1975), "Gravity and Crustal Thickness in Indo-Gangetic Plains and Himalayan Region, India", *Geophysical Journal of the Royal Astronomical Society*, 40, 441-452.

Chun, K. Y., (1986), "Crustal Block of the Western Ganga Basin: A Fragment of Oceanic Affinity", *Bull. Seismol. Soc. Am.*, 76, No. 6, 1687-1698.

Dewey, J. F. and Bird J. M., (1970), "Mountain Belts and New Global Tectonics", *Journal Geophysical Research*, 75, 2625-2647.

Dobrin, M. B. and Savit, C. H., (1988), "Introduction to Geophysical Prospecting", *McGraw-Hill International Editions*.

Edward, R. N., Bailey, R. C. and Garland, G. D., (1981), "Conductivity Anomalies: Lower Crust or Asthenosphere ?", *Physics of the Earth and Planetary Interior*, 25, 263-272.

Edwards, R. N., Nobes, D. C. and Gomez-Trevino, E., (1984), "Offshore Electrical Exploration of Sedimentary Basin: The Effects of Anisotropy in a Horizontally Isotropic, Layered Medium", *Geophylies*, 49, 566-576.

Fisher, G., Schnegg, P. A., Peguiron, M. and Le luang, B. V., (1981), "An Analytic One-Dimensional Magnetotelluric Inversion Scheme", *Geophysical Journal of the Royal Astronomical Society*, 67, 257-278.

Gansser, A., (1964), "The Geology of the Himalayas", *Wiley Interscience* New York, 289.

Gansser, A., (1974), "Himalaya, Mesozoic, Cenozoic Orogenic Belts", *Geological Society of London*, Special publication", No. 4, 207-218.

Glenn, W. E. and Ward, S. H., (1976), "Statistical Evaluation of Electrical Sounding Methods, Part I: Experimental Design", *Geophysics*, 41, 1207-1221.

Gokaran, S. G., Rao, C. K. and Singh B. P., (1992), "Magnetotelluric Investigation Across the Kurdavadi Rift Region", Paper presented at the *International Symposium on Deep Electromagnetic Exploration*, held at IIT Kharagpur, 13-16 January, (1992).

Gomez-Trevino, E., (1987a), "Nonlinear Integral Equations for Electromagnetic Inverse Problems", *Geophysics*, 52, 1297-1302.

Gomez-Trevino, E., (1987b), "A Simple Sensitivity Analysis of Time Domain and Frequency Domain Electromagnetic Measurements", *Geophysics*, 52, 1418-1423.

Gomez-Trevino, E. and Edwards, R. N., (1983), "Electromagnetic Soundings in the Sedimentary Basin of Southern Ontario - a Case history", *Geophysics*, 48, 311-330.

Green, A. G., Mikereit, B., Mayrand, L., Spencer, C., Kurtz, R. D. and Clowes, R. M., (1987), "Lithoprobe Seimic Reflection Profiling Across Vancouver Island", *Geophys. J. Roy. Astr. Soc.*, 89, 85-90.

Griffel, D. H., (1981), "Applied Functional Analysis", *Ellis Horwood Limited*.

Gupta, P. P., (1971), "Study of the Tectonic Trends in Punjab Plains and Western Uttar Pradesh by the Use of Gravity Residuals", (*ONGC unpublished report*).

Gupta, J. C. and Jones, A. G., (1990), "Electrical Resistivity Structure of the Flathead Basin in Southeastern British Columbia, Canada", *Canadian Journal of Earth Science*, 27, 1061-1073.

Gupta, H. K. and Narain, H., (1967), "Crustal Structure in Himalayas and Tibet Plateau Region from a Surface Wave Dispersion", *Bull. Seismol. Soc. Am.* 57, 235-248.

Gupta, H. K., Nyman, D. C. and Landisman, M., (1977), "Shield-Like Upper Mantle Velocity Structure Below the Indo-Gangetic Plains: Inferences drawn from Long-Period Surface Wave Disperison Studies", *Earth Planet. Sci. Lett.* 34, 51-55.

Guptasarma, D., (1978), "On: The Interpretation of Direct Current Resistivity Measurements", *Geophysics*, 264-265.

Haak, V. and Hutton, V. R. S., (1986), "Electrical Resistivity in Continental Lower Crust, in: The Nature of the Lower Continental Crust", J. B. Dawson, J. Hall and K. H. Wedephol, eds. *Geol. Soc. London, Spec. Publ.*, 24, 35-49.

Hermance, J. F., (1982), "The a Symptotic Response of Three-Dimensional Basin Offsets to Magnetotelluric fields at Long Periods- the Effects of Current Channeling", *Geophysics*, 47, 1562-1573.

Hermance, J. F. and Neumann G. A., (1988), "Evidence for Multiple Boundary Faults Beneath the North West of Long Valley Caldera: MT Results", *G.R.let.*, 15, 1437-1440.

Hjelt, S. E., (1984), "Deep Electromagnetic Studies of the Baltic Shield", *Journal of Geophysics*, 55, 144-152.

Hutton, V. R. S., Gough, D. I., Dawes, G. J. K. and Travassos, J., (1987), "Magnetotelluric Soundings in the Canadian Rocky Mountain", *Geophysical Journal of the Royal Astronomical Society*, 90, 245-263.

Ingham, M. R., (1988), "The Use of Invariant Impedances in Magnetotelluric Interpretation", *Geophysical Journal*, 92, 165-169.

Ingham, M. R. and Hutton, V. R. S., (1982), "Crustal and Upper Mantle Electrical Structure in Southern Scotland", *Geophysical Journal of the Royal Astronomical Society*, 69, 579-594.

Isacks, B., Oliver J. and Sykes L. R., (1968), "Seismology and the New Global Tectonics", *Journal of Geophysical Research*, 73, 5855.

Jackson, D. D., (1972), "Interpretation of Inaccurate, Insufficient and Inconsistent Data", *Geophysical Journal of the Royal Astronomical Society*, 28, 97-110.

Jones, A. G. and Craven J. A., (1990), "The North American Central Plains Conductivity Anomaly and its Correlation With Gravity, Magnetic, Seismic and Heat Flow Data in Sakatchewan, Canada", *Physics of the Earth and Planetary interior*, 60, 169-194.

Jones, A. G. and Garland, G. D., (1986), "Preliminary Interpretation of the Upper Crust Structure Beneath Prince Edward Island", *Ann. Geophys*, 48, 157-164.

Jupp, D. L. B. and Vozoff, K., (1975), "Stable Iterative Methods for the Inversion of Geophysical Data", *Geophysical Journal of the Royal Astronomical Society*, 42, 957-976.

Kaila, K. L., Reddy, P. R. and Narain, H., (1968), "Crustal Structure in the Himalayan Foothills of North India from P Wave Data of Shallow Earthquakes", *Bull. Seism. Soc. Am.*, 58, No. 2, 597-612.

Kao, D., (1981), "Magnetotelluric Response on Vertically Inhomogeneous Earth", *J. Geophys. Res.*, 86, 3027-3038.

Kao, D., (1982), "Magnetotelluric Response on Vertically Inhomogeneous Earth Having Conductivity Varying Exponentially With Depth", *Geophysics*, 47, No. 1, 89-99.

Kao, D. and Rankin, D., (1980), "Magnetotelluric Response on Inhomogeneous Layered Earth", *Geopysics*, 45, 1793-1802.

Kaofoed, O., (1979), "Resistivity Sounding on an Earth Model Containing Transition Layers With Linear Change of Resistivity With Depth", *Geophys. Prosp.*, 27, 862-868.

Kaufman, A. A. and Keller, G. V., (1981), "The Magnetotelluric Sounding Method (SERIES on Methods in Geochemistry and Geophysics, 15)", Elsevier Scientific Publication Company.

Kumar, R., (1979), "Theoretical Magnetotelluric Response of a Two-Dimensional Dyke", *Geophysical Research Bulletin*, 17, 129-138.

Kumar, R., Sarma, S. V. S. and Narayana, P. V. S., (1981), "Short Note on Detectability of an Intermediate Layer of Magnetotelluric Sounding", *Geophysics*, 46, 333-342.

Kunetz, G., (1972), "Processing and Interpretation of MT Sounding", *Geophysics*, 37, 1005-1021.

MacBain, J., (1986), "On the Fréchet Differentiability of the One-Dimensional Magnetotelluric Problem", *Geophysical Journal of the Royal Astronomical Society*, 86, 669-672.

MacBain, J., (1987), "On the Fréchet Differentiability of the One-Dimensional Magnetotelluric Problem", *Geophysical Journal of the Royal Astronomical Society*, 88, 777-785.

Mallick, K., (1970), "Magnetotelluric Sounding on a Layered Earth With Transitional Boundary", *Geophysical prospecting*, 18, 738-757.

Mallick, K., (1971), "Can Transition in the Electrical Properties of the Earth be Detected", *Geophysical prospecting*, 19, 156-162.

Mallick, K., (1972), "Conducting Sphere in Electromagnetic Input Field", *Geophysical Prospecting*, 20, 293-303.

Mallick, K., (1973), "Conducting Infinite Horizontal Cylinder in Electromagnetic Input Field (superposition)", *Geophysical Prospecting*, 21, 102-108.

Mallick, K. and Jain, S. C., (1979), "Resistivity Sounding on a Layered Transitional Earth", *Geophys. Prosp.*, 27, 869-875.

Mallick, K. and Roy, A., (1968), "Resistivity Sounding on Two-Layer Earth With Transitional Boundary", *Geophys. Props.*, 16, 436-446.

McGillivray, P. R. and Oldenburg, D. W., (1990), "Methods for Calculating Fréchet Derivatives and Sensitivities for the Non-Linear Inverse Problem: A Comparative Study", *Geophysical Prospecting*, 38, 499-524.

Mckenzie, D. P., (1969), "Speculations on the Cause and Consequence of Plate Motions", *Geophysical Journal of Royal Astronomical Society*, 18, 1-32.

Mckenzie, D. P. and Sclater, J. G., (1971), "Evolution of the Indian Ocean Since and Late Cretaceous", *Geophysical Journal of Royal Astronomical Society*, 24, 437-528.

McMechan, G. A. and Barrodale, I., (1985), "Processing Electromagnetic Data in Time Domain", *Geophysical Journal of the Royal Astronomical Society*, 81, 277-293.

Menke, W., (1984), "Geophysical Data Analysis: Discrete Inverse Theory", *Academic Press, Inc.*

Menvielle, M. and Mouel, J. L. L., (1990), "Electrical Structure of the Crust in South Eastern Tibet", *Proc. Indian Acad. Sci. (Earth Planet. Sci.)* 49, 717-738.

Morrison, H. F., Phillips, R. J. and O'Brien, D. R., (1969), "Quantitative Interpretation of Transient Electromagnetic Fields Over a Layered Half-Space", *Geophysical Prospecting*, 17, 82-101.

Naidu, P.S., (1965), "Telluric Field and Apparent Resistivity Over an Inclined Fault", *Canadian Journal of Earth Sciences*, 2, 351-360.

Negi, J. G., (1974), "Progress in Theoretical Geophysics", *National Geophysical Research Institute, Hyderabad*, (Unpublished).

Negi, J. G. and Saraf, P. D., (1989), "Anisotropy in Geoelectromagnetism: Method in Geochemistry and Geophysics", *Elsevier Science Publication, B. U.*, 28.

Oldenberg, D. W., (1978), "The Interpretation of Direct Current Resistivity Measurements", *Geophysics*, 43, 610-625.

Oldenberg, D. W., (1979), "One-Dimensional Inversion of Natural Source Magnetotelluric Observation", *Geophysics*, 44, 1218-1244.

Oldenberg, D. W., (1984), "An Introduction to Linear Inverse Theory", *IEEE Transactions on Geoscience and Remote Sensing* GE-22, 665-674.

Oldham, R. D., (1917), "The Structure of the Himalayas and of the Gangetic Plains as Elucidated by Geodetic Observations in India", *Geological Society of India Mem.*, 42, 1-12.

Orange, A. S., (1989), "Magnetotelluric Exploration for Hydro Carbons", *Proceedings of IEEE*, 77, No. 2, 287-317.

Park, S. K., (1985), "Distortions of Magnetotelluric Sounding Curves by Three-Dimensional Structures", *Geophysics*, 50, 785-797.

Park, S. K. and Lively Brooks, D. W., (1989), "Quantitative Interpretation of Rotationally Invariant Parameters in Magnetotellurics", *Geophysics*, 54, 1483-1490.

Park, S. K., Orange, A. S. and Madden, T. R., (1983), "Effects of Three-Dimensional Structure on MT Sounding Curves", *Geophysics*, 48, 1402-1405.

Parker, R. L., (1970), "The Inverse Problem of Electrical Conductivity in the Mantle", *Geophysical Journal of the Royal Astronomical Society*, 22, 121-138.

Parker, R. L., (1972), "Inverse Theory With Grassly Inadequate Data", *Journal of the Royal Astronomical Society*, 22, 121-138.

Parker, R. L., (1977a), "The Fréchet Derivative for the One-Dimensional Electromagnetic Induction Problem", *Geophysical Journal of the Royal Astronomical Society*, 49, 543-547.

Parker, R. L., (1977b), "Understanding Inverse Theory", *Annual Reviews of Earth and Planetary Sciences*, 5, 35-64.

Parker, R. L., (1980), "The Inverse Problem of Electromagnetic Induction: Existence and Construction of Solutions Based Upon the Incomplete Data", *Journal of Geophysical Research*, 85, 4421-4428.

Parker, R. L., (1986), "Comment Concerning on Fréchet Differentiability of the One-Dimensional Magnetotelluric Problem ?", *Geophysical Journal of the Royal Astronomical Society*, 86, 673.

Patella, D., (1977), Resistivity Sounding on a multilayered Earth With Transitional Layer, Part 1: Theory", *Geophys. Prosp.*, 25, 699-729.

Pedersen, L. B., (1982), "The Magnetotelluric Impedance Tensor-its Random Errors", *Geophysical Prospecting*, 30, 188-210.

Pedersen, L. B. and Rasmussen, T. M., (1989), "Inversion of Magnetotelluric Data: A Non-Linear Least Squares Approach", *Geophysical Prospecting*, 37, 669-696.

Pham, V. N., Boyer, D., Therne, P., Yuan, X. C., Li, L. and Jira, G. V., (1986), "Partial Melting Zones in the Crust in Southern Tibet from Magnetotelluric Results", *Nature*, 319, 310-314.

Porstendorfer, G., (1975), "Principles of MT Prospecting: Gebruder Borntraeger", *Berlin-west struttgart*.

Powell, C. and Conagham, P. J., (1973), "Plate Tectonics and the Himalayas", *Physics of the Earth and Planetary Interior*, 20, 1-12.

Qureshy, M. N., (1969), "Thickening of Basalt Layer as a Possible Cause for the Uplift of the Himalayas- a Suggestion Based on Gravity Data", *Tectonophysics*, 7, 137-157.

Qureshy, M. N., (1971), "Relation of Gravity to Elevation and Rejuvenation of Blocks in India", *Journal of Geophysical Research*, 76, 545-557.

Qureshy, M. N. and Midha, R. K., (1986), "Deep Crustal Signatures in India and Contiguous Regions from Satellites and Ground Geophysical data, In: M. Barazangi and L.Brown (Eds.), Reflection Seismology : The Continental Crust", *Geodynamic Series*, 14(AGU), 77-94.

Raiverman, V., Kunte, S. V. and Mukherjea, A., (1983), "Basin Geometry, Cenozoic Sedimentation and Hydrocarbon Prospects in North Western Himalaya and Indo-Gangetic Plains", *Asia Journal*, 6, 67-92.

Ranganayaki, R. P., (1984), "An Interpretative Analysis of Magnetotelluric Data", *Geophysics*, 49, 1730-1748.

Reddy, I. K. and Rankin, D., (1972), "On the Interpretation of MT Data in the Plains of Alberta", *Canadian Journal of Earth Science*, 9, 514-527.

Roy, K. K., (1973), "Theoretical Analysis of Telluric Field Over a Faulted Basement", *Pageoph*, 105, 835-846.

Roy, K. K. and Ghose, R., (1985), "Magnetotelluric and Seismic Evidences for Crust-Mantle Heterogeneities", *Physics of the Earth and Planetary Interiors*, 41, 143-153.

Roy, K. K. and Naidu, P. S., (1970), "Computation of Telluric Field and Apparent Resistivity Over an Anticline", *Pure and Applied Geophysics*, 80, 205-217.

Roy, K. K., Rao, C. K. and Chattopadhyay, A., (1989), "Magnetotelluric Survey Across Singhbhum Granite Batholith", *Proc. Indian Acad. Science (Earth Planetary Science)*, 98, No. 2, 147-165.

Roy, K. K., Rathi, O. P. and Rao, K. P., (1982), "Telluric Fields and Their Gradients Over a Step Fault", *Geophysics*, 47, 1078-1090.

Sarma, S. V. S., Harinarayana, T., Gupta, M. L., Sarma, S. R., Kumar, R. and Sankernarayan, P. V., (1983), "A Reconnaissance Telluric Survey in Northern Parts of Konkan Geothermal Province, India", *Geophysical Research Bulletin*, 21, 91-99.

Sarma, S. V. S., Sastri, T. S. and Sarma, Y. S., (1991), "On the Latitudinal Variation of Magnetotelluric Source Field in the Equatorial Region of India", *Journal of Geomagnetism and Geoelectric*, 43, 677-684.

Sarma, S. V. S., Ramanujachary, K. K and Narayana S., (1970), "Results of Magnetotelluric Soundings at Choutupal (Near Hyderabad, India)", *Proceedings pf the second symposium on Upper Mantle Project, Hyderabad)*, NGRI contribution NO. 71-225, 175-181.

Sasaki, Y., (1989), "Sensitivity Analysis of Magnetotelluric Measurements in Relation to Static Effects", *Geophysical Prospecting*, 37, 395-406.

Sastri, V. V., Bhandari, L. L., Raju, A. T. R. and Datta, A. K., (1971), "Tectonic Framework and Subsurface Stratigraphy of the Ganga Basin", *Journal Geological Society of India*, 12, 222-223.

Satpathy, B. N., (1974), "A Paradox in Apparent Resistivity Masurements Over a Ground Section With Conductive Substratum", *Geophysics*, 39, 93-94.

Sengupta, S. N., (1977), "Basement Configuration of the Indo-Gangetic Plains Shown by Aeromagnetic Surveys", *Geophysical case histories of India AEG*, Hyderabad, 1, 1-7.

Shanker, R., (1988), "Heat Flow Map of India and Discussions on its Geological and Economic Significances", *Indian Minerals*, 2, 89-110.

Spies. B. R., (1989), "Depth of Investigation in Electromagnetic Sounding Methods", *Geophysics*, 54, 872-888.

Spies, B. R. and Eggers, D. E., (1986), "The Use and Misuse of Apparent Resistivity in Electromagnetic Methods", *Geophysics*, 51, 1462-1471.

Spies, B. R. and Eggers, D. E., (1988), "Erratum on the Use and Misuse of Apparent Resistivity in Electromagnetic Methods", *Geophysics*, 53(12), 1637.

Srivastava, S. P., (1963), "Application of the Magnetotelluric Method to Anisotropic and Inhomogeneous Bodies", *Journal of Geophysical Research*, 68, 38-52.

Srivastava, S. P., (1965), "Method of Interpretation of Magnetotelluric Data When Source Field is Considered", *J. Geophys. Res.*, 70, 945-954.

Srivastava, S. P., (1966), "Theory of the Magnetotelluric Method for a spherical Conductor", *Geophys. J. R. Astron. Soc.*, 11, 373-387.

Srivastav, B. J., Singh, B. P. and Lilley, F. E. M, (1984), "Magnetometer Array Studies in India and the Lithosphere", *Tectonophysics*, 105, 355-371.

Swift, C. M., Jr., (1967), A Magnetotelluric Investigation of an Electrical Conductivity Anomaly in the Southwestern United States: Ph.D. Thesis, M.I.T.".

Tandon, A. N. and Dube, R. K., (1973), "A Study of the Central Structure Beneath the Himalayas from Body Waves", *Pure and Applied Geophysics*, 111, 2207-2215.

Tikhonov, A. N., (1950), "Determination of the Electrical Characteristics of the Deep Strata of the Earth's Crust", *dokl. Akad. Nank, USSR*, 73, No. 2, 295-297.

Valdiya, K. S., (1976), "Himalayan Transverse Faults and Folds and Their Parallelism With Subsurface Structures of North Indian Plains", *Tectonophysics*, 32, 353-386.

Wadia, D. N., (1931), "The Syntaxis of the Northwest Himalaya: Its Rocks, Tectonics and Orogeny", *Records Geological Survey of India*, 65(2), 189-220.

Wannamaker, P. E., Hohmann, G. W. and Ward, S. H., (1984), MT Responses of Three-Dimensional Bodies in Layered Earth", *Geophysics*, 49, 1517-1534.

Ward, S. H., Smith, B. D., Glenn, W. E., Rijo, L. and Inman, J. R., (1976), "Statistical Evaluation of Electrical Sounding Methods Part II: Applied Electromagnetic Depth Sounding", *Geophysics*, 41, 1222-1235.

Weidelt, P., (1972), "The Inverse Problem of Geomagnetic Induction", *Zeitschrift for Geophysik*, 38, 257-289.

Weidelt, P., (1985), "Construction of Conductance Bounds from Magnetotelluric Impedances", *Journal of Geophysics*, 57, 191-206.

Wieladek, R. and Ernst, T., (1977), "Application of the Method of Least Squares to Determining Impulse Response and Transfer Function", *Publ. Inst. Geophysics Poland Academic Science*, G-1, 3-12.

Wiggins, R. A., (1972), "The General Linear Inverse Problem: Implication of Surface Wave and Free Oscillations for Earth Structure", *Reviews of Geophysics and space Physics*, 10, 251-285.

Wright, J. A., (1970), "Anisotropic Apparent Resistivities Arising from Two-Dimensional Structures", *Canadian Journal of Earth Science*, 7, 527-531.

Woodhouse, J. H., (1976), "On the Rayleigh Principle", *Geophysical Journal of the Royal Astronomical Society*, 46, 11-22.

Wu, F. T., (1968), "The Inverse Problem of Magnetotelluric Sounding", *Geophysics*, 37, 972-979.

Yee, E., Kosteniuk, P. R. and Paulson, K. V., (1988), "The Reconstruction of the MT Impedance Tensor: An Adaptive Parametric Time Domain Approach", *Geophysics*, 53, 1080-1087.

Zhang, P., Roberts, R. G. and Pederson, L. B., (1987), "Magnetotelluric Strike Rules",*Geophysics*, 52, 267-278.

Zhang, P., Rasmussen, T. M. and Pedersen. L. B., (1988), "Electric Resistivity Structure of the Siljan Impact Region", *Journal of Geophysical Research*, 93, 6485-6501.

Zeidler, E., (1985), "Nonlinear Functional Analysis and its Applications III-Variational Methods and Optimization", *Springer-Verlag, Inc.*